Origin, growth and demise of the cold-water coral mound Challenger (IODP Site 1317)

Dissertation

Zur Erlangung des Doktorgrades

Dr. rer. nat

Der Mathematisch-Naturwissenschaftlichen Fakultät
der Christian-Albrechts-Universität

zu Kiel

vorgelegt von

Jacek Raddatz

Kiel, 2011

Referent: Prof. Dr. Wolf-Christian Dullo

Koreferent: Prof. Dr. Anton Eisenhauer

Tag der Disputation: 15.11.2011

Zum Druck genehmigt: Ja

gez., der Dekan

“I'm going down to sleep on the bottom of the ocean
cause I couldn’t let go when the water hit the setting sun**”**

Rocky Votolato

Erklärung

Hiermit erkläre ich an Eides statt, dass ich diese Dissertation selbständig und nur mit Hilfe der angegeben Quellen und Hilfmittel erstellt habe. Weiterhin versichere ich, dass der Inhalt dieser Arbeit weder in dieser, noch in veränderter Form, einer weiteren Prüfungsbehörde vorliegt. Die Arbeit wurde unter Einhaltung der Regeln guter wissenschaftlicher Praxis der Deutschen Forschungsgemeinschaft verfasst.

Kiel, den

(Jacek Raddatz, Dipl. Geogr.)

Table of Contents

Abstract

The Integrated Ocean Drilling Program (IODP) Expedition 307 was proposed to obtain evidence for understanding the origin and evolution of a 155 m high deepwater carbonate mound in the Porcupine Seabight. The major aim of this study is the reconstruction of environmental parameters using well-developed paleoceanographic proxies derived from calcareous tests and skeletons of benthic organisms based on sediment cores from this expedition. In particular, this study uses different archives such as scleractinian cold-water corals and calcitic foraminifers.

The second chapter (published in Marine Geology 2011) reports on a high-resolution record of the mound base. Stable oxygen and carbon isotopes measured in several benthic and planktonic foraminifers as well as sortable silt analyses document the start-up phase of coral growth. Mound initiation and further development coincide with the intensification of Mediterranean Outflow Water (MOW) characterized by oceanographic conditions favourable for rapid cold-water coral growth. Furthermore excursions in foraminiferal $\delta^{13}C$ values and increased flow conditions indicate erosional intervals, which overprinted probably diagenetically the original geochemical signals.

The third chapter (to be submitted to Geology), also based on sediments from the mound base, shows that these ecosystems only thrive under specific oceanographic conditions. Based on core material, not only from Challenger Mound (IODP Expedition 307) but also from the Propeller Mound, we reconstructed paleo-seawater densities from oxygen isotope ratios in benthic foraminifera. Results clearly indicate results demonstrate that cold-water coral mound development occurred when a density window of sigma-theta (σ_Θ) = 27.35–27.55 kg m^{-3} was present in the ambient bottom water. Therefore we conclude that seawater density is reflecting one of the major controlling factors favoring mound growth and highlights the sensitivity of these ecosystems to environmental changes.

The fourth chapter (submitted to Earth Planetary Science Letters) demonstrates the use of paleotemperature proxies in the scleractinian reef building cold-water coral *Lophelia pertusa*. Temperature calibrations are based on *L. pertusa* samples from temperature range of 5.9°-13.65°C originating from the European continental margin and the Mediterranean Sea.

Results could not confirm earlier findings of Rüggeberg et al. (2008) that $\delta^{88/86}Sr$ in *Lophelia* skeleton is positively correlated with temperature and may serve as a potential paleotemperature proxy. Results rather show that $\delta^{88/86}Sr$ is inversely correlated with temperature in samples from the North Atlantic. However, this temperature effect appears to be superimposed by changes in the ocean carbonate system. Furthermore, this sample set of *L. pertusa* clearly shows the temperature dependency of elemental ratios such as Mg/Li and Sr/Ca. The Mg/Li ratio may serve as a new paleotemperature proxy in scleractinian cold-water corals, whereas the Sr/Ca ratio needs more detailed research.

The fifth chapter (to be submitted) focuses on the long-term controlling mechanisms of cold-water coral mound growth in the Porcupine Seabight. Here, different paleo-proxies such as Mg/Ca, $\delta^{13}C$ and $\delta^{18}O$ in foraminifera and Mg/Li, Ba/Ca and U/Ca in cold-water coral *L. pertusa* were used to reconstruct paleoenvironmental parameters. Based on existing and additional age determinations ($^{87}Sr/^{86}Sr$, Th/U) previous findings were supported. However, our data point to an earlier mound initiation at ~3 Ma coincidently with the intensification of the Mediterranean Ouflow Water (MOW). Foraminiferal temperature records reveal that early mound development occurred in glacial and interglacial conditions, whereas the recent mound decline was caused by high amplitude excursions of the last interglacial/glacial cycles. In particular, coral $Mg/Li_{Lophelia}$ temperatures indicate that coral growth occurred within a temperature range of 8 to 10°C, comparable to the recent measured settings in the Porcupine Seabight. Hence, results imply that the variations in intermediate water masses (Mediterranean Outflow Water, Eastern North Atlantic Water,) are the main trigger for mound growth and decline in the Porcupine Seabight. Moreover prior to the mid-Pleistocene rapid Challenger Mound growth benefited from a stable boundary layer between the MOW and the Eastern North Atlantic Water (ENAW) at which organic matter and nutrients settled on.

Zusammenfassung

Die Expedition 307 des internationalen Bohrprogrammes IODP wurde durchgeführt um das Verständnis des Ursprungs und der Entwicklung eines 155 m hohen Kaltwasserkorallen-Karbonathügels (Challenger Mound) in der Porcupine Seabight zu verbessern. Das Hauptziel dieser Studie ist die Rekonstruktion von Umweltparametern durch die Verwendung von etablierten und neuen Proxies an kalzitischen Gehäusen und Skeletten benthischer Organismen aus den Bohrkernen der IODP Expedition 307. Im Besonderen werden in dieser Studie zwei verschiedene benthische Archive benutzt: aragonitische Kaltwasserkorallen und kalzitische Foraminiferen.

Das zweite Kapitel (publiziert in Marine Geology 2011) konzentriert sich auf eine hoch auflösenden Untersuchung der Basis des Karbonathügels und somit dem Beginn des Korallenwachstums. Sauerstoff- und Kohlenstoffisotope, gemessen an verschiedenen benthischen und planktonischen Foraminiferen, sowie Korngrößenanalysen dokumentieren die Startphase des Korallenhügels. Der Beginn und die weitere Entwicklung des Challenger Mounds fanden gleichzeitig mit der Intensivierung des Mittelmeeraustromwassers statt, wodurch das Korallenwachstum begünstigt wurde. Weiterhin zeigen starke Abnahmen in den Kohlenstoffsignaturen und verstärkte Strömungsbedingungen mögliche Intervalle von Erosionen auf, die das ursprüngliche geochemische Signal der Foraminiferen diagenetisch überprägt haben könnten.

Das dritte Kapitel (wird eingereicht bei Geology) basiert ebenfalls auf Sedimenten von der Hügelbasis und macht deutlich, dass dieses Ökosystem nur unter ganz bestimmten ozeanographischen Vorrausetzungen gedeiht. Anhand von Sauerstoffisotopen in benthischen Foraminiferen haben wir an Kernmaterial von IODP Expedition 307 und auch am nahe gelegenem Propeller Mound die Paläodichte des Seewassers rekonstruiert. Ergebnisse zeigen deutlich auf, dass Kaltwasserkorallenhügel wuchsen, sobald die Meerwasserdichte (sigma-theta, σ_Θ) Werte zwischen 27.35 und 27.55 kg m^{-3} aufzeigte. Daher scheint die Dichte des Seewassers einer der Hauptparameter zu sein, der das Korallenwachstum mit steuert.

Das vierte Kapitel (eingereicht bei Earth and Planetary Science Letters) veranschaulicht den Gebrauch von Paläotemperaturproxies in der skleraktinen und, riffbildenden Kaltwasserkoralle *Lophelia pertusa*. Temperatur-Kalibrationen basieren auf *L. pertusa* Proben vom gesamten Europäischen Kontinentalschelf und dem Mittelmeer aus

Temperaturen von 5,9°-13,8°C. Die Resultate konnten vorherige Untersuchungen von Rüggeberg et al. (2008) nicht bestätigen, welche vorschlagen dass $\delta^{88/86}$Sr im Skelett von *L. pertusa* positiv mit Wassertemperatur korreliert und als potentieller Temperatur-Proxy dient. Unsere neuen Ergebnisse zeigen, dass $\delta^{88/86}$Sr in Proben aus dem Nord-Atlantik invers abhängig von der Temperatur ist. Nichtsdestotrotz scheint dieser Temperatureffekt von Veränderungen im Karbonatsystem des Ozeans überlagert zu sein. Darüber hinaus zeigt dieser Probensatz aber auch eine deutliche Temperaturabhängigkeit von Elementverhältnissen wie Mg/Li und Sr/Ca. Hierbei könnte besonders das Mg/Li Verhältnis als neuer Paläotemperatur-Proxy in skleraktinen Kaltwasserkorallen dienen, wobei das Sr/Ca Verhältnis noch einer eingehenden Untersuchung unterzogen werden muss.

Das fünfte Kapitel (wird eingereicht) konzentriert sich auf die Kontrollmechanismen des Wachstums der Kaltwasserkorallenhügel in der Porcupine Seabight. Hierbei wurden verschiedene Paläo-Proxies wie Mg/Ca, δ^{13}C in Foraminiferen und Mg/Li, Ba/Ca in der Kaltwasserkoralle *Lophelia pertusa* benutzt um Paläoumweltparameter zu rekonstruieren. Basierend auf einem existierenden Altersmodell konnten vorherige Erkenntnisse durch zusätzlichen Altersbestimmungen (^{87}Sr/^{86}Sr, Th/U) unterstützt werden. Jedoch zeigen unsere Daten, dass ein Beginn des Hügelwachstum schon vor ~3 Millionen Jahren begonnen haben könnte, zeitgleich mit dem Einströmen des Mittelmeeraustromwassers. Foraminiferen-Temperaturaufnahmen zeigen auf, dass der frühe Hügelwachstum in Gazialen und Interglazialen stattgefunden hat, wobei der derzeitige Rückgang des Hügelwachstums durch die starken Amplituden der letzten Interglazial/Glaziale Zyklen verursacht wurde. Im Besonderen zeigen die Korallen-Mg/$Li_{lophelia}$ Temperaturen, dass die Korallen innerhalb eines Temperaturfensters von 8–10°C wuchsen, vergleichbar zu den heutigen Verhältnissen in der Porcupine Seabight. Variationen in den Zwischenwassermassen (Mittelmeeraustromwasser, östliches Nordatlantikwasser) sind der Hauptauslöser für Wachstum und Rückgang der Karbonathügel in der Porcupine Seabight. Darüber hinaus wurde das schnelle Wachstum des Challenger Mounds vor dem mittleren Pleistozän von einer stabilen Grenzschicht zwischen dem Mittelmeeraustromwasser und dem östlichen Nordatlantikwasser begünstigt, da sich hier verstärkt organisches Material und Nährstoffe ansammeln konnten.

Acknowledgements

First of all I would like to thank Prof. Dr. Wolf-Christian Dullo for giving me the opportunity to carry out this PhD-Thesis and for being a patient and helpful supervisor in every circumstance. I learned a lot by your philosophy of life! Moreover, your door was always open for me! I really appreciated that!

I thank also Prof. Dr. Anton Eisenhauer for co-correcting this thesis. Moreover, you also supported and helped me during my doctoral studies with many helpful und fruitful discussions, thanks!

Special thanks go out to Andres and Volker! My “little” supervisors! I honestly have to say that I benefited from your knowledge, experience and inexhaustible support! Thank you very much for your convenient way!

Jan-Rainer and Hauke I thank you for being good friends and flat mates! I’ll never forget the great times we had in the Wulfsbrook!

Further, I also thank André for developing great ideas with me and sometimes distracting me from work whenever it was needed.

I thank Ed and Kai for becoming friends and for making me swim faster! Thanks go out to all my colleagues & friends at the Geomar or wherever you may roam: Sascha, Anneleen, Stephan, Armin, Karen & Jürgen, Dirk, Martin, Thor, Nico, Jan, Torben, Nabil, David, Florian, Paddy, Claudia, Clauschi, Steffie, Kristin and Matthias!

Roland & Moritz next door (!), thanks for the beer, the rides home, the sunrises, the helicopter flight and everything else!

I also would like to express my gratitude to Nadine, Ana, Jutta, Lutz and Folkmar for their technical support during my research!

Life wouldn’t be the same without my close friends! Thank you Daniel, Rene, Priggi, Hasi, Jörn, Monti, Jan-Pierre, Gerit and Ariane!

Last but certainly not least! I thank my Family and my better half Steffi for their love, support and time! I cannot imagine missing that!

Chapter I

Introduction

1.1 Motivation, main objectives and aim of this study

Continental margins mediate between the deep sea and the shelf and are linked to processes of both ocean areas. Climate data and environmental data are locked in calcareous tests and skeletons of benthic organisms. This study focuses on cold-water coral reefs and carbonate mound provinces discovered several years ago in the Porcupine Seabight and the Rockall Trough of the North Atlantic (Henriet et al. 1998; De Mol et al. 2002), especially on Challenger Mound drilled during IODP Expedition 307. These cold-water coral ecosystems build up spectacular, several 100-m high mound structures. The controlling mechanism of initial mound growth and development are still under debate. However, their recent development is dependent on sedimentary, oceanographic and climatic processes (De Mol et al. 2002; Freiwald 2002; Rüggeberg et al. 2005, 2007; Dorschel et al. 2005). Explanations of the origin and evolution of the Porcupine mounds revolve around two scenarios that may be expressed as either competing or complementary hypotheses: (a) hydrocarbon seepage initiates microbial-induced carbonate formation and indirectly fuels coral growth (endogenous control: Hovland et al. 1998; Henriet et al. 2001), and (b) oceanographic and environmental conditions control mound initiation and growth (e.g. Frederiksen et al. 1992).

(a) The seepage hypothesis was first proposed by Hovland et al. (1994), who correlated the distribution between coral mounds with areas showing high dissolved light hydrocarbon contents in water. Hydrocarbon seepage may initiate favourable conditions for deep-sea corals, in terms of raised inorganic carbon for skeletal accretion (Hovland et al. 1998) and - possibly more important - may contribute to early submarine lithification providing stable or at least firm substrates (Liebetrau et al. 2010). The aligned occurrence seen in some mounds of the Porcupine Seabight suggests that mounds were established along linear structures, such as faults (Hovland et al. 1994). However, since no significant quantities of gas could be found in the Challenger mound during IODP Expedition 307 and no further evidence is still supporting this hypothesis, it is assumed that geofluids are no prime triggers for mound initiation and formation (IODP Expedition 307 Shipboard Scientific Party).

(b) The oceanographic or environmental hypothesis highlights that the most important

conditions stimulating mound development is the interaction of water currents and sediment dynamics. Enhanced currents provide nutrient for the corals and may keep stable substrates free for coral larvae to settle (Colman et al. 2005; De Mol et al. 2002; Frederiksen et al. 1992; Freiwald et al. 1997; Kenyon et al. 2003). The overall aim of this study is focusing on the oceanographic and environmental hypothesis and therefore intends to reconstruct the paleoceanographic conditions causing cold-water coral mound growth and try to give explanations on mound decline in the Porcupine Seabight.

Cold-water coral mounds or carbonate mounds are known to occur widespread within the Porcupine Seabight. Sediment cores recovered during IODP Expedition 307 at Challenger Mound have the potential to shed light into the debate which ocean dynamics and changes favored mound start-up, growth and which cause mound decline. Geochemical signals in biogenic tests of planktonic and benthic foraminifers, as well as in skeletons of cold-water corals allows to understand the mechanisms of these environmental changes, especially the intermediate water mass variability such as the Mediterranean Outflow Water (MOW).

This study is based on the following chapters:

Chapter 2 and 3

These studies focus on lower sediments from the base of Challenger Mound and explain the paleoenvironmental conditions during mound initiation by the use of stable isotopes of benthic and planktonic foraminifera, as well as grain size analyses.

(2) Paleoenvironmental reconstruction of Challenger Mound initiation in the Porcupine Seabight, NE Atlantic, 2011. Jacek Raddatz, Andres Rüggeberg, Stephan Margreth, Wolf-Christian Dullo and the IODP Expedition 307 Scientific Party, Marine Geology, 282, 79-90. doi:10.1016/j.margeo.2010.10.019

(3) The seawater density code: a key to decipher cold-water coral carbonate mound development (to be submitted to Geology). Andres Rüggeberg, Sascha Flögel, Wolf-Christian Dullo, Jacek Raddatz, Volker Liebetrau.

Chapter 4

This proxy calibration contributes to the understanding of coral skeletons as paleo-archives with the focus on different potential paleo-thermometers in recent-live samples of cold-water coral *Lophelia pertusa*.

(4) Temperature dependence of stable Sr-isotopes, Sr/Ca and Mg/Li in the scleractinian cold-water coral *Lophelia pertusa* (submitted to Earth and planetary Science Letters). Jacek Raddatz, Andre Krabbenhöft, Volker Liebetrau, Andres Rüggeberg, Ed Hathorne, Anton Eisenhauer, Florian Böhm, Matthias López Correa, Paolo Montagna, Hauke Vollstaedt, Jan Fietzke and Wolf-Christian Dullo

Chapter 5

The last study is based on an extended record from upper mound sediments but also from selected intervals throughout the entire mound sequence. This study reveals the long-term history of the Challenger Mound by the use of different age determinations on coral skeletons and other geochemical signals in foraminifera and corals.

These investigations help to understand the role of intermediate water masses of southern origin (Mediterranean, Bay of Biscay) with their pole-ward transport and the colonization of cold-water corals during their first introduction to the Porcupine Seabight and the long-term history of Challenger Mound (IODP Site 1317) by the use of paleo-proxies.

(5) Control mechanisms of long-term cold-water coral growth in the Porcupine Seabight (in preparation for submission). Jacek Raddatz, Andres Rüggeberg, Volker Liebetrau, Anneleen Foubert, Ed Hathorne, Anton Eisenhauer, Dirk Nürnberg, Jan Fietzke, and Wolf-Christian Dullo

1.2 History of scleractinian cold-water corals research

Corals and their reefs are often associated with warm and bright tropical waters, but in fact they are not restricted to these habitats (Fig 1). More than 50 % of approximately 5100 coral species inhabit deep and cold waters. In general, corals belong to the phylum cnidaria and include stony corals (*Scleractinia*), soft corals (*Octocorallia*), black corals (*Antipatharia*), and hydrocorals (*Stylasteridae*, Roberts et al. 2009). Scleractinian cold-water corals are azooxanthellate (without symbionts) and can therefore live in the aphotic zone.

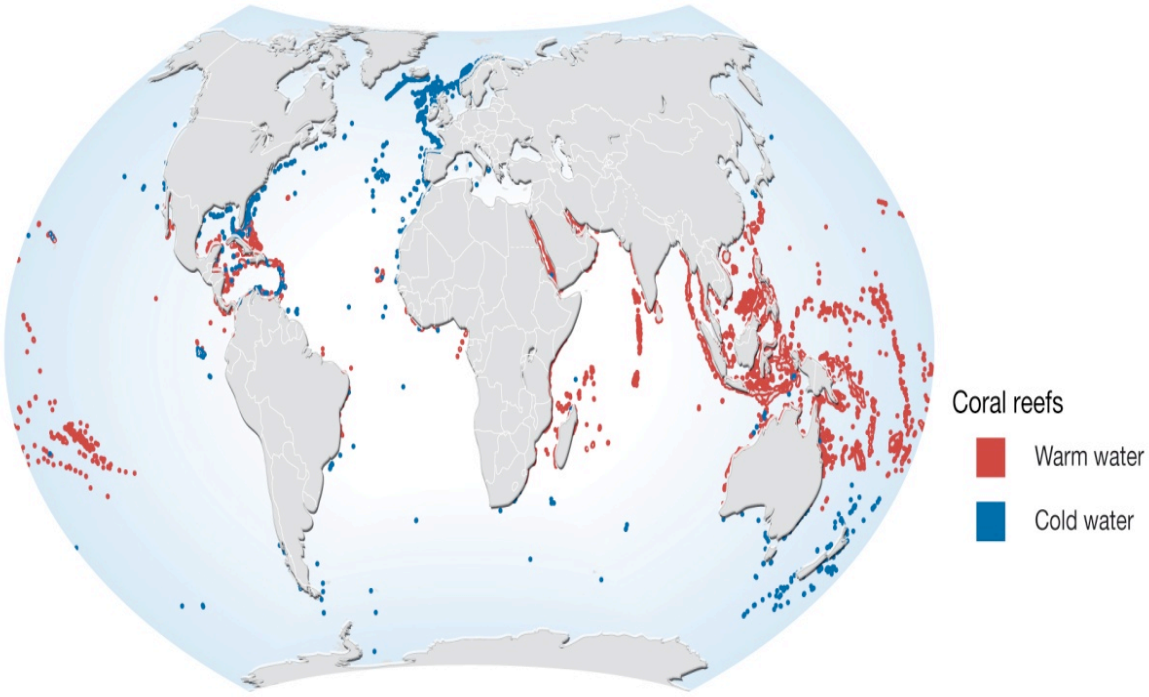

Figure 1: Distribution of cold-water and tropical coral reefs. UNEP/GRID-Arendal Maps and Graphics Library. February 2008. Available at: http://maps.grida.no/go/graphic/distribution-of-coldwater-and-tropical-coral-reefs. Accessed July 06, 2011.

They were first mentioned and drawn by the Norwegian Bishop Erich Pontoppidan in 1755. Later these species were described in more detail in the fundamental work of Carl von Linné (1758) and other early studies such as Gunnerus (1768) and Flemming 1846). Further exploration of the deep-sea, including cold-water corals was possible by the pioneering global expedition of *Challenger* and subsequently the *HMS Lighting* and *Porcupine* that found cold-water corals in their dredges (Thomson 1873). In the mid 20th century Le Danois (1948) first speculated that cold-water corals probably also build reef-like structures as their tropical

counterparts. Technical developments to map the seafloor such as survey sonar, manned submersibles and more recent developments such as the multibeam echosunder, ROV (Remotely Operating Vehicle) and TOBI (Toded Ocean Bottom Instrument) sidescan sonar made it possible to record in detail cold-water coral growth in the deep ocean. Sedimentary carbonate sequences from coral reefs and mounds have also been accessed by gravity cores and big drill ships like the RV *Joides Resolution* (IODP Exp. 307) in order to understand the origin, evolution and development of these cold-water corals reefs and to explore their potential as paleoceanographic archives. In the last two decades intensive research has been carried out in several EU projects (ECOMOUND, GEOMOUND, AGES, HERMES, HERMIONE) as well as ESF Projects (MOUNDFORCE, CARBONATE, MICROSYSTEMS) and smaller national projects for example TRISTAN & ISOLDE focusing on these research topics.

1.3 *Lophelia pertusa* distribution and occurrence

Recent investigations clearly revealed that species such as *L. pertusa* (Fig. 2) produce complex three dimensional reef frameworks especially in the Northeast Atlantic (Freiwald 2002). Initially, these corals being heterotrophic sessile filter feeders need a hard substrate to settle on, strong bottom currents and large organic fluxes (Freiwald 2002, Freiwald et al. 2004). *L. pertusa* tolerates a wide range of environmental factors such as temperatures of 4–14 °C and salinity values of 32–38.8 psu (Freiwald 2002; Freiwald et al. 2009) where the higher values for temperature and salinity are related to the Mediterranean Sea. Furthermore, *L. pertusa* tolerates values of dissolved oxygen ranging from 3.75 to 6.65 ml/l (Dodds et al. 2007; Dullo et al. 2008). The shallowest living colonies are found in 40 m water depth in the Trondheimsfjord, Norway (Fosså et al. 2005) while the deepest colonies occur in > 3000 m water depth on the New England Seamount Chain (Freiwald et al. 2004). Another controlling parameter for living cold-water coral reef distribution in the Northeast Atlantic is the density of seawater.

Figure 2: A stock of *L. pertusa* redrawn by Moen (2006) after Gunnerus (1768)

The study of Dullo et al. (2008) demonstrated a relationship between the distribution of living cold-water coral reefs and the hydrography on the Celtic and Norwegian Margin. Living reef ecosystems of cold-water corals in the Northeast Atlantic seem to occur within a density range of sigma-theta (σ_Θ)= 27.35 to 27.65 kg m^{-3}. However, cold-water corals in the Mediterranean Sea tolerate a seawater density value of up to 29.1 kg m^{-3} (Freiwald et al. 2009). According to Freiwald et al. (2009) oceanographic conditions in the Mediterranean Sea are marginal for the coral physiology, which in turn caused that living corals here only occur in small patches.

On the continental slopes of the European Margin *Lophelia* reefs are widely distributed (Roberts et al. 2006; Freiwald et al. 2004). They occur from northern Norway in the Barents Sea (Fig. 3, 70°N, Lindberg et al. 2007) to NW Africa off Mauretania (16°N, Colman et al. 2005). On the Norwegian margin large flourishing reefs developed after the retreat of the

glaciers to large living cold-water corals reefs (Frank et al. 2011; Freiwald et al. 2004; Fosså et al. 2005;). The margin southwest of Ireland represents one major region of abundant carbonate mounds associated to cold-water coral growth. These mounds tend to cluster in provinces (De Mol et al. 2007; Freiwald et al. 2004) and vary in height from a few metres up to > 380 m (Wheeler et al. 2007). A coral mound can vary strongly in appearance, but the framework of a vivid coral ecosystem is often dominated by the cold-water corals *L. pertusa* and *Madrepora oculata* (Foubert et al. 2005).

In the Porcupine Seabight coral mound growth occurs in a specific depth interval between the eastern North Atlantic Water (ENAW) and the underlying saline Mediterranean Outflow Water (MOW). The ENAW is originating in the Bay of Biscay and the MOW in the Mediterranean Sea and stream poleward into the Irish Sea (Hargreaves 1984; White and Bowyer 1997). Topographically steered by the slope of the Porcupine Seabight, these water masses change into a southwestward flow direction. Due to the large differences in density between the MOW and ENAW a pycnocline forms at around 775 m. In particular cold-water corals benefit from the density gradient of transition zone between the ENAW and the MOW (Dullo et al. 2008). Corals are fed by organic matter and nutrients from high productive surface waters and are kept clean by a vigorous current regime (White et al. 2007). At depth of the pycnocline bottom currents can be amplified by internal waves of up to 45 cm/s (Dorschel et al. 2007b; White et al. 2007).

Cold-water coral growth on the slopes of the European margin initiated on erosional surfaces with dynamic boundary currents (De Mol et al. 2002; van Weering et al. 2003) at the Pliocene/Pleistocene boundary and repeated reef growth has build-up huge carbonate mounds (Kano et al. 2007; Foubert & Henriet 2009). Carbonate mound growth on the Irish margin is restricted to interstadial and interglacial conditions (Dorschel et al. 2005; Rüggeberg et al. 2007). Further south in the Bay of Biscay corals tend to grow rather at terminations (Schröder-Ritzrau et al. 2003) or during glacial periods in the Gulf of Càdiz and off Mauritania (Wienberg et al. 2009; Eisele et al. 2011). In the Mediterranean Sea McCoulloch et al. (2010) showed that cold-water corals growth have persisted at least for the last 480 ka. Growth especially occured in colder interstadials and during the Younger Dryas.

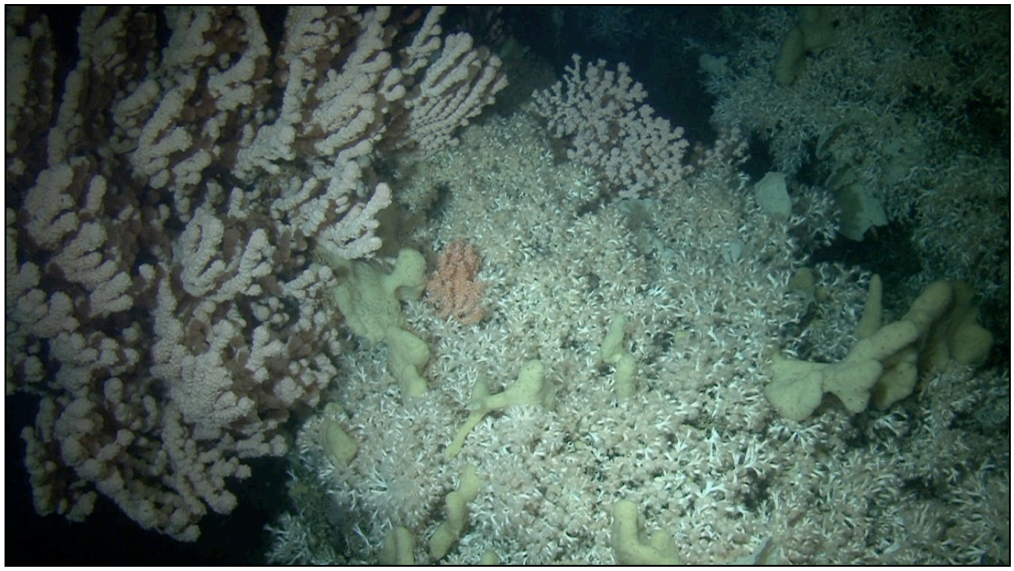

Figure 3: Flourishing *Lophelia*-Reef (and associated fauna) off northern Norway, Lopphavet. Picture taken during Dive 1102 with manned submersible JAGO (IFM-GEOMAR) during research cruise POS391.

1.4 The Challenger Mound

In 2005 the IODP Expedition 307 sailed to drill for the first time complete records through the entire sediment body of a huge carbonate mound. The 155 m high Challenger Mound was chosen due to its dead coral cover. It is located in the Porcupine Seabight at 52°23'N and 11°43'W in ~ 800 m below sea level (Fig. 4). The Porcupine Seabight is characterized by over 1000 buried and exposed mounds (Huvenne et al. 2007). The recovered sediment cores contained mainly the scleractinian cold-water coral *Lophelia pertusa* and only to a minor degree *Madrepora oculata*. The presence of corals throughout the mound sequence made it possible to state that corals played a major role in the initiation of mound growth and further development (Williams et al. 2006).

Generally the Challenger Mound can be subdivided into two units M1 (Fig. 4155–22.98 mbsf, 1317 E) and M2 (22.98–0 mbsf 1317 E). The mound sits on an unconformity with a lower age of 16.58 (Kano et al. 2007). Moreover, stratigraphic work carried out on the Challenger Mound by Kano et al. (2007, strontium isotope stratigraphy) and Foubert and Henriet (2009, magnetostratigraphy) showed that growth was initiated at around 2.6 Ma.

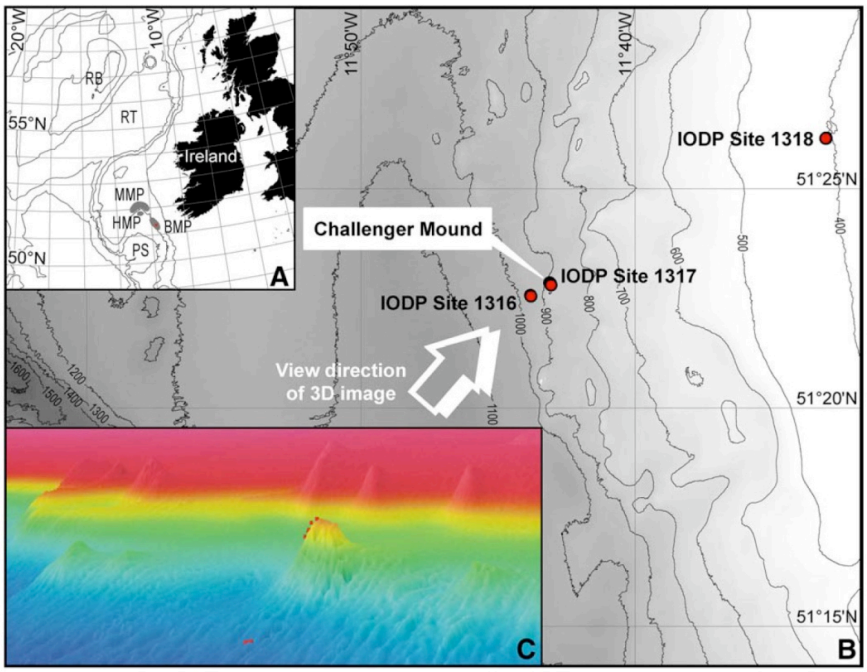

Figure 4: A: Location map showing the Porcupine Seabight (PS) with the Mound Provinces MMP: Magellan Mound Province, HMP: Hovland Mound Province, BMP: Belgica Mound Province. B: Location map of the hole transect drilled during IODP Expedition 307. C: 3D-visualisation of the BMP (adapted from Titschack et al. 2009)

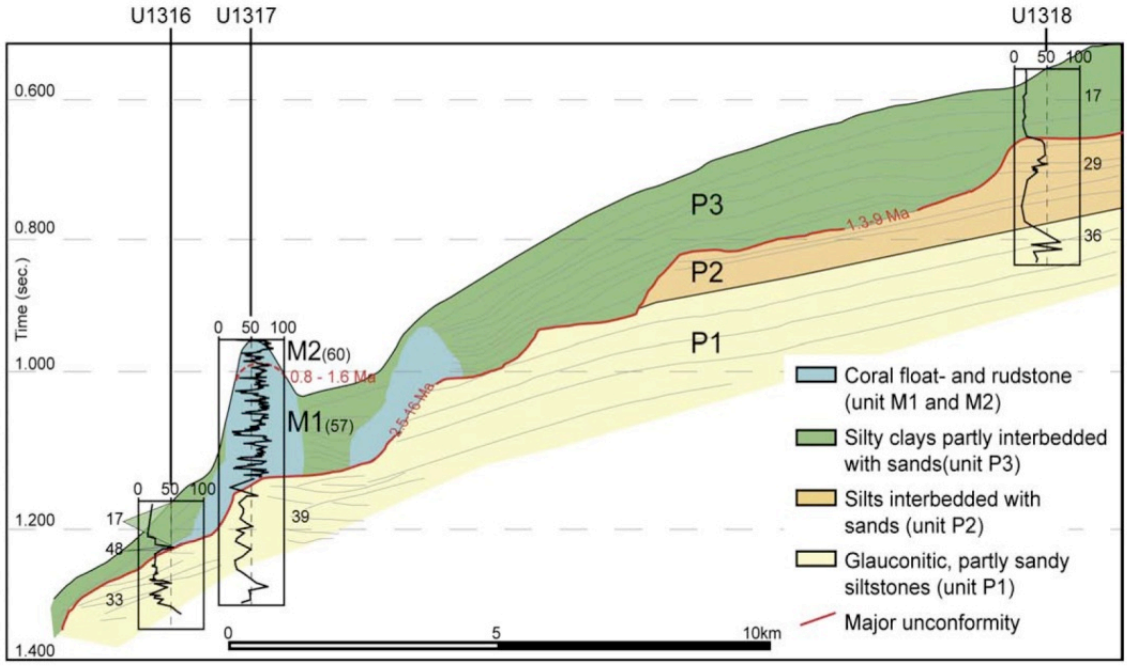

Figure 5: Sedimentary facies of the IODP 307 site transect (after De Mol et al., 2002). Key unconformities are shown in red with the duration of their hiatus (based on $^{87}Sr/^{86}Sr$-dates of Kano et al. 2007). Total carbonate contents are plotted (small numbers, adapted from Titschack et al. 2009)

Both studies recognized a significant hiatus at around 23.6 m depth in IODP Site 1317 E. This major hiatus separates the mound record into a period of fast growth (2.6–1.7 Ma) and slower growth (1.0–0.5 Ma). An oxygen isotope stratigraphy of the planktonic foraminifera species *Globigerina bulloides* for the Challenger Mound presented by Sakai et al. (2009) highlighted an even faster development during its initial growth phase. They suggested that the mound initiated during marine isotope stage 92 (2.24 Ma) and growth lasted until 1.85 Ma. The restart of growth occurred in MIS 19 at 750 ka. Growth of the Challenger Mound therefore seems to have been connected to major global climatic changes, such as the major initiation of Northern Hemisphere Glaciation and the Mid-Pleistocene Transition (Kano et al. 2007). Moreover, the Challenger Mound grew in periods in which no deposition occurred in the surrounding areas. Hence, the sedimentary sequence of the mound can serve as an extraordinary archive for high resolution paleoceanographic reconstructions of intermediate water masses in the Porcupine Seabight (Titschack et al. 2009; Kano et al. 2007).

1.5 Cold-water corals as paleo-archives

Since we are in a period of rapid climate change it is important to reconstruct the past seawater conditions and circulation to improve our ability to predict future climate and oceans scenarios such as temperature increase and acidification of the deep sea. Compared to traditional sedimentary archives, deep-sea corals have several advantages. Scleractinian corals incorporate high concentrations of uranium in their aragonite skeleton and hence can be accurately dated by the U/Th method (Cheng et al. 2000b; Mortlock et al. 2005). Paired measurements of ^{14}C and U/Th in deep-sea corals have the potential to directly measure the $\Delta^{14}C$ of the past ocean and hence can be used as a ocean circulation tracer (Adkins et al. 1998; Goldstein et al. 2001; Schröder-Riztrau et al. 2003). Moreover, in combination with Neodymium isotopes they can serve as a valuable new tool for rapid climate change (Van de Fliert et al. 2010). Growth rates in *L. pertusa* vary between 4–26 mm/year and therefore can provide high-resolution records for seawater temperature and paleoceanographic reconstructions (Mortensen 2001; Gass & Roberts 2010).

The first work focusing on temperature records in scleractinian cold-water corals was the study by Smith et al. (2000). They examined a strong relationship between the linear regression of $\delta^{18}O$ and $\delta^{13}C$ of aragonite and the $\delta^{13}C$ seawater DIC to seawater temperature, which is the so called “lines technique”. However, this approach is biased by coral vital effects, offsets in slopes of the lines, uncertainty of seawater values and an induced variability

due to the centres of calcification (Adkins et al. 2003; Sherwood & Risk 2007). Moreover, this method requires an enormous sample procedure and > 15 measurements of stable isotope analyses for one determined temperature value.

Another potential temperature proxy was introduced by Mitsuguchi et al. (1996) in scleractinian warm-water corals. They found a significant relationship between seawater temperature and the Mg/Ca ratio in the coral skeleton, but further studies by Cohen et al. (2006) and Gagnon et al. (2007) could not support these findings. Elemental ratios with known temperature dependency in scleractinian corals are B/Ca (Sinclair et al. 2006), U/Ca (Min et al. 1995; Shen et al. 1995) and Sr/Ca (Beck et al. 1992; Smith et al. 1979). The Sr/Ca ratio of warm-water corals is a widely used robust temperature proxy (e.g. Beck et al. 1992; Gagan et al. 1998), although other environmental and biological factors can distort the temperature signal of cold-water corals (Montagna et al. 2005; Cohen et al. 2006). Cohen et al. (2006) found a temperature dependency of Sr/Ca in the cold-water coral *Lophelia pertusa*. However, the amplitude of the Sr/Ca variability was too large to be simply explained by temperature. Vital effects seem to have a much larger control on the element incorporation. Often the measured trace element ratio is different from the thermodynamically expected value which is ascribed to the so called "vital effect" and may be distinctly different between species (Weber and Woodhead 1972; Gagnon et al. 2007; Gaetani et al. 2011). The temperature dependency of the U/Ca ratio could also not be confirmed by recent studies. In particular, the U/Ca ratio in the cold-water coral *Desmophyllum dianthus* is rather affected by CO_3^{2-} concentrations of seawater (Anagnostou et al. 2011) and its temperature dependence in warm-water corals is largely superimposed by pH and/or CO_3^{2-} concentrations (Inoue et al. 2011). Anagnostou et al. (2011) also highlighted that the Ba/Ca ratio in scleractinian cold-water corals is rather related to the Ba/Ca ratio of seawater and hence may serve as a proxy for nutrient reconstructions.

Recently Mg/Li has been introduced as a potential paleotemperature proxy in aragonitic foraminifera (Bryan and Marchiotto 2008) and scleractinian cold-water corals (Case et al. 2010; Montagna et al. 2008). High resolution laser ablation analysis of *L. pertusa* and other scleractinian cold-water corals collected from different water temperatures suggest that Mg/Li ratios are primarily controlled by temperature as combining Li/Ca and Mg/Ca ratios remove some of the vital effect and are not affected by changes in salinity and carbonate ion concentration (Case et al. 2010).

The first paleotemperature proxy introduced in scleractinian cold-water corals using non-traditional stable isotopes was the work by Rüggeberg et al. (2008). Based on the results of Fietzke and Eisenhauer (2006) who examined a temperature dependent fractionation of $\delta^{88/86}Sr$ in the tropical coral *Pavona clavus* Rüggeberg et al. (2008) found a similar temperature relationship in the cold-water coral *L. pertusa.* They investigated *L. pertusa* samples from contrasting water temperatures along the European continental margin. They suggested $\delta^{88/86}Sr$ might serve as new proxy for the reconstruction of intermediate water mass temperatures independent from any vital effects.

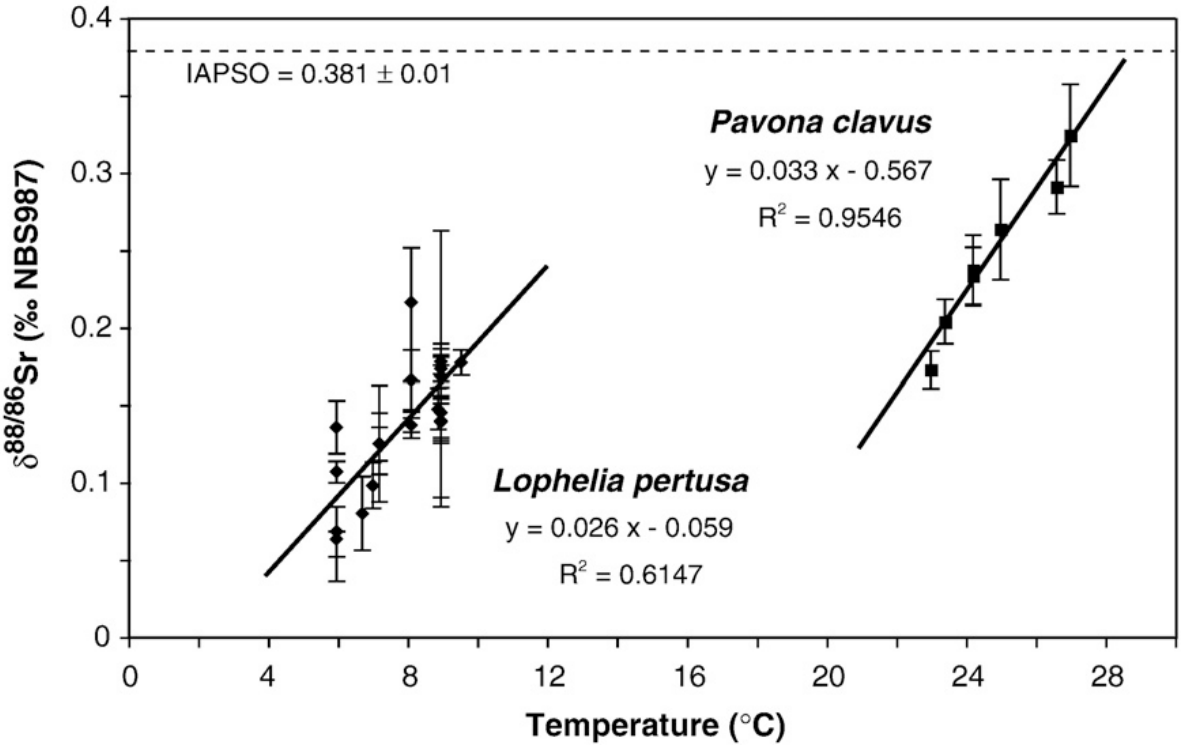

Figure 6: Temperature dependency of stable strontium isotope fractionation in scleractinian cold-water coral *L. pertusa* (Rüggeberg et al. 2008) and shallow warm-water coral *P. clavus (*Fietzke and Eisenhauer 2006) in comparison to IAPSO seawater standard (adapted from Rüggeberg et al., 2008).

In summary several proxy calibrations and several geochemical signals have been developed and established in scleractinian cold-water corals to identify past ocean conditions, see Table 1.

Table 1: Proxies and several other geochemical signals used in scleractinan cold-water corals *(e.g L. pertusa* and *Desmophyllum dianthus)*

Proxy/ Parameter	Sr/Ca	Mg/Li	U/Ca	Mg/Ca	Ba/Ca	P/Ca	$\delta^{18}O$/ $\delta^{13}C$	$\delta^{88/86}Sr$	$\delta^{14}C$	U/Th	ε_{Nd}
Temperature	x	x					x	x			
Salinity							x				
CO_3^{2-}			x								
Nutrients					x	x					
Age									x	x	
Circulation/ Water masses									x		x
Vitally effected	x			x			x				
References	e.g Cohen et al. (2006)	Case et al. (2010)	Anagnostou et al. (2010)	e.g. Sinclair et al. (2005)	Anagnostou et al. (2011)	e.g. Montagna et al. (2008)	e.g Smith et al. (2000)	Rüggeberg et al. (2008)	e.g Adkins et al. (1998)	e.g Cheng et al. (2000)	e.g Van de Flierdt et al. (2010)

Still, our knowledge about cold-water coral basic processes lag behind that of warm-water corals, but we know that cold-water corals record a detailed history of past seawater conditions. Therefore, they are good archives for paleoceanographic reconstructions and provide new and independent constraints in ocean sciences especially for intermediate water dynamics. Finally, a better understanding of past waxing and waning of coral reefs will then in turn improve our ability for future predictions such as ocean warming and acidification.

Chapter II

Paleoenvironmental reconstruction of Challenger mound initiation in the Porcupine Seabight, NE Atlantic

Based on*: Paleoenvironmental reconstruction of Challenger mound initiation in the Porcupine Seabight, NE Atlantic*. Jacek Raddatz, Andres Rüggeberg, Stephan Margreth, Wolf -Christian Dullo and the IODP Expedition 307, 2011. Paleoenvironmental reconstruction of Challenger Mound initiation in the Porcupine Seabight, NE Atlantic. Marine Geology 282, 79-90. doi;10.1016/j.margeo.2010.10.019

Abstract

The understanding of the paleoenvironment during initiation and early development of deep cold-water coral carbonate mounds in the NE Atlantic is currently focus of international research. The Integrated Ocean Drilling Program (IODP) Expedition 307 drilled the 155 m high Challenger Mound in the Porcupine Seabight (SW off Ireland) in order to investigate for the first time sediments from the base of a giant carbonate mound. In this study we focus in high resolution on 12 meters of sediments from Site 1317 encompassing the mound base. The mound initiation and start-up phase coincides with the intensification of the Northern Hemisphere Glaciation (INHG) at around 2.7 Ma. Further carbonate mound development seems to be strongly dependent on rapid changes in paleoceanographic and climatic conditions at the Pliocene-Pleistocene boundary, especially characterized and caused by the interaction of intermediate water masses, the Mediterranean Outflow Water (MOW), the Eastern North Atlantic Water (ENAW) and the influence of Southern Component Water (SCW).

This study is based on well-established proxies such as $\delta^{18}O$ and $\delta^{13}C$ of planktonic (*Globigerina bulloides)* and benthic foraminifera (*Fontbotia wuellerstorfi*, *Discanomalina coronata*, *Lobatula lobatula, Lobatula antarctica, and Planulina ariminensis*) as well as grain size parameters to identify the paleoenvironmental and paleoecological setting favourable for the initial coral colonization on the mound. Stable oxygen and carbon isotope records of benthic foraminiferal species indicate that *L. lobatula* provides a reliable isotopic signature for paleoenvironmental reconstructions. In particular, $\delta^{18}O$ values of *L. lobatula* indicate initial mound growth started in a glacial mode with moderate excursions in $\delta^{18}O$ values.

Carbon isotope values of *D. coronata* are significantly offset compared to other epibenthic species. This offset may be related to vital effects. Bottom water temperatures, calculated using standard equations based on $\delta^{18}O$ of foraminiferal tests, range between 7 and 11°C, consistent with the known temperature range conducive for cold-water coral growth and development.

Bottom currents transporting intermediate water masses of southern origin (Mediterranean, Bay of Biscay) enhanced at 2.6 Ma supporting first coral settlements with the INHG. The benthic $\delta^{13}C$ and the sortable silt records indicate that the early Pleistocene hydrodynamic regime was characterized by weaker current intensities associated with vertical movements of MOW or its replacement by SCW at intermediate depth. After these sluggish phases enhanced MOW flow dominated again and led to stronger current intensities and most probably sediment erosion on Challenger Mound. Erosion in combination with early diagenetic (oxidation) processes overprinted the sediment layers as indicated by dissolved coral skeletons, the increase in Ca-content and sediment density, minimum $\delta^{13}C_{planktonic}$ values, as well as the occurrence of gypsum and pyrite, implying a careful evaluation of original and overprinted geochemical signals. We conclude that the Challenger Mound development was already influenced by short-term variability of water masses from southern origin and possible erosional events comparable to the late Pleistocene setting.

2.1 Introduction

The European continental margin is colonized by cold-water coral reefs. Large deep-water carbonate mounds formed by the interaction between reef-building cold-water corals and sedimentary processes are only found on the margins from Ireland to the Gulf of Cadiz (Roberts et al. 2006; Wheeler et al. 2007). Azooxanthellate reef-building corals are mainly *Lophelia pertusa* and to a minor degree *Madrepora oculata* (Freiwald 2002; Wienberg et al. 2008). Cold-water coral reefs are carbonate factories (Dorschel et al. 2007a; Titschack et al. 2009) occurring in water depths between 500 and 1000 m (Foubert et al. 2005; Wheeler et al. 2007) and reaching heights of up to 350 m and can be several kilometres in diameter.

In general, cold-water corals tolerate a wide range of environmental factors such as temperatures of 4–12°C (Freiwald 2002) and salinity values of 32–36 psu in the North Atlantic. In the Mediterranean Sea they thrive in waters with temperatures up to 14°C and salinities up to 38.8 psu (Freiwald et al. 2009). Furthermore, cold-water corals tolerate values of dissolved oxygen ranging from 3.75–6.65 ml/l and grow in a large range of water depths

(Dullo et al. 2008). The shallowest living colonies are found in 40 m water depth in the Trondheimsfjord, Norway (Fosså et al. 2005), while the deepest colonies are reported from 3273 m on the New England Seamount Chain in the northwest Atlantic (Freiwald et al. 2004). A controlling parameter for living cold-water coral reef distribution is the density of seawater. Dullo et al. (2008) demonstrated a relationship between the distribution of cold-water coral reefs and the hydrography on the Celtic and Norwegian Margin. Living reef ecosystems of cold-water corals in the Northeast Atlantic seem to occur within a density range of sigma-theta (σ_Θ) = 27.35 to 27.65 kg m^{-3}. However, cold-water corals in the Mediterranean Sea seem to tolerate a different seawater density value of 29.1 kg m^{-3} (Freiwald et al. 2009).

Many studies have investigated the carbonate mounds in the North Atlantic during the last decade (De Mol et al. 2002, 2007; Dorschel et al. 2005, 2007a; Eisele et al. 2008; Hovland et al. 1994; Huvenne et al. 2005, 2007; Mienis et al. 2006, 2007, 2009; Rüggeberg et al. 2005, 2007; van Weering et al. 2003; Wienberg et al. 2008; Wheeler et al. 2005a, 2005b, 2007), but the initiation and start-up phase of these structures have been only recently studied (Sakai et al. 2009; Huvenne et al. 2009; Titschack et al. 2009; Kano et al. 2007; Foubert and Henriet 2009; Louwye et al. 2007).

It is presently known that cold-water coral mound growth is initiated by the correct interplay of all necessary environmental condition and that mound growth occurred in cycles along the European continental margin. Previous works (e.g., Roberts et al. 2006; Rüggeberg et al. 2007) showed that mound development generally occurred during interglacials, whereas mounds are inactive during glacial times. During warmer periods (interglacial) stronger currents supply more nutrients making cold-water coral growth favourable. During glacial times weak currents, decreased nutrient supply and enhanced sedimentation rates do not support coral growth (Rüggeberg et al. 2005, 2007; Dorschel et al. 2005, 2007a; Roberts et al. 2006). However, the most-recent models are based on short gravity cores from the Porcupine Seabight (PSB), and hence span only the last interglacial/glacial cycles. The studies of Kano et al. (2007), Titschack et al. (2009) and Foubert and Henriet (2009) unveiled for the first time the full duration of a cyclic mound build-up at the Challenger Mound.

This study focuses on the stable isotopic signature ($\delta^{18}O$ and $\delta^{13}C$) of planktonic (*Globigerina bulloides)* and benthic foraminifera (*Fontobtia wuellerstorfi*, *Discanomalina coronata*, *Lobatula lobatula, Lobatula antarctica* and *Planulina ariminensis*), and sediment grain size data (mean sortable silt) of sediments from IODP Exp. 307 Site U1317C. Our aim is to quantitatively reconstruct at a high-resolution the paleoenvironmental and paleoecological setting favourable for initial coral settling and development on the Challenger Mound.

2.1.1 Regional setting and hydrography

The Porcupine Seabight is an amphitheatre-shaped embayment. It is about 150 km long, 65 km wide and located southwest of Ireland in the North Atlantic (Fig. 1). To the southwest the Porcupine Seabight passes into the Porcupine Abyssal Plain at a depth of 3000 m, while it is limited by the Slyne Ridge in the north at a depth of 250 m. More than 1600 carbonate mounds possibly occur in the region (Foubert et al. 2005).

Five main mound provinces are present in the Porcupine Seabight (Fig. 1): (1) the Magellan Mound Province in the north, (2) the Hovland Mound Province further south, (3) the recently discovered Viking Mound Province southeast of the Hovland Mound Province, (4) the Belgica Mound Province including the Challenger Mound at its eastern margin, and (5) the Enya Mound Province (5) south to southeast of the Belgica Mound Province (Hovland et al. 1994; De Mol et al. 2002; De Cock 2005; Van Rooij et al. 2007). The Belgica Mound Province is about 45 km long. Here De Mol et al. (2002) described 66 conical mounds, occurring in water depths of 550 to 1025 m.

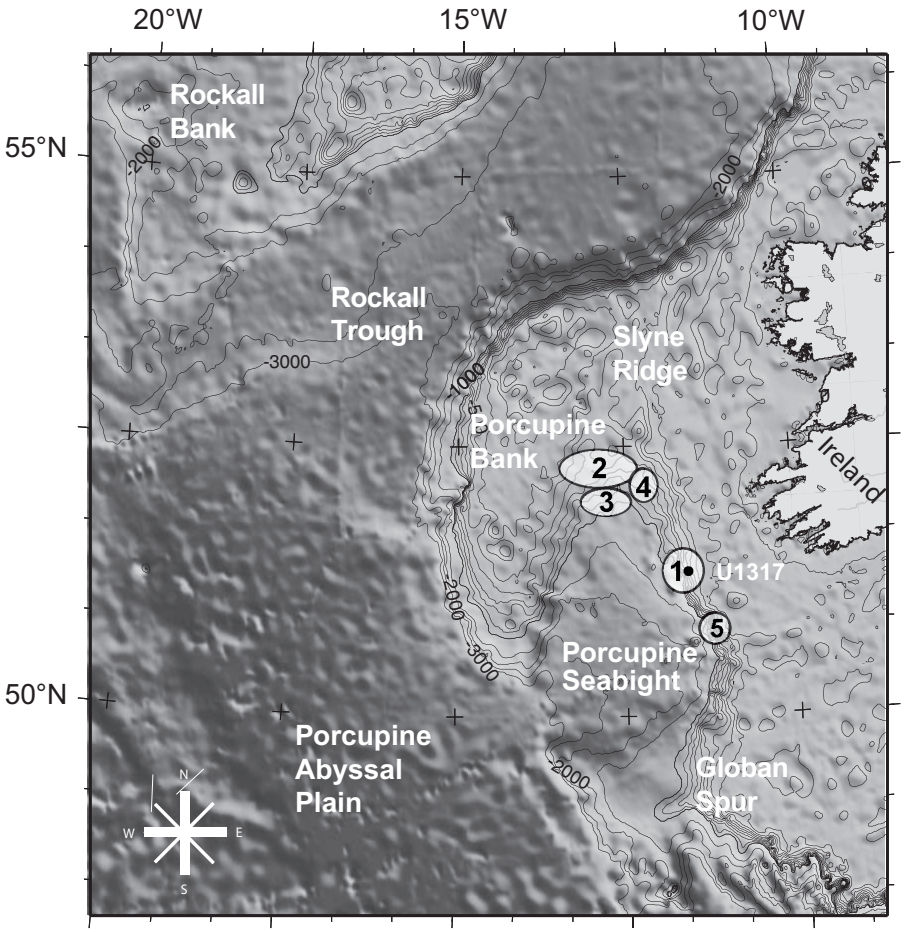

Figure 1: Map showing the bathymetry of the North-East Atlantic with the Irish and Celtic Margin. The studied sediment drill core (Site U1317 C) is indicated within the Belgica Mound Province (1). Other mound provinces are the Magellan (2), the Hovland (3), the Viking (4), and the Enya Mound Province (5). Datasets for the map are based on the ETOPO5 digital elevation file (http://www.ngdc.noaa.gov/).

A detail review of the present-day oceanographic setting of the Porcupine Seabight in relation to the carbonate mounds is given by White et al. (2005). A general northward along-slope current system originates at the Iberian Margin and flows along the East-Atlantic margin into the Norwegian Sea. The most important water masses at intermediate depths are the Eastern North Atlantic Water (ENAW) and the Mediterranean Outflow Water (MOW). The Eastern North Atlantic Water reaches a water depth down to 800 m and is underlain by the MOW. At 950 m water depth the MOW is characterized by an oxygen minimum and a salinity maximum (Pollard et al., 1996). The Labrador Sea Water and the Norwegian Sea Deep Water are reported to occur at greater depths below the MOW (Rice et al. 1991). In the Belgica Mound Province the strong hydrodynamic regime is combined with the presence of internal

waves and tides at the boundary between ENAW and MOW, hence underlining the unique setting of the Belgica Mound Province (Rice et al. 1991; De Mol et al. 2002).

The Challenger Mound, located on the eastern margin of the Porcupine Seabight, is a 155 m high carbonate mound covered with dead cold-water coral fragments (Foubert et al. 2007). It was drilled during IODP Expedition 307 at Site U1317 (Fig. 1, 51°22.8' N, 11°43.1' W; 781–815 m water depth) (Williams et al. 2006). The up to 155 m long coral-bearing sedimentary successions have great potential to shed light on the processes triggering the colonization of cold-water corals on the mounds and the driving mechanisms of mound growth itself. A thick sedimentary cover is documented on the upslope flank of the mound, while a thinner one occurs on the downslope flank. The Challenger Mound is characterized by different growth phases and an erosional boundary overlying glauconitic and silty sandstone drift deposits at the mound base (Kano et al. 2007; Expedition Scientists 2005; Foubert and Henriet 2009). Sediments below the base of the Challenger Mound are of middle Miocene age (14.78-15.16 Ma; Louwye et al. 2007), whereas the mound base is about 2.6 Ma old (Kano et al. 2007; Foubert and Henriet 2009). A second major hiatus identified at 1.7 Ma suggests that during this time the mound was not active. The overlaying sediments are dated at 1 Ma and indicate a possible re-activation of the mound (Kano et al. 2007; Foubert and Henriet 2009).

2.2 Material and methods

This study is based on sediments from Hole U1317C recovered during IODP Expedition 307 with R/V JOIDES RESOLUTION in 2005 (Expedition 307 Scientists, 2006). In order to obtain undamaged half cores, they were frozen before splitting (Dorschel et al. 2005; Foubert et al. 2007).

At 147.95 mbsf (= metres below seafloor) sediments from core U1317C are characterized by an unconformity, marked by a sharp colour change from the grey, coral bearing sediments to the greenish-grey underlying unit. Samples were taken every 10 cm in the interval between 141 and 151 mbsf just above and below the mound base using 10 cm^3 syringes. All samples were dried at 50°C, weighed and then wet sieved through a 63-µm sieve. The suspended fine fraction (< 63 µm) was collected in 3-litre jars for fine fraction analysis. The coarse fraction was again oven dried, weighed and dry sieved at 125 µm and 250 µm to obtain the correspondent size fraction.

2.2.1 Grain size analyses

Grain-size distribution of the fine fraction (<63 μm) was determined from the collected fine fraction with a Micromeritic Sedigraph 5100. This device measures the concentration of sediment in suspension by the attenuation of a X-Ray beam. Water in the samples was replaced by a sodium polyphosphate solution (0.05 %) to avoid flocculation of particles. After homogenisation on a rotating carousel (at least 12 hours), the samples were placed in the ultra-sounds for 10 seconds. Afterwards they were analysed with a density setting of calcite (2.71 g cm^{-3}) at a constant water temperature of 35°C and with an analysis range from 1 to 63 μm. Cumulative and mass frequency data output was used to calculate mean silt (0–63 μm) and mean sortable silt (10–63 μm) distributions, along with size frequency distributions. Finally raw data were converted into weight percentages (wt.-%).

2.2.2 Stable isotopes analyses

Stable oxygen and carbon isotope analyses ($\delta^{18}O$ and $\delta^{13}C$) were carried out on well-preserved and clean foraminifera specimens. The benthic species *F. wuellerstorfi* (3 specimens), *P. ariminensis* (5), *L. antarctica* (3), *L. lobatula* (5), *and D. coronata* (3), were picked from the size fraction larger than 250 μm and the planktonic species *Globigerina bulloides* (15) was picked from the >125 μm size fraction (Plate 1). Oxygen and carbon isotopes were measured with a Finnigan 252 mass spectrometer with a Kiel CARBO device at IFM-GEOMAR in Kiel for the species *L. lobatula* and *G. bulloides* and due to technical problems also at the Isotope Laboratory of the Institute of Geology and Mineralogy at the University of Erlangen for the species *F. wuellerstorfi, D. coronata, L. antartica and P. ariminensis*. Approximately 0.1 mg of $CaCO_3$ was measured for each sample. Reproducibility was ±0.045 ‰ for $\delta^{18}O$ and ±0.012 ‰ for $\delta^{13}C$. Isotopes ratios are presented relative to the PeeDee Belemnite (PDB) standard based on calibration with National Bureau of Standards (NBS).

Bottom-water temperatures were calculated using the equation of Shackleton (1974) for benthic foraminifera: $T\ (°C) = 16.9 - 4.38\ (\delta^{18}O_c - \delta^{18}O_w) + 0.10 * (\delta^{18}O_c - \delta^{18}O_w)^2$ using a $\delta^{18}O_w$ of 0 ‰ for the Early Pleistocene/Late Pliocene and -0.25 ‰ for the Miocene (Zachos et al. 2001).

Sea Surface Temperature (SST) was calculated using the $\delta^{18}O_c$ values of the planktonic species *G. bulloides.* The equation of Erez and Luz (1983) was applied using a $\delta^{18}O_w$ of 0 ‰ for the Early Pleistocene/Late Pliocene and -0.25 ‰ for the Miocene (Zachos et al. 2001) as

follows: T (°C) = 16.998 - 4.52 ($\delta^{18}O_c$ - $\delta^{18}O_w$)+ 0.028 ($\delta^{18}O_c$ - $\delta^{18}O_w$)^2.

2.3 Results

2.3.1 Stable oxygen and carbon isotopes in foraminifera

Variations in the oxygen and carbon isotope records of benthic foraminifera are shown in figures 2 and 3. Oxygen isotope values of benthic foraminifera have a similar mean value of ~2 ‰ for all species. High frequency variations characterize the patterns at small scale. *Fontbotia wuellerstorfi* displays a variability of ~0.8 ‰ in the investigated interval above the mound base <149 mbsf. Oxygen isotope values of the other species vary by ~0.8 ‰ (*L. antartica*), ~1 ‰ (*L. lobatula*), ~1.3 ‰ (*D. coronata*), and ~1.1 ‰ (*P. ariminensis*). Downcore the $\delta^{13}C$ values have a different pattern with respect to $\delta^{18}O$.

The mean $\delta^{13}C$ values are ~0.25 ‰ for *F. wuellerstorfi*, ~0.6 ‰ for *D. coronata* and *P. ariminensis*, ~0.1 ‰ for *L. antartica*, and ~0.15 ‰ for *L. lobatula*. The variability of $\delta^{13}C$ values is much larger than for the $\delta^{18}O$. Carbon isotope values of *F. wuellerstorfi* vary by ~1.8 ‰ and are comparable to *P. ariminensis. L. antartica and L. lobatula* show slightly higher variability of ~2 ‰ and ~2.2 ‰, respectively. Overall, $\delta^{13}C$ variations of *D. coronata of* ~2.5 ‰ are the highest of all the species investigated.

Oxygen and carbon isotope ratios of *G. bulloides* change rapidly at ~148 mbsf (Figs. 2–4) with an $\delta^{18}O$ increase by 2.5 ‰ and a $\delta^{13}C$ decrease by about 2 ‰. Similar $\delta^{18}O$ values of *L. lobatula* increase by about 2 ‰, and the $\delta^{13}C$ values decrease by 1 ‰ (Figs. 2–4).

Temperature reconstructions were performed following Shackleton (1974) for the benthic and Erez and Luz (1983) for the planktonic species. Both records display a distinct shift at the mound base at ~ 148 mbsf. Temperature estimates decrease from 21° to 10° for the sea surface and from 17° to 9°C for the deep waters between the Mid Miocene and the mound initiation in the Pliocene (Fig. 4). Over the whole record Sea-Surface-Temperature (SST) values estimated from *G. bulloides* display a higher variability than Bottom-Water-Temperature (BWT) estimates (3–4°C). The same pattern is visible in the $\delta^{13}C$ records, where the variability of planktonic $\delta^{13}C$ values is about 2 ‰ larger than the benthic.

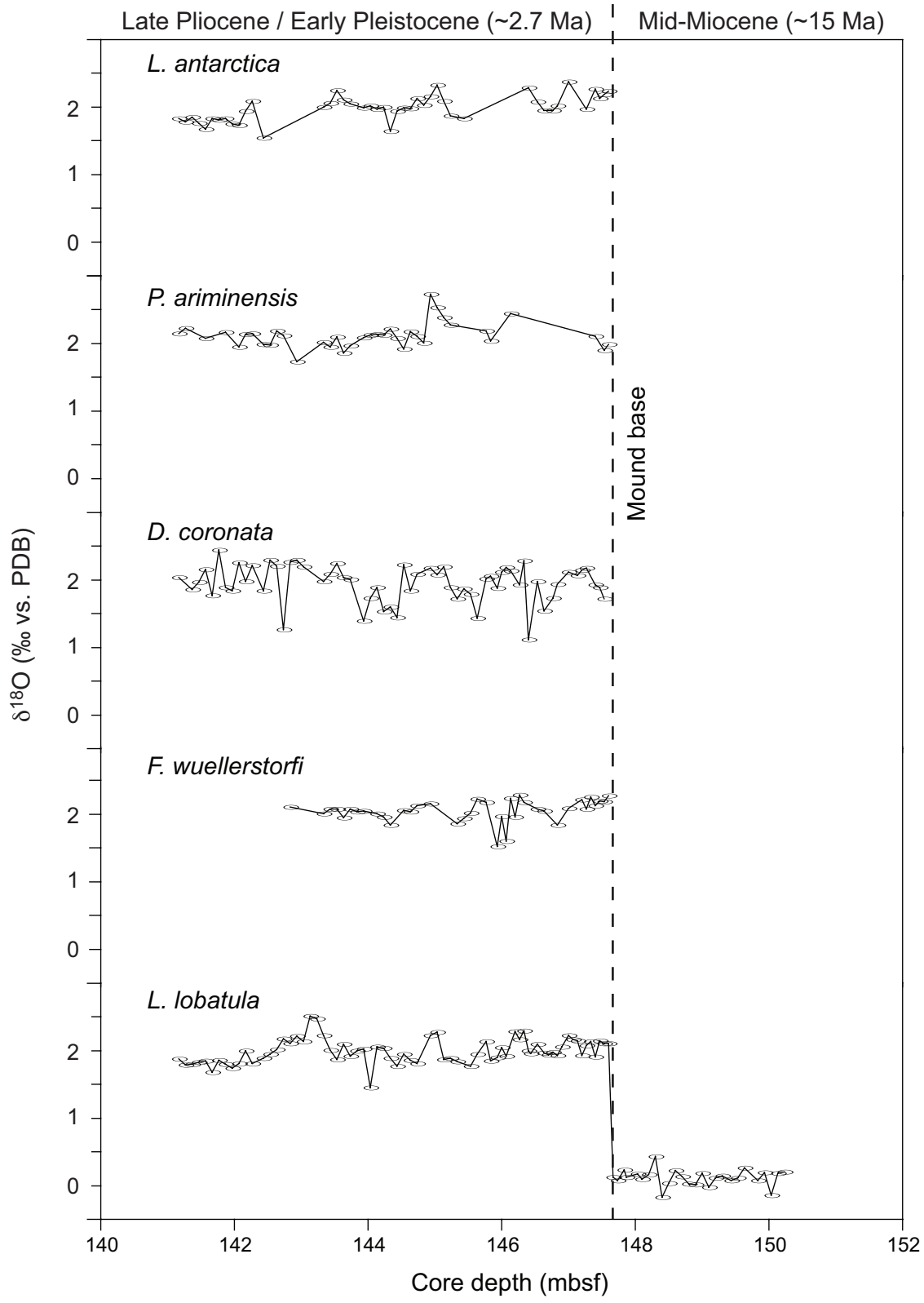

Figure 2: $\delta^{18}O$ values (in ‰ vs. PDB) of benthic foraminifera *Lobatula lobatula*, *Fontbotia wuellerstorfi*, *Discanomalina coronata*, *Planulina ariminensis*, and *Lobatula antartica*.

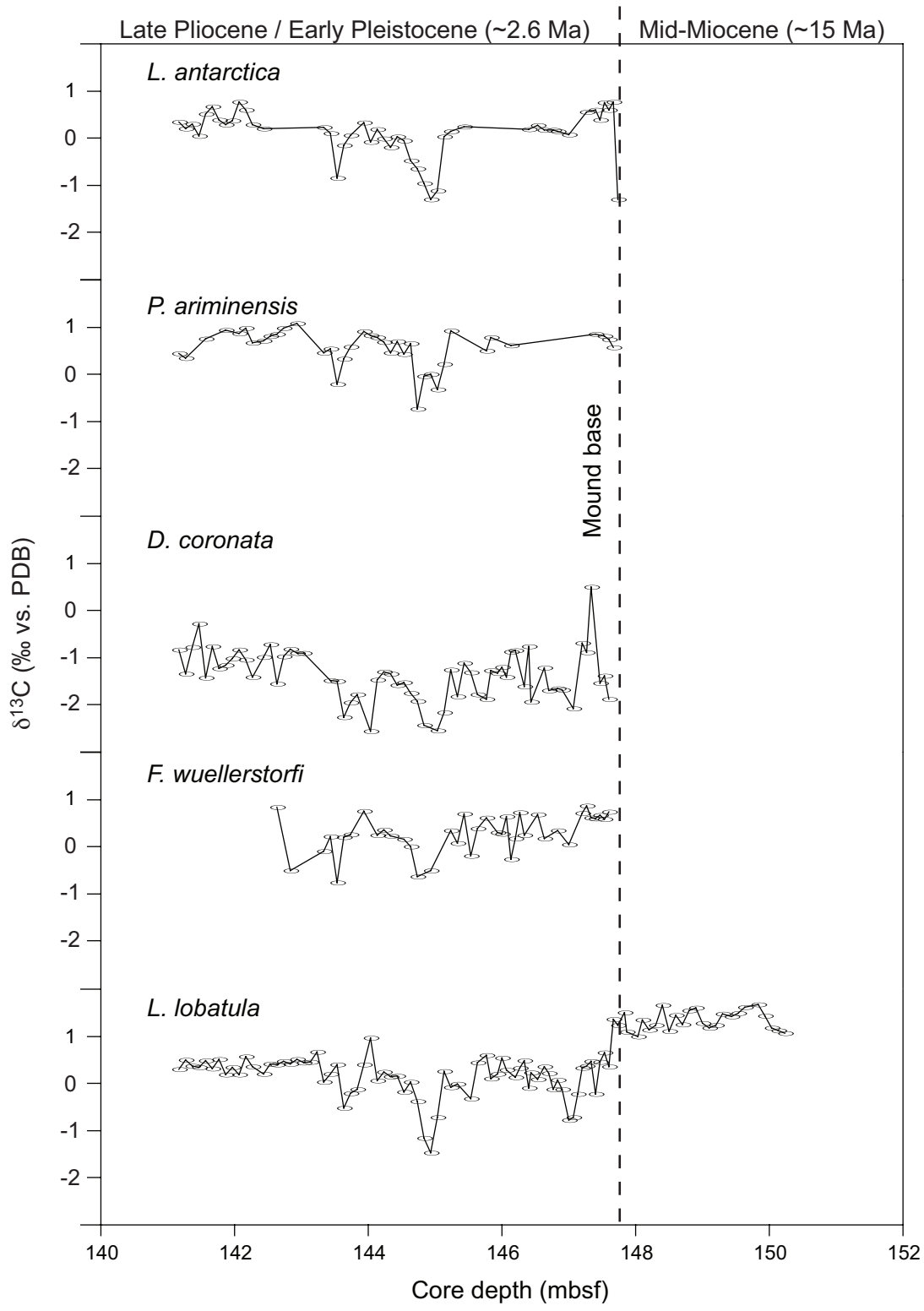

Figure 3: $\delta^{13}C$ values (in ‰ vs. PDB) of benthic foraminifera *Lobatula lobatula*, *Fontbotia wuellerstorfi*, *Discanomalina coronata*, *Planulina ariminensis*, and *Lobatula antartica*.

2.3.2 Grain Sizes Analyses

The sortable silt fraction of carbonate free sediment is sensitive to hydrodynamic processes and can be used to estimate variations in paleo-current intensities (McCave et al. 1995). In core U1317C, mean sortable silt is characterized by two different patterns: (1) values in the upper interval (~141 to ~148 mbsf depth) vary from about 21 to 27 μm, whereas (2) values in the lower interval (~148 to ~151 mbsf) only vary from 18 to 22 μm (Fig. 4). The calculated means for each interval are 23.66 (±2.76) μm for the upper part and 19.74 (±1.90) μm for the lower part.

2.4 Discussion

2.4.1 Species Reliability

Stable isotope measurements on foraminifera are an important tool in paleoceanographic studies and are routinely used for paleoenvironmental reconstructions. In general oxygen isotope ratio of foraminiferal calcite reflects the $\delta^{18}O$ value of seawater ($\delta^{18}O_w$), which varies with the global ice volume as a function of seawater salinity (Lynch-Stieglitz et al. 1999). Additionally, the foraminiferal calcite exhibits $\delta^{18}O$ fractionation dependent on temperature and therefore $\delta^{18}O$ is used as a proxy for temperature.

The $\delta^{13}C$ value of foraminiferal calcite tests is primarily a function of the $\delta^{13}C$ value of dissolved inorganic carbon (DIC) in the seawater (Emiliani 1955; O'Neil et al. 1969; McClorke et al. 1990) and has been used in studies as a proxy for productivity and to trace water masses. Further factors influencing the $\delta^{13}C$ are interspecies offsets (Duplessy et al. 1970; Shackleton, 1974) attributed to the microhabitat preferences of benthic foraminifera (deep infaunal, epifaunal, elevated substrates or even fauna-attached; Mackensen et al. 2000; McCorkle et al. 1990), vital effects (species-specific metabolic variation), and any potential diagenetic overprint. Hence, prior to any interpretation of paleoceanographic relevance we compare isotopic data of multiple species for their reliability of isotopic information.

Not all of the benthic foraminiferal species studied here occur continuously in middle Miocene sediments (below the mound base). Only *L. lobatula* is abundant throughout the entire analysed section, while *D. coronata*, *L. antarctica*, *F. wuellerstorfi*, *P. ariminensis* occur from 148 mbsf upward. Lutze and Thiel (1987) have shown that *F. wuellerstorfi* only colonize elevated epibenthic microhabitats up to 14 cm above the seafloor. Hence the $\delta^{13}C$ signal of this species can be used as a recorder of the ambient bottom water properties (Graham 1981; McCorkle et al. 1990; Zahn et al. 1997).

Although measured at different laboratories, the oxygen and carbon isotope values of the benthic foraminifera *F. wuellerstorfi*, *L. antarctica*, *P. ariminensis* and *L. lobatula* are similar and therefore useful for deep-water paleoceanographic reconstructions at this location. Where present, all the investigated species display stable oxygen and carbon isotope values that are consistent with those of *F. wuellerstorfi*, indicating that they respond to similar environmental conditions and are influenced by similar bottom waters. Only $\delta^{13}C$ values of *D. coronata* are significantly offset from other species by around -2 ‰. This species is generally associated with cold-water coral ecosystems (Margreth et al. 2009) and lives attached on elevated substrate like a dead coral framework. The $\delta^{13}C$ offset of *D. coronata* with respect to the other species most likely results from a strong vital effect, also known for some other benthic species (Wilson-Finelly et al. 1998). These species have a strong metabolic effect causing low $\delta^{13}C$ values, whereas kinetic effects result in even more depleted $\delta^{13}C$ values (Mackensen and Bickert 1999). As *G. bulloides* and *L. lobatula* provide a continuous downcore record across the base of Challenger Mound, we only use their $\delta^{18}O$ and $\delta^{13}C$ records for downcore paleoenvironmental interpretation.

Plate 1

List of genera and species used in this study. The families are listed in taxonomic order following Loeblich and Tappan (1988), genera and species are listed in alphabetical order.

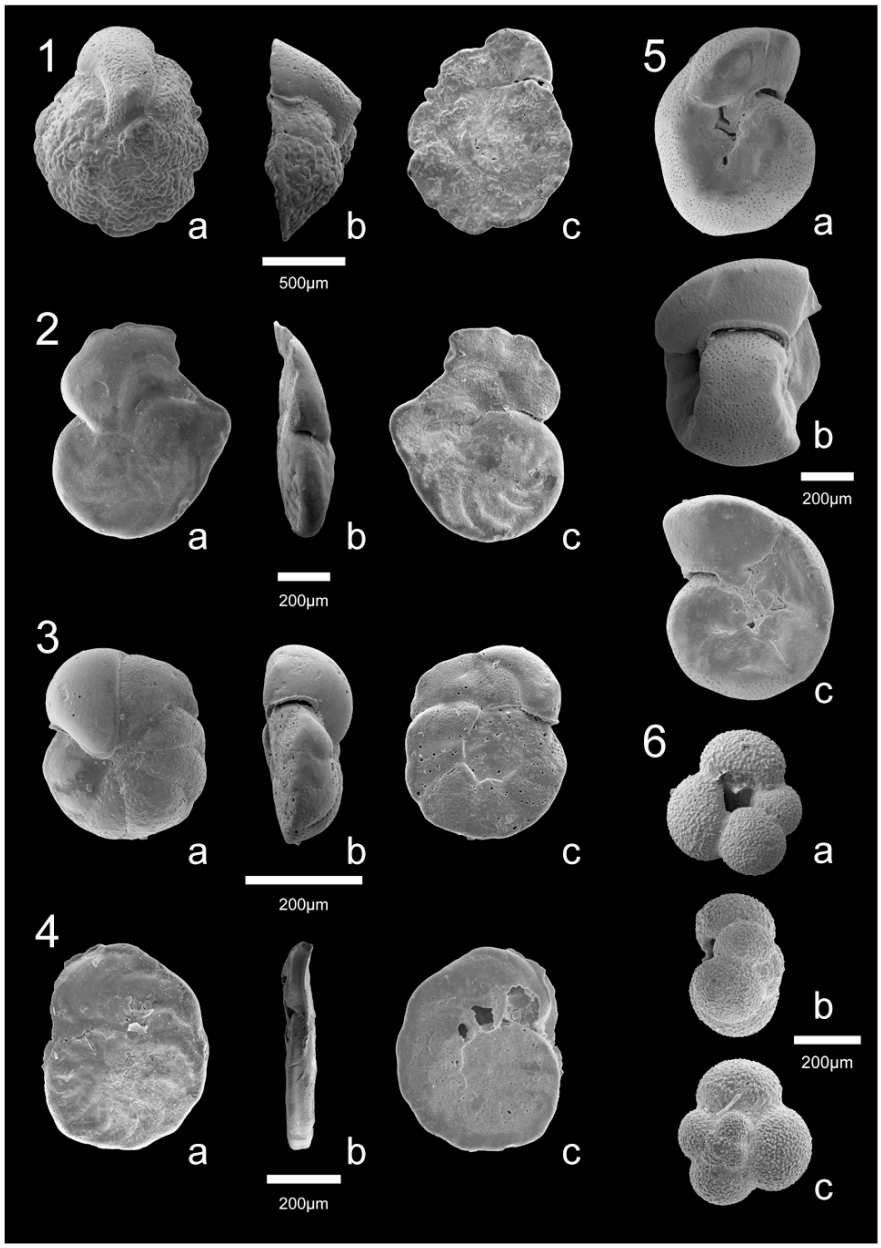

1 a–c *Lobatula antarctica* (Saidova, 1975), sample 1317 C, 17-1, 54–55 cm.

2 a–c *Fontbotia wuellerstorfi* (Schwager, 1866), sample 1317c C, 17-1, 44–45 cm,

3 a–c *Lobatula lobatula* (Walker and Jacob, 1798), sample 1317 C, 17-4, 90–91 cm,

4 a–c *Planulina ariminensis* (d'Orbigny, 1826), sample 1317 C, 17-3, 27–28 cm.

5 a–c *Discanomalina coronata* (Parker and Jones, 1857), sample 1317 C, 17-4, 90–91 cm.

6 a–c *Globigerina bulloides* (d'Orbigny, 1826), sample 1317 C, 17-1, 24–25 cm.

a = umbilical views, b = side views, c = spiral views

2.4.2 Paleoenvironmental conditions during initiation and early development of Challenger Mound

Carbonate mound growth on the European margin is generally controlled by environmental conditions. In particular the first settlement of cold-water coral larvae is thought to result from the introduction of the MOW into the PSB (De Mol et al. 2002; Freiwald 2002). Development of a single mound occurs from localised coral larvae settlements, supporting the build-up of a giant carbonate mound (Huvenne et al. 2009). Further development is driven by environmental changes following glacial-interglacial cycles (Rüggeberg et al. 2007). Initial growth of the Challenger Mound occurred at the beginning of the Northern Hemisphere Glaciation at ~ 2.6 Ma (Kano et al., 2007) and mound growth within the entire PSB probably occurred at the same time (De Mol et al., 2002).

Our study provides insight into the paleoenvironmental setting during the start-up phase and initiation of Challenger Mound. In the following discussion we concentrate on the setting of the middle Miocene recorded in the sediments below the mound base around 15 Ma, the mound initiation at ~2.6 Ma and first episode of mound growth at the mound base after a hiatus of ~12 Myr, and on the climatic and oceanographic variability indicating variations in early mound development in comparison to present-day settings.

2.4.2.1 Below the mound base

The period of the middle Miocene between 14 and 17 Ma was the warmest of the Neogene and is known as the Miocene Climatic Optimum (MCO) (Zachos et al. 2001). Several studies of the middle Miocene indicate warm SST ranging between 15° and 21°C at a latitude of around 50°N (e.g., Shevenell et al. 2004; Pagani et al. 1999; Nikolaev et al. 1998; Savin et al. 1977). Our middle Miocene SST data from IODP Site U1317C based on *G. bulloides* are consistent with the reported SST's varying between 16 and 22°C (Fig. 4).

The reconstructed BWT of ~15°C also indicate a very warm intermediate water mass for the MCO at ca. 800 m water depth. Such warm BWT or light benthic stable oxygen isotope values are also reported from the low latitude Atlantic during the latest early Miocene (15-17 Ma; Nikolaev et al. 1998) and from deeper sites in the central North Atlantic (Wright et al. 1992; Pagani et al. 1999). During this time a weak circulation pattern occurred in the North Atlantic caused by a reduction of the Northern Component Water formation (Miller and Fairbanks 1983; Zachos et al. 2001), while warm and saline intermediate waters of southern origin prevailed (Wright et al. 1992; Flower and Kennett, 1994). Relatively high planktonic

and benthic foraminiferal $\delta^{13}C$ values between 1 and 2 ‰ support the origin of this warm and saline, possibly Tethyan intermediate water mass (Fig. 4).

High $\delta^{13}C$ values during the early to middle Miocene are also considered to be the result of large-scale changes in organic carbon deposition relative to carbonate sedimentation, the so-called "Monterrey Carbon Excursion" (Vincent and Killingley 1985). Intervals of high organic carbon accumulation in marginal basin sediments are marked by distinct $\delta^{13}C$ maxima in the benthic record between 17 and 15 Ma with values of 1.5–2 ‰ (Flower and Kennett 1994; Wright et al. 1992). Remarkable high planktonic and benthic $\delta^{13}C$ signals may reflect this pivotal point in Cenozoic climatic evolution at Hole U1317C (Fig. 4).

The reconstructed BWT of ~15°C also indicate a very warm intermediate water mass for the MCO at ca. 800 m water depth. Such warm BWT or light benthic stable oxygen isotope values are also reported from the low latitude Atlantic during the latest early Miocene (15-17 Ma; Nikolaev et al. 1998) and from deeper sites in the central North Atlantic (Wright et al. 1992; Pagani et al. 1999). During this time a weak circulation pattern occurred in the North Atlantic caused by a reduction of the Northern Component Water formation (Miller and Fairbanks 1983; Zachos et al. 2001), while warm and saline intermediate waters of southern origin prevailed (Wright et al. 1992; Flower and Kennett 1994). Relatively high planktonic and benthic foraminiferal $\delta^{13}C$ values between 1 and 2 ‰ support the origin of this warm and saline, possibly Tethyan intermediate water mass (Fig. 4).

High $\delta^{13}C$ values during the early to middle Miocene are also considered to be the result of large-scale changes in organic carbon deposition relative to carbonate sedimentation, the so-called "Monterrey Carbon Excursion" (Vincent and Killingley, 1985). Intervals of high organic carbon accumulation in marginal basin sediments are marked by distinct $\delta^{13}C$ maxima in the benthic record between 17 and 15 Ma with values of 1.5–2 ‰ (Flower and Kennett 1994; Wright et al. 1992). Remarkable high planktonic and benthic $\delta^{13}C$ signals may reflect this pivotal point in Cenozoic climatic evolution at Hole U1317C (Fig. 4).

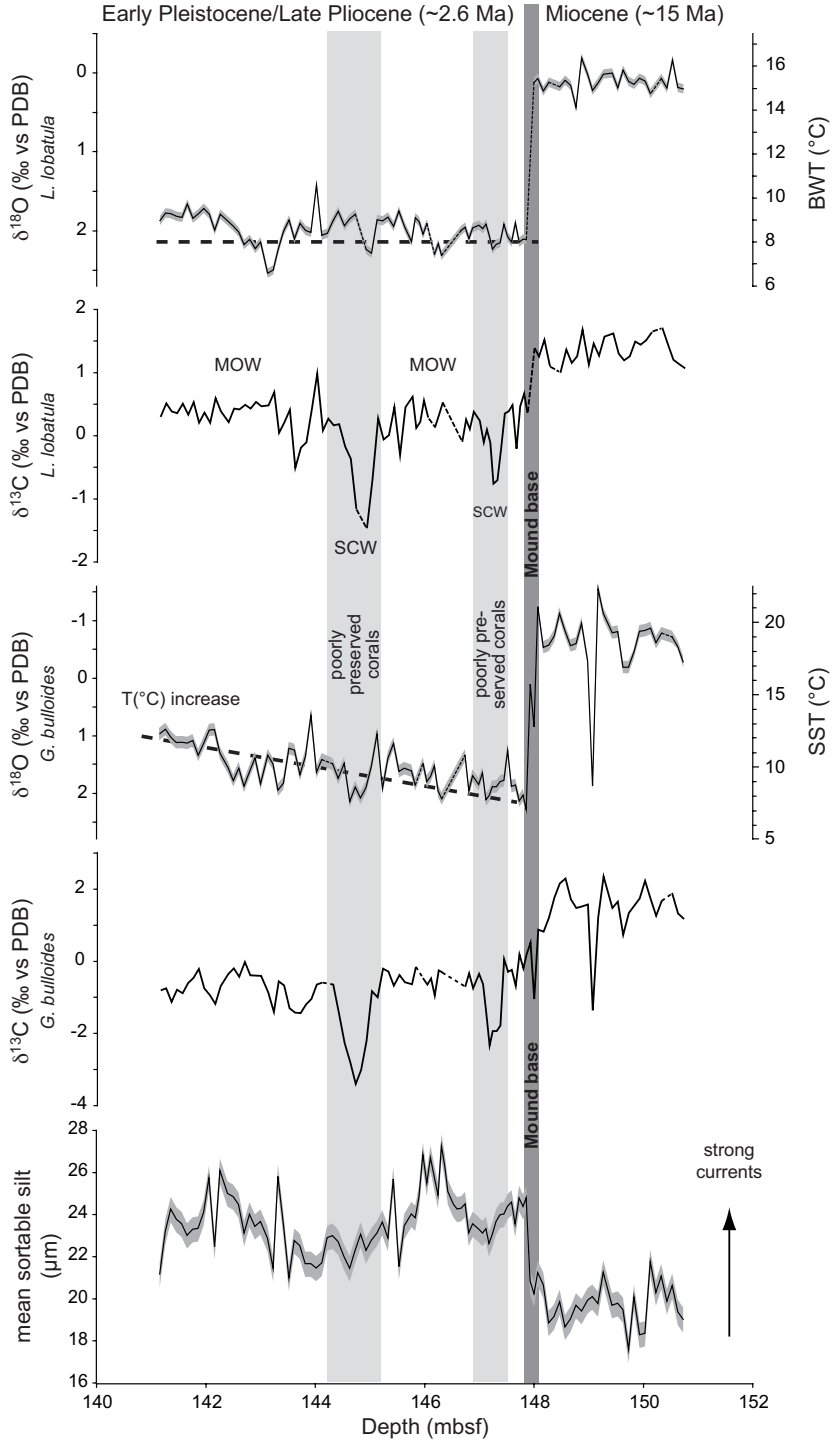

Figure 4: High-resolution records of IODP Site U1317 C, 141–151 m below seafloor (mbsf). Mean sortable silt (in µm), stable oxygen and carbon isotopes (in ‰ vs. PDB) from *Lobatula lobatula* and *Globigerina bulloides*. Stable oxygen isotope values were converted into Sea Surface Temperatures (SST in °C) and Bottom Water Temperatures (BWT in °C). Grey envelope indicates error of reconstructed temperatures. Dotted line between 141 and 148 mbsf at benthic $\delta^{18}O$ indicates mean Mediterranean Outflow Water (MOW) temperatures of ~8°C (from Khelifi et al. 2009). Light grey bars indicate sections of poorly preserved corals coherent with possible occurrence of Southern Component Water (SCW).

The MCO-following cooling phase is not documented in the cores of IODP Site 1317. Long hiatuses of more than 3 Myr were common in the late Miocene to Pliocene NE Atlantic and represent major erosional (and/or non depositional) events in low-productivity regions or paths of strong bottom currents (Keller and Barron, 1983; Pearson and Jenkins, 1986). According to these authors Neogene hiatuses (NH) occurred at 13.5 to 12.5 Ma (NH3), 12–11 Ma (NH4), 10–9 Ma (NH5), 7.5–6.2 Ma (NH6), and 5.2–4.7 Ma (NH7) documented in different DSDP cores along the European continental margin at water depths between 1600 and 4500 m. All these hiatuses at intermediate depth developed during cold periods and may therefore rather be attributed to changes in the hydrodynamic regime at intermediate waters as suggested by Louwye et al. (2007) than to low productivity.

This is comparable to dynamics described for the carbonate mound settings during glacial-interglacial cycles of the late Pleistocene (Dorschel et al., 2005; Rüggeberg et al. 2007; Van Rooij et al. 2007). The sum of hiatuses NH3–NH7 (13.5–4.7 Ma) give a reasonable explanation for the lack of sediments spanning ~12 Myr in core 1317C and the erosional unconformity, on which Challenger Mound started to develop at ~2.6 Ma (Kano et al., 2007).

2.4.2.2 Mound initiation and first episode of mound growth

The initiation of coral mound growth is indicated by the sharp increase in planktonic (benthic) $\delta^{18}O$ values of ~3 (2) ‰, 4 µm increase of mean sortable silt and $\delta^{13}C$ decrease of ~1.5–2 ‰, respectively (Fig. 4). Compared to $\delta^{18}O$ values of the same species from core 1317E (Sakai et al. 2009), our $\delta^{18}O$ values of *G. bulloides* are ~0.5 ‰ heavier. This offset cannot be simply explained by differences in the resolution of data. Sakai et al. (2009) defined the beginning of mound growth to Marine Isotope Stage (MIS) 92 at ~2.24 Ma, which is a cold or early glacial period. However, Kano et al. (2007), Foubert and Henriet (2009) and Huvenne et al. (2009) argue for an earlier onset of mound initiation in core 1317E. A diachronous growth of Challenger Mound is the best explanation for different initiation dates between the cores of Site U1317. Foubert and Henriet (2009) were able to show this diachronous mound growth using spectral analyses on geophysical and geochemical parameters. They demonstrated that the nucleation of Challenger Mound started before 2.58 Ma close to Hole U1317E and later at Hole U1317C (< 2.58 Ma), reflecting therefore not the entire mound history in the latter hole. Despite the different mound start-up phases in Holes U1317E and U1317C, the heavier planktonic oxygen isotope values of ~2 ‰ at site 1317C (Fig. 4) point to mound development

during an early Pleistocene glacial period. The $\Delta^{18}O$ between glacial and interglacial phases ~2.5 Ma ago is ca. 0.7–1.3 ‰ (Lisiecki and Raymo 2005). The small-scale variability in planktonic oxygen isotope data of core 1317C is in the same order of ~1 ‰ and the general trend form the mound initiation to the end of the record at 141 mbsf as well (Fig. 4, see 4.2.3). Taking a constant sedimentation rate of 15 cm kyr^{-1} (max. 24 cm kyr^{-1}) without any hiatus into account (Kano et al. 2007), the investigated section (141–148 mbsf) comprises only a part of a glacial-interglacial cycle with ~47 kyr (~30 kyr), respectively. Therefore, we assume that Challenger Mound initiation may have occurred in an early Pleistocene glacial phase, amplified by that fact that glacial periods were less extreme at that time than the more recent ones (Lisiecki and Raymo 2005). This is in contrast with Huvenne et al. (2009), which relate the mound initiation to warmer conditions reconstructed from the characterization of the sedimentation mode and bottom current intensities. However, their planktonic foraminiferal assemblages display no clear difference within the sedimentary facies between 141 and 148 mbsf. This is also expressed in the relatively small variability of BWT of mean 8.56 ± 0.73°C supporting small glacial-interglacial changes at that time and being still in the range of tolerated temperatures for the reef-building coral *L. pertusa* (Freiwald 2002).

Small variations in BWT are generally related to the interplay of different water masses or vertical movements of an intermediate water mass (see 4.2.3). During the initial glaciation of the northern hemisphere Mediterranean Outflow Water (MOW) dominated the oceanographic setting at intermediate water depths in the Porcupine Seabight (Khelifi et al. 2009). Accordingly, BWT from Site U1317C show a striking similarity to Mg/Ca-based BWT of *Cibicides mundulus* from DSDP Site 548 (South of the Porcupine Seabight, 1250 m water depth) from 3.4 and 3.1 Ma (Khelifi et al. 2009). At this site BWT values around 8°C indicate the influence of MOW in the North Atlantic.

It remains questionable why the build-up of Challenger Mound and possibly the other carbonate mounds in the Porcupine Seabight started several 100 ka after the intensification of MOW at 3.5–3.3 Ma (Khelifi et al. 2009), since MOW is assumed to be the main carrier of cold-water coral larvae from the Mediterranean Sea into the North Atlantic (De Mol et al. 2002). Probably vertical movements and a progressing shallowing of MOW after 3.3 Ma led to the initiation of coral development at the site of Challenger Mound. However, the inaccuracy of radiogenic Sr age determinations for that period should be kept in mind indicating a mound initiation between 2.329–3.614 Ma (Kano et al. 2007). Therefore the start-up of carbonate mound growth may be still linked to the introduction of MOW to the NE Atlantic.

2.4.2.3 Mound growth and short-term decline

The variability of stable isotope and grain size data indicate variations in the paleoenvironment during the early development of Challenger Mound. Bottom water temperatures remain relatively stable around 9°C while SST show an increase of ~3°C indicating a shift from an early glacial phase (~144–148 mbsf) to an interglacial period (~141–144 mbsf) with comparable values as reported by Hopper and Funnell (1986) from Hole 552A between 2.4–2.6 Ma (Fig. 4).

Paleocurrent reconstructions from sortable silt analyses present a distinct increase of 4 μm, respectively, indicating a stronger current regime in the early Pleistocene compared to the Mid-Miocene (Fig. 4). Small-scaled variations in current velocities describe the early mound development with phases of reduced currents around 147 mbsf and between 144 and 145 mbsf, and intensified currents at the mound base, around 146 mbsf and between 142 and 143 mbsf. Schönfeld and Zahn (2000) described a similar cyclic pattern with ~5 μm amplitude at the Portuguese margin and relate it to changes of current intensities and short-term vertical movements of MOW within one glacial-interglacial cycle. After the Messinian salinity crisis (5.9–5.2 Ma; Soria et al. 2008) MOW underwent major changes in response to the successive glacial and interglacial stages, when sea level dropped by 50–120 m below to present level. Enhanced currents at greater depth and weaker current strength at shallower water depth characterized MOW during glacial periods. During terminations, when sea level rose and glaciers shrank, a MOW more similar to the recent one was established at shallower depth (Zahn et al. 1997; Schönfeld and Zahn 2000). Such a dynamic behaviour of MOW was probably not only restricted to recent glacial/interglacial cycles, but was active, although less pronounced, in times of initial mound growth in the early Pleistocene.

Mean sortable silt values of 20 to 26 μm are comparable to modern and Holocene values of Propeller Mound (Hovland Mound Province; Rüggeberg et al. 2005), where residual currents of mean 2–5 cm s^{-1} occur (White 2007). However, modern current intensities on top of Galway Mound, a mound 8 km north of Challenger Mound, reach 16 cm s^{-1}, whereas current speeds on its flanks appear to be slightly lower (Dorschel et al. 2007b). This suggests that current intensities in times of mound initiation were significantly weaker in the Belgica Mound Province than today. Huvenne et al. (2009) discussed a hydrodynamic regime characterized by an intermediate current strength optimal for cold-water corals to grow facilitating a fast, early mound development.

Trends in current intensity, productivity and sediment supply can be directly linked to episodes where non-deposition or erosion occurred. Titschack et al. (2009) showed that the early mound growth phase might also be disturbed by episodes of non-deposition and/or erosion. At Hole U1317C a gradual weakening of current strength and negative benthic $\delta^{13}C$ anomalies may be associated to changes in the bottom waters. Episodes of reduced currents at ~144.5 mbsf and at ~147.5 mbsf directly coincide with peak minima in the benthic and planktonic $\delta^{13}C$ values (Fig. 4). Extremely low planktonic $\delta^{13}C$ values of -2.5 ‰ and less can be related to upwelling of nutrient rich and $\delta^{13}C$ depleted waters during times of stronger advection (Naidu and Niitsuma 2004; Naidu 2004), whereas low benthic $\delta^{13}C$ values may reflect less ventilated bottom waters. The small temperature difference between bottom and surface waters at 144–148 mbsf may indicate a period of enhanced upwelling. This is supported by findings of Nikolaev et al. (1998) showing several vertical $\delta^{18}O$ profiles from the NE Atlantic (foraminiferal zone N21, 2–3 Ma) having ± constant oxygen isotope values of the upper 400 m of the water column. In the recent PSB, benthic $\delta^{13}C$ values of ~1 ‰ are recorded, while Holocene values are more depleted (0.3–0.5 ‰). During glacial periods with well-ventilated water masses, benthic $\delta^{13}C$ values were heavier with ~1.5 ‰ (Peck et al. 2007). Therefore, mean benthic $\delta^{13}C$ values of ~0.5 ‰ probably reflect relatively poorly ventilated bottom waters compared to the glacially enriched values resulting from the nutrient-depleted MOW mixing with ENAW (Frank et al. 2004).

The drop to extremely depleted $\delta^{13}C$ values at ~144.5 mbsf and at ~147.5 mbsf coincides with poorly preserved and partly dissolved coral skeletons (Fig. 4). What caused these extreme $\delta^{13}C$ decreases? Peck et al. (2007) also found brief episodes of depleted benthic $\delta^{13}C$ values during the last glacial/interglacial cycles in the Porcupine Seabight. They related these depleted $\delta^{13}C$ values to decreases in the ventilation of the Glacial North Atlantic Intermediate Water (GNAIW). These events are associated with melt water pulses from North Western European Ice Sheets (NWEIS). Becker et al. (2006) showed that the Late Pliocene/Early Pleistocene (~2.6 Ma) climatic system of the North Atlantic was influenced by similar short-term variations comparable to the recent oceanographic setting.

Additionally, Thierens et al. (2009) showed a deposition of ice-rafted detritus already in the early stage of mound development. However, the maximum extent of NWEIS during the late Pliocene is not comparable to that of the last glaciations (Zachos et al. 2001). Therefore, other factors are required to explain the observed benthic $\delta^{13}C$ excursions.

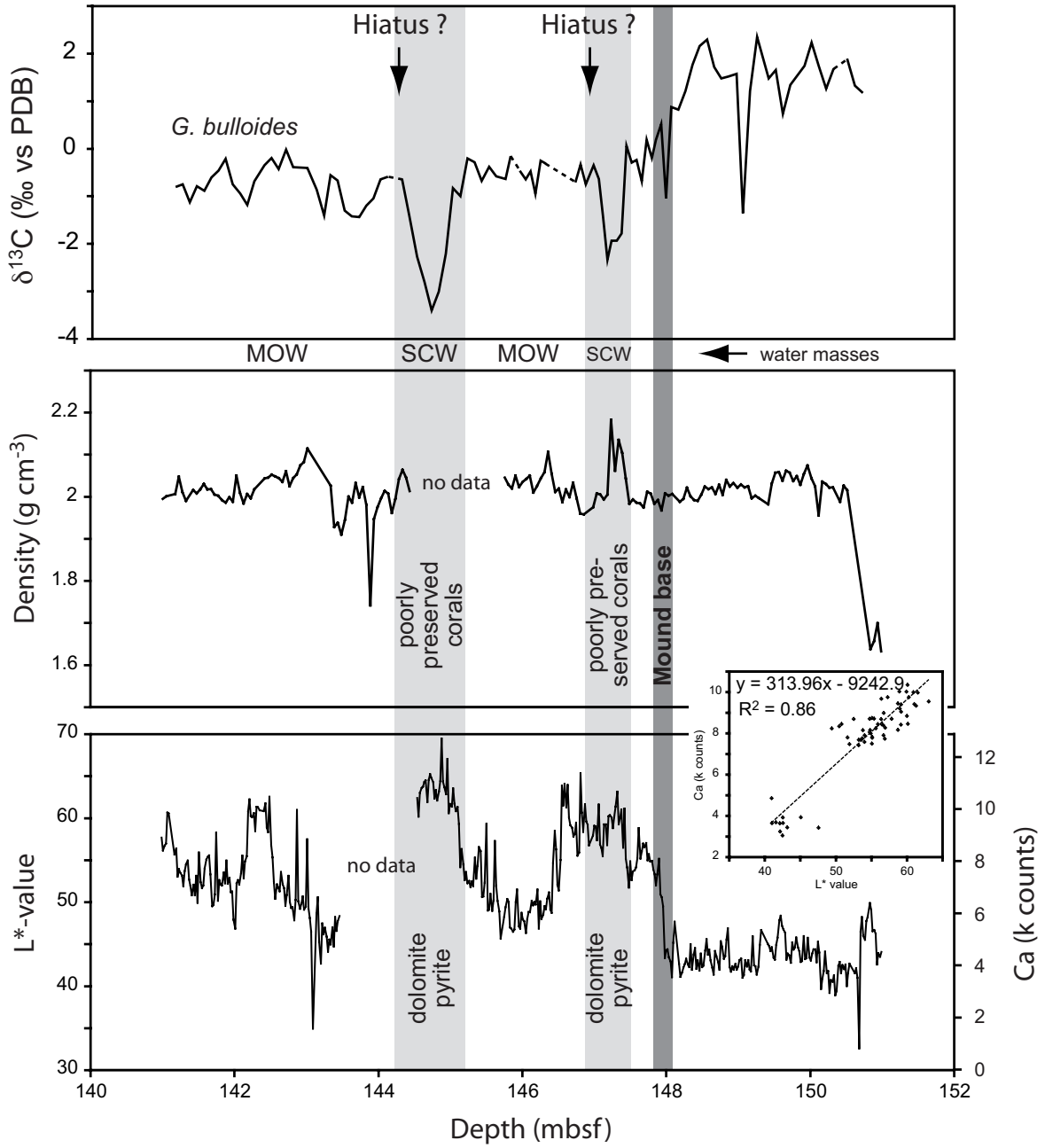

Figure 5: Core logging data of sediment density (in g cm^{-3}), colour reflectance L*-value (in percent) and XRF Ca-counts (in k counts) of the investigated interval (Expedition 307 Scientists, 2006; Foubert and Henriet, 2009) are presented in relation to planktonic stable carbon isotopes (in ‰) and interpretations from figure 4. XY-plot indicates linear relation between L*-values and Ca-counts with correlation coefficient R^2 of 0.86. Sediment erosion after and early diagenetic (oxidation) processes within the grey intervals may have overprinted the sediments leading to dissolution of coral skeletons, the extreme $\delta^{13}C$ decreases, maxima in Ca-counts and sediment density, and the formation of pyrite and gypsum according to Pirlet et al. (2010).

Sarnthein et al. (1994) observed that the nutrient-rich $\delta^{13}C$-depleted Southern Component Water (SCW) replaces MOW at intermediate depth during glacial periods. Decreased GNAIW formation and weak MOW flow during the early Pleistocene glacial periods may have lead to vertical redistribution of water masses along the European Margin (Peck et al. 2007; Zahn et al. 1987, 1997). This potentially led to the introduction of SCW into the Porcupine Seabight causing the observed depleted benthic $\delta^{13}C$ values.

Therefore we conclude, that rather a glacial version of SCW influenced the oceanographic regime of the PSB during cold phases of the Early Pleistocene. In addition, occurrence of the cold-water benthic foraminiferal species *L. antartica* underlines the appearance of a glacial SCW at these times (Fig 2. and 3). However, the introduction of SCW to intermediate depth in the PSB does not explain the even heavier drop of planktonic $\delta^{13}C$ values at the same time. Naidu and Niitsuma (2004) also reported of $\delta^{13}C$ values of *G. bulloides* about 1 ‰ lower than that of benthic foraminifera at a site in the Arabian Sea during the last glaciation. Pirlet et al. (2010) relate the occurrence of dissolved corals within a distinct sediment layer to the interplay of increased currents with possible sediment erosion and increased oxidation processes within the surface sediment layer. The result of this process is a distinct layer with a) dissolved coral skeletons, b) increased carbonate content and sediment density, c) the occurrence of gypsum crystals, d) first- and second-generation pyrite, and e) depleted $\delta^{13}C$ values of bulk sediment down to -5 ‰. Transferring these implications to the early development of Challenger Mound, both sections with low $\delta^{13}C$ values, and poorly preserved coral skeletons correlate well with higher sediment densities and Ca content (Fig. 5). A re-examination of the coarse sediment fraction from samples of dissolved coral layers showed that in these horizons pyrite and gypsum minerals are abundant compared to sediments with well-preserved coral skeletons. We therefore conclude that both, changes in the hydrography at surface and intermediate depth (SCW, upwelling, and MOW characteristics) and early diagenetic (oxidation) processes induced by erosional events describe the sediments at the mound base of Site U1317C.

However, it is not possible to estimate the length of the hiatuses and how much material might have been eroded. A comparison of the $\delta^{18}O$ record of Challenger Mound with other records to determine Marine Isotope Stages (Sakai et al., 2009) must therefore be treated with caution due to the temporal gaps in the sedimentary record. A multi-proxy data set in

combination with early diagenetic structures as proposed by Pirlet et al. (2010) could resolve possible hiatuses through the whole Challenger Mound record.

2.5 Conclusion

This study provides detailed stable isotope records as well as grain size analyses from the base of IODP Site U1317C at Challenger Mound, Porcupine Seabight. These records encompass the sedimentary sequence from the Middle Miocene to the Early Pleistocene and reveal the presence of an extended hiatus between the middle Miocene and the Late Pliocene/Early Pleistocene. Mound growth coincided with the intensification of the Northern Hemisphere Glaciation, characterized by moderate glacial conditions that were still favourable for cold-water corals to grow. Temperatures calculated from benthic $\delta^{18}O$ are between 7 and 11°C, consistent with the range of the known temperature tolerance (4–12°C) for the reef forming cold-water coral *Lophelia pertusa*. Bottom current intensities are characterized by a cyclic pattern that can be associated to vertical movements of Mediterranean Outflow Water (MOW) and its replacement by Southern Component Water (SCW). Peak events of these gradual movements are clearly observed in both planktonic and benthic $\delta^{13}C$ values indicating the influence of $\delta^{13}C$-depleted SCW in the Porcupine Seabight during that time. After these sluggish phases enhanced MOW flow replaced SCW and led to stronger current intensities and most probably sediment erosion on Challenger Mound. Erosion and early diagenetic (oxidation) processes overprinted the sediment layers as indicated by dissolved coral skeletons, the increase in Ca-content and sediment density, minimum $\delta^{13}C$ values, as well as the occurrence of gypsum and pyrite, implying a careful evaluation of original and overprinted geochemical signals.

2.6 Acknowledgements

This study was financially supported by the Deutsche Forschungsgemeinschaft DFG-Project ISOLDE (Contract No. Du 129/45-1), which is gratefully acknowledged. AR acknowledges funding of DFG-Projects TRISTAN and Paläo-TRISTAN (Contract No. Du129/37-2 and 37-3). The authors are grateful to captains, crews, chief scientists, and scientific parties of the research drill campaign IODP Exp. 307 with RV JOIDES RESOLUTION. Anneleen Foubert is greatly acknowledged for providing the XRF calcium data to correlate with colour reflectance data. Furthermore we would like to thank Lulzim Haxhiaj (IFM-GEOMAR, Kiel) and Matthias López Correa (GeoZentrum Nordbayern, Erlangen) for their convenient corporation,

as well as Volker Liebetrau (IFM-GEOMAR) for many patient and fruitful discussions. Ed Hathorne is gratefully acknowledged for improving the language. Furthermore, we would like to thank Veerle Huvenne and an anonymous reviewer for their valuable comments to this manuscript. We are indebted to guest-editor Silvia Spezzaferri for thorough suggestions improving the manuscript considerably!

Chapter III

The Seawater Density Code: a key to decipher cold-water coral carbonate mound development

Based on*: The Seawater density Code: a key to decipher cold-water coral carbonate mound development.* Andres Rüggeberg, Sascha Flögel, Wolf-Christian Dullo, Jacek Raddatz, Volker Liebetrau (to be submitted to Geology).

Abstract

Cold-water coral carbonate mounds (CCMs) are marine benthic ecosystems acting as important hot spots of biodiversity and living resources, being at risk due to global environmental change. The most prominent examples of modern CCMs occur in the northeast Atlantic, where these complex biogenic build-ups started to grow around 2.6 Ma (Kano et al. 2007) Here we show for the first time that these ecosystems only thrive under specific oceanographic conditions. Based on core material from Challenger Mound (IODP Expedition 307) and Propeller Mound we reconstructed paleo-seawater densities from oxygen isotope ratios in benthic foraminifera. Our results demonstrate that CCMs grew when a density window of sigma-theta (σ_Θ) = 27.35–27.55 kg m^{-3} was present in the ambient bottom water. We conclude that seawater density is reflecting one of the major controlling factors favoring CCM growth, thus highlighting their sensitivity to environmental changes and potential for paleoceanographic reconstruction of these ecosystems and water mass dynamics.

3.1 The Seawater Density Code: a key to decipher cold-water coral carbonate mound development

Cold-water coral carbonate mounds (CCMs) are among the most spectacular marine ecosystems on this planet supporting immense biodiversity and high density of marine life comparable to shallow-marine tropical reefs. These vitally important systems are under varying degrees of pressure due to bottom trawling, hydrocarbon extraction, deep-sea mining and bioprospecting (European Commission 2007). The European continental margin is known for its high density of CCMs, which occur in distinct provinces (Henriet et al. 1998; Roberts

et al. 2006). All mounds along this margin started to develop above a distinct seismic unconformity (De Mol et al. 2002), which has been dated to ~5 Ma (Stoker et al. 2002). Recently, IODP Expedition 307 drilled through this unconformity and assigned the earliest phases of mound growth in the Porcupine Seabight off SW-Ireland to 2.5 – 2.7 Ma (Kano et al. 2007).

The formation of CCMs strongly relies on the sediment baffling capacity of their major frame builders, which are azooxanthellate cold-water corals. Since they depend on particulate organic matter (POM) as prime nutrients, it was hypothetically argued that their distribution along the margin follows distinct water mass signatures (Freiwald 2002; Sakai et al. 2009). Detailed regional and local oceanographic studies have shown the significance of physical parameters (Davies et al. 2008) on living cold-water coral occurrences among which seawater density, sigma-theta, is the key factor (Dullo et al. 2008). Today, all prolific growing CCMs along the Atlantic continental margin from the Bay of Biscay to northern Norway are restricted to a density window of s_Q = 27.35 – 27.65 kg m^{-3}.

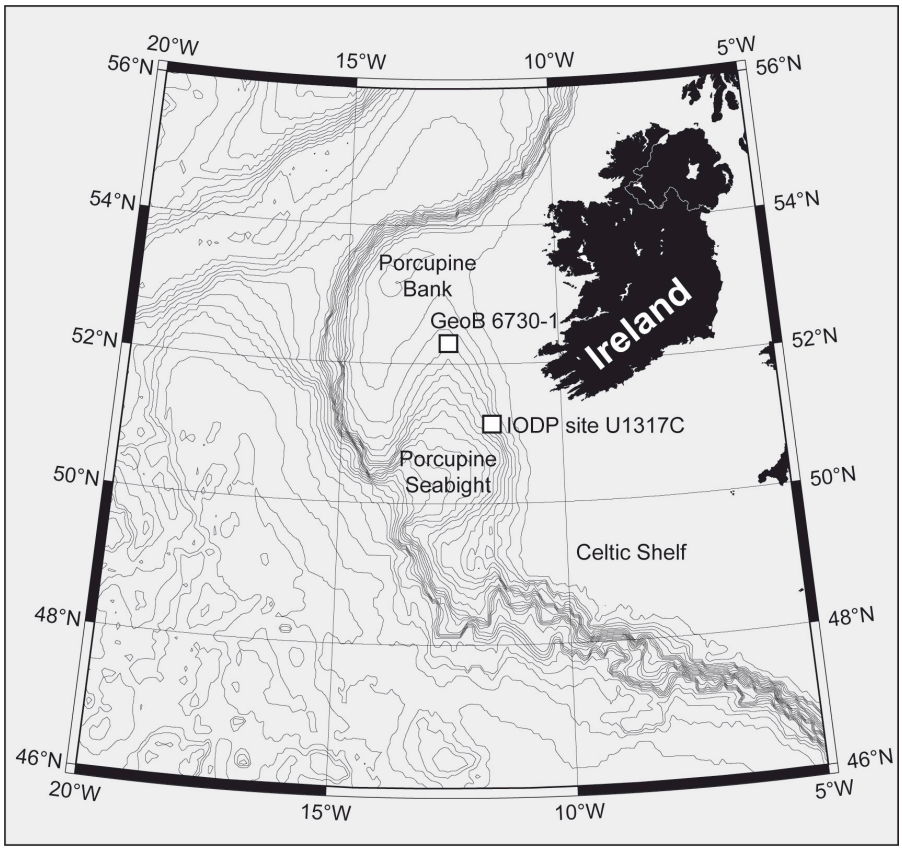

Figure 1: Core localities within the Porcupine Seabight. Depth lines correspond to 200-m intervals.

Addressing the question whether this present-day envelope of sigma-theta is a limiting factor of mound formation through time, we explored benthic foraminifera of CCMs and analyzed core samples from Propeller Mound, GeoB 6730-1, and from Challenger Mound, IODP core U1317C (Fig. 1). Phases of mound growth were identified applying precise U/Th-geochronology [Supplementary Information]. In order to determine paleo-densities we followed the established approach of Lynch-Stieglitz et al. (1999a, 1999b), who used stable oxygen isotopes of calcite tests ($\delta^{18}O_{calcite}$) of benthic foraminifera. Principle behind is the fact, that an increase of seawater density and $\delta^{18}O_{calcite}$ is driven by two independent parameters, increasing salinity and decreasing temperature, respectively. The dependence of seawater density on salinity and temperature is well known and is assumed to be constant throughout the oceans and geological time (Lynch-Stieglitz et al. 1999a). Eight different equations (Lynch-Stieglitz et al. 1999b) were proposed to reconstruct paleo-densities from $\delta^{18}O_{calcite}$ accounting for different oceanographic settings and temperature regimes. For our Holocene interval (Marine Isotope Stage MIS 1) we used equation 1 (best estimate: $\sigma_\theta = 26.0 + 1.1 \bullet \delta^{18}O_{calcite} - 0.16 \bullet \delta^{18}O_{calcite}^2$) by applying present-day $\delta^{18}O_{water}$ values from the Porcupine Seabight. Since all recovered time intervals older than the Holocene experienced different climatic/oceanographic conditions we selected among the established equations those representing past interglacial and glacial conditions (*Interglacial*: equation 6: $\sigma_\theta = 25.7 + 1.0 \bullet \delta^{18}O_{calcite} - 0.12 \bullet \delta^{18}O_{calcite}^2$ for MIS 5.3-5.4, 7, 9.1 // *Glacial*: equation 7: $\sigma_\theta = 25.9 + 1.0 \bullet \delta^{18}O_{calcite} - 0.15 \bullet \delta^{18}O_{calcite}^2$ for MIS 6.5). The onset of mound growth ~2.6 Ma ago occurred at the beginning of the Northern Hemisphere Glaciation (Haug & Tiedemann 1998). However, the early phase was still characterized by oceanographic and climatic conditions closer to those of interglacials, which justifies the use of equation 6.

Figure 2a displays the studied core from the top of Propeller Mound encompassing 350 cm of length. According the U-Th geochronology of 11 cold-water coral fragments, the core spans a time interval back to MIS 9.1 (~300 ka), reflecting discontinuous accumulation phases resulting in a mean growth rate around 1.1 cm ky^{-1} at the S-spur of the Propeller Mound. The core is characterized by several but well recognized hiatuses, (indicated by dashed lines of the σ_θ values in Fig. 2a) comprising times of non-deposition, equivalent to time intervals of "shut-off" mound growth and subordinate to times of erosion (Dorschel et al. 2005). The uppermost part represents the Holocene (MIS 1) with mean σ_θ values of 27.3 ± 0.05 kg m^{-3} indicating a rather marginal position on the envelope defined for prolific recent mound growth. This is due to the fact, that Propeller Mound is located in a shallower bathymetric range than the active mound growth. We were obliged to select that mound in terms of

environmental protection rules not to disturb active coral reef growth. This applies also for the selection of the IODP-site. The first hiatus downcore comprises the time interval between the MIS 2 and MIS 5.2. The section below, MIS 5.3 and 5.4, shows active mound growth and reconstructed σ_θ values of 27.36 ± 0.05 kg m^{-3}. Based on our dating and SPECMAP data (Imbrie et al. 1984), the second hiatus covers the time from MIS 5.5 to MIS 6.4.

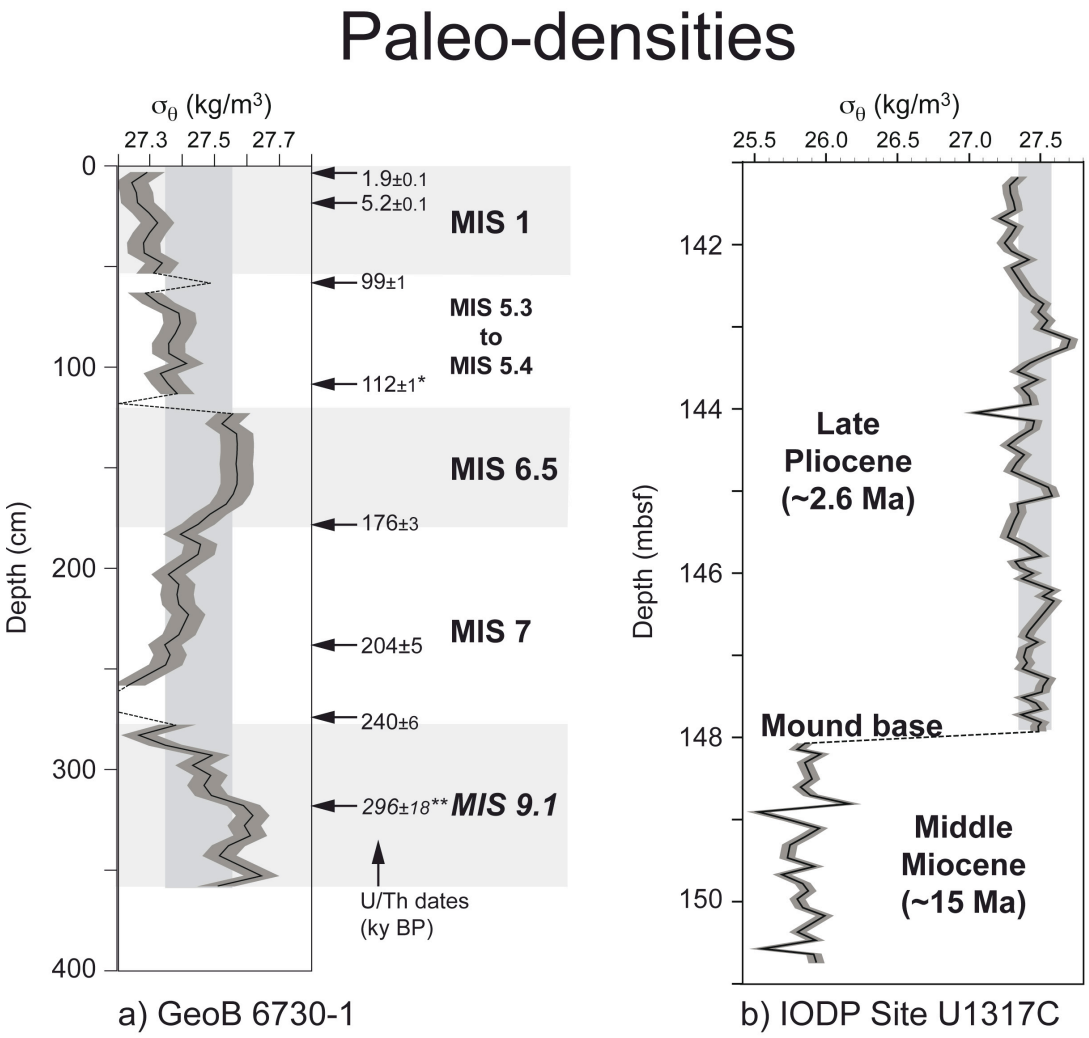

Figure 2a: displays the recorded Marine Isotope Stages (MIS) together with U/Th age data of core GeoB 6730-1. The vertical gray bar indicates the present day density envelope of s_Q = 27.35 – 27.55 kg/m^3. Plotted on top are reconstructed paleo-densities indicating time intervals of mound growth. * Mean value of three age determinations, ** large error comprising MIS 8.3 to MIS 9.2 (see supplementary discussion in SOM). **2b** displays data from core IODP Site U1317C between 151 m and 141 m below the seafloor (mbsf). Reconstructed s_Q-values show a pronounced shift from Middle Miocene to the onset of mound growth at 2.6 Ma.

Although MIS 6 represents a glacial period, there is one warmer phase defined as MIS 6.5. Propeller Mound recorded that specific time window by active accumulation reflecting characteristic s_q values of 27.54 ± 0.05 kg m^{-3} and cold-water coral growth with an age of 176 ± 3 ka for the basal layer at 178 cm core depth. The interglacial stage of MIS 7 displays prolific mound growth of more than one meter having mean σ_θ values of 27.39 ± 0.05 kg m^{-3} back to an age of 204 ± 5 ka. Before, there is still mound growth but more on a marginal position of the σ_θ envelope illustrated by minor coral contributions to silty sediments (Rüggeberg et al. 2007). The lowermost section of the core where mound growth is recorded has a calculated s_q range of 27.26 – 27.64 kg m^{-3}. The upper part, from 273 down to 318 cm, is interrupted by a hiatus around 303 cm. Below, the reconstructed σ_θ values of 27.57 ± 0.05 kg m^{-3} cover a marginal position of the envelope. The U/Th systematic implies an age of cold-water coral formation around 300 ka covering within uncertainty the glacial/interglacial transition between MIS 9.1 and MIS 8.4. The corresponding core section is characterised by generally minor coral content (Rüggeberg et al. 2007) with intercalated layers enriched in small coral fragments.

IODP core 1317C displays the transition from middle Miocene times where no mound growth is recorded to the onset of mound growth ~2.6 Ma ago (Fig. 2b). Applying the method of reconstructing paleo densities shows a dramatic shift of σ_θ values from 25.83 ± 0.13 kg/m^3 to 27.41 ± 0.11 kg m^{-3} across the middle Miocene to Late Pliocene transition recorded in the IODP core from Challenger mound. With respect to the available time resolution, our reconstructed densities plot within the defined density envelope. Recent publications indicate that early mound growth might have been interrupted by hiatuses (Raddatz et al. 2011; Thierens et al. 2010; Titschack et al. 2009) as known from sediments of the past ~300 kyr (Dorschel et al. 2005; Rüggeberg et al. 2007).

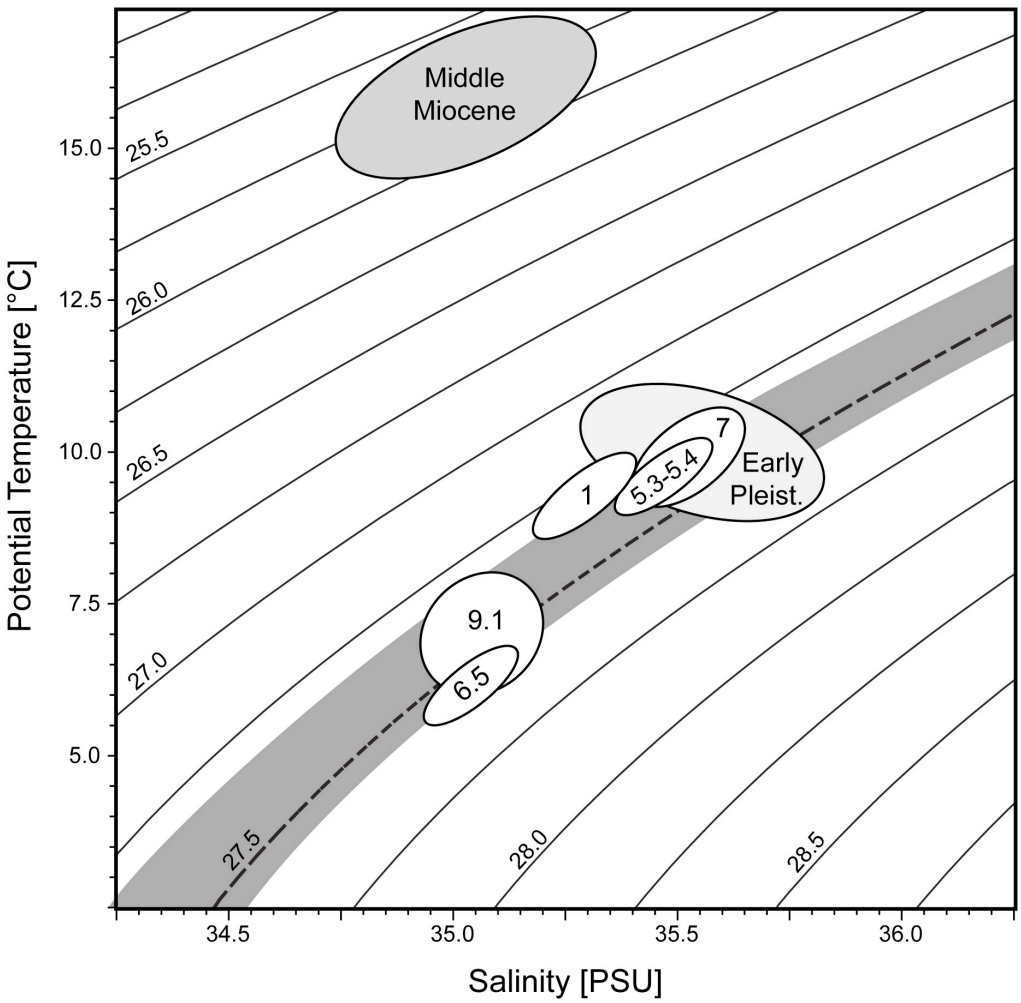

Figure 3: Potential temperature and salinity plot including lines of equal density (s_Q) in kg/m^3. Reconstructed densities of selected time intervals are displayed. The paleo-densities derived for the Middle Miocene (pink patch) before mound initiation is too light since also paleo-temperatures are much elevated with respect to modern conditions. The onset of mound growth at 2.6 Ma (light grey patch) plots into the area of the present-day density envelope of s_Q = 27.35 – 27.55 kg/m^3 (grey band) as well as the time intervals of Marine Isotope Stages (MIS) 1, 5.3, 5.4, 7 and 9.1 (white patches). The MIS 6.5 fit also to the modern density envelope, since it represents warm phases within a glacial. Therefore, they exhibit cooler temperatures equivalent to modern cold-water coral reefs of northern Norway (Dullo et al. 2008).

Excursions to lighter and heavier values outside the density envelope in IODP core U1317C therefore may indicate periods of non-deposition and/or erosion, thus supporting these studies (Raddatz et al. 2011; Thierens et al. 2010; Titschack et al. 2009).

In conclusion, our reconstructed data on paleo-densities show that periods of mound growth coincide with the presence of a density envelope identical to the modern one around sites of recent to subrecent cold-water coral reef formation (Fig. 3). In comparison to former studies

(Dorschel et al. 2005) mound growth is not entirely limited to interglacial periods. Warmer phases of glacials also provide conditions for prolific coral growth as seen during MIS 6.5 in Propeller Mound. This combined record of IODP 1317 drill core and RV-Poseidon 265 gravity core demonstrates that the dynamics of ocean gateways play a major role on the carbonate mound formation in the NE-Atlantic. Mediterranean Outflow intensified 3.3 – 3.5 Ma ago resulting in a gradual density rise of bottom waters (Khélifi et al. 2009). The closure of the Isthmus of Panama around 2.7 Ma (Haug and Tiedemann 1998) resulted in an enhanced subsurface water transport to higher latitudes in the Atlantic establishing the necessary density contrast in water masses (Eastern North Atlantic Water / Mediterranean Outflow Water) enabling active mound growth. Overall, prolific marine benthic ecosystem development portrayed in CCM growth is controlled already by minor changes in ambient bottom water densities. These results show that marine benthic ecosystems occupy very narrow and specific ecologic niches, which are very sensitive and even at risk to the actual global environmental changes, such as bottom water warming and acidification. As a consequence, our findings have lead to a robust diagnostic key-tool for interpretation of basin-wide sudden onset or shutdown of carbonate mound growth during Earth history (Wood 1999).

Methods

Uranium-series geochronology

U-Th isotope analyses: Uranium-series measurements for U/Th coral ages were performed at the Leibniz Institute of Marine Sciences at the University Kiel (IFM-GEOMAR) on a Finnigan MAT 262 RPQ+ (Mat262), a Thermo-Finnigan Triton-RPQ (Triton) thermal ionization mass spectrometer (TIMS), and a VG Axiom multi collector – inductively coupled plasma – mass spectrometer (MC-ICP-MS) applying lab-procedures and methods of (Edwards et al. 1986; Fietzke et al. 2005) and decay constants of (Cheng et al. 2000a). Sample 108 is measured twice for Th with MC-ICP-MS in independent sessions (Axiom 1 & 2) and for U with TIMS (MAT262 & Triton) and MC-ICP-MS as well. The resulting mean value of multiple measurements reflects reproducibility and robustness of applied methods.

For isotope dilution measurements a combined $^{233/236}U/^{229}Th$-spike was used, with stock solutions calibrated for concentration using NIST-SRM 3164 (U) and NIST-SRM 3159 (Th), as combi-spike calibrated against CRM-145 uranium standard solution (also known as NBL-112A) for U-isotope composition and against a secular equilibrium standard (HU-1, uranium ore solution) for determination of $^{230}Th/^{234}U$ activity ratio. Characteristic whole procedure

blanks at time of sample preparation were around 14 to 60 pg for U, 6 to 9 pg for ^{232}Th and 0.5 to 5 fg for ^{230}Th. Calculation of geochronological data and activity ratios are based on the decay constants (Cheng et al. 2000a).

The applied data reduction includes a correction for isotopic composition of incorporated Th of detrital origin, according to continental crust values (Wedepohl 1995) as approximation for potentially involved shelf sediments. Note, in most cases this correction is negligible due to sufficiently high ^{230}Th/^{232}Th activity ratios and low Th concentrations in the corals. Due to the generally high ages in this sample set, the impact of age correction on the interpretation of δ^{234}U values is significant and criteria for isotopic reliability of ^{230}Th age data may be applied. Recent reef forming cold-water corals showed within their uncertainties similar $\delta^{234}U_{(0)}$ values of 145.5 ± 2.3 ‰ (Cheng et al. 2000b) and 146.3 ± 3.9 ‰ (Liebetrau et al. 2010) for different depth and location, supporting the application of the $\delta^{234}U_{(T)}$ reliability criteria presented for tropical corals (Blanchon et al. 2009).

Stable oxygen isotope analyses

Seawater: Water samples from the Porcupine Seabight were collected during expeditions of the RV METEOR and RV POSEIDON in April (M61/1), June (M61/3) and August (P316) 2004. Water samples for isotope analysis were filled into 100 ml crimp sealed glass bottles crimp and 0.2 ml of a saturated $HgCl_2$ solution was added to stop biological activity. Oxygen isotopes were analyzed at the Leibniz Laboratory at Kiel University (Germany) applying the CO_2-water isotope equilibration technique on 4 ml sub-samples on the Kiel Equi unit on-line coupled to a Finnigan Delta E isotope ratio mass spectrometer and on 0.5 ml sub-samples on a Finnigan gas bench II unit coupled to a Finnigan DeltaPlusXL (Bauch et al. 2005). The ^{18}O/^{16}O ratio is given versus VSMOW in the usual d-notation. The measurement precision for δ^{18}O analysis is ± 0.05 ‰ and ± 0.4 ‰, respectively.

Benthic foraminifera: Stable oxygen isotope ratios of water samples (^{18}O/^{16}O) are given versus VSMOW in the usual δ-notation (Craig 1961). The thermohaline gradient within the water column, internal waves at depth, and different seasons during sampling account for the wider spread of the δ^{18}O results from water depths of carbonate mounds. Additionally, due to the small salinity range of DS < 0.3 psu and the concentration of samples from coral reefs, the correlation coefficient is low. However, GEOSECS data (Schmidt et al. 1999) support our findings.

Paleo-seawater density reconstruction

Paleo-seawater densities were reconstructed using $\delta^{18}O$ data from benthic foraminifera derived from cores GeoB 6730-1 and IODP core U1317C. We converted the $\delta^{18}O_{calcite}$ to density using the technique described by Lynch-Stieglitz et al. (1999b)

3.2 Acknowledgements

We thank Captains, crews, and shipboard scientific parties of cruises P265, IODP-expedition 307. The study received funding from the Deutsche Forschungsgemeinschaft projects TRISTAN and ISOLDE (Du 129/37 and DU 129/45). Additional financial support was provided by the Leibniz-Award (Du 129/33), which is gratefully acknowledged. We greatly acknowledge Nils Andersen, Leibniz Laboratory at Kiel University, for conducting stable oxygen isotope measurements of water samples. Dr. J. Fietzke is especially acknowledged for maintaining the Axiom MC-ICP-MS on high performance for the U-Th measurements and analytical collaboration. Dr. Folkmar Hauff is gratefully acknowledge for supporting the TIMS work, as well as A. Kolevica for her clean-lab support, J. Heinze for XRD measurements on smallest sample amounts and L. Haxhiaj for performing C and O isotope measurements on the carbonate samples. A. Eisenhauer is thanked for providing the MS facilities at IFM-GEOMAR. We are indebted to the A. P. Laudenbacher Foundation in La Punt Chamues-ch providing an excellent atmosphere for a working and research retreat.

3.3 Author contribution

A.R. and C.W.D. designed the research program. IODP Expedition 307 Scientists collected drill cores and carried out work at sea. A.R., J.R., V.L. analyzed the samples. A.R., S.F., W.C.D. and V.L. analyzed the data and wrote the paper and supplementary information. A.R., S.F., W.C.D., J.R., and V.L. discussed the results and commented on the manuscript.

3.4 Supplementary information

Uranium-series geochronology

Sample preparation

In several depth intervals of core GeoB 6730-1 coral fragments of *Lophelia pertusa* were selected to determine absolute age data using the U/Th isotope systematic of the aragonite skeleton. All samples were first scrubbed with dental tools and ultrasonically cleaned to remove exterior contaminants (sediments, iron-manganese crusts and coatings) from the fossil coral fragments. Each sample was bathed in 50/50 mixture of 30 % H_2O_2 and 1M NaOH and MQ-water alternately for 15 minutes with ultrasonification (Cheng et al. 2000b). This procedure was performed up to three times to ensure total removal of particles, organic stains and oxides left after mechanical procedure on the coral and within the open pore space. However, the last $HClO_4$ cleaning step described by Cheng et al. (2000b) was skipped due to the related risk of increased sample loss on small fragments. Before element separation, all samples were checked again for the cleanness and purely aragonitic crystal structures under the binocular. X-ray diffraction (XRD) on selected samples additionally helped to determine calcite content below the detection limit (<1%). All sub-samples were taken with a micro-driller from freshly cut surfaces of cleaned fragments of *L. pertusa*, after discarding first drill steps as additional surface cleaning procedure. Element separation procedure was based on Eichrom-UTEVA resin (Cheng et al. 2000b).

U-Th isotope analyses

The U/Th analyses on *L. pertusa* of core GeoB 6730-1 are summarized in table S1. Data from fossil zooxanthellate corals back in time to ~300 ka suggest that interglacial seawater $\delta^{234}U$ was generally within the uncertainty of the modern value. Only few data from glacial periods are reported, suggesting initial $\delta^{234}U_{(T)}$ was as low as 136 ‰ during most of the past glaciation (Delanghe et al. 2002). However, our $\delta^{234}U_{(T)}$ data set varies between 119 and 164 ‰ and according to reliability criteria (Blanchon et al. 2009) only 8 of 11 samples are considered for geochronological interpretation.

Supplementary discussion on Uranium-series dating

Ages presented in Fig. 2a of the manuscript are restricted to samples matching the reliable ("R") and strictly reliable ("SR") quality criteria after (Blanchon et al. 2009), avoiding

preference to less precise measurements by disregarding the range of individual analytical uncertainties for $\delta^{234}U_{(T)}$.

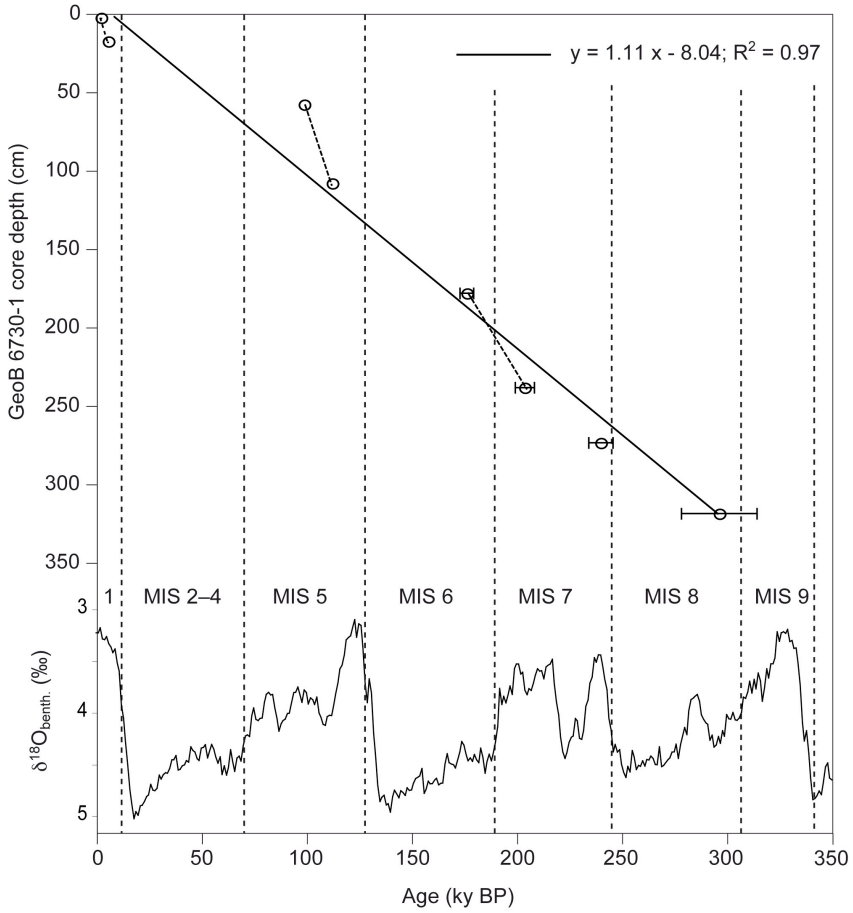

Figure S1: Longterm growth rate of core GeoB 6730-1 for the past 300 ky and Marine Isotope Stages (MIS) 1, 5, 7 (dashed lines). MIS follows the $\delta^{18}O$ LR04-record (Lisiecki & Raymo 2005). See text for detailed values and discussion.

Nevertheless, the age at 318 cm core depth (sample 6730-1/318, 296 ± 18 ky BP) is still considered and given in italics due to two observations. (i) The data are reaching the highest quality level "SR" within the range of slightly elevated age uncertainty, which is mainly due to highest ^{232}Th content and the related uncertainty of correction for detrital impact. (ii) Calculating the ^{234}U excess age, independent from Th systematic and considering a $\delta^{234}U_{(T)}$ value of 146 ± 2 ‰ for modern seawater (Henderson & Anderson 2003) as reliable starting point, ends up in an age of 314 ± 15 ky BP (overlapping with at comparable precision). This time span required for the decay of the unsupported (excess) ^{234}U of the initially incorporated U until the today measured $^{234}U/^{238}U$ activity ratio is determined by ($T=(1/\lambda^{234}U)$ * LN

($\delta^{234}U_{(modern\ seawater)}$ / $\delta^{234}U_{(sample\ measured)}$). Furthermore, following suggestions by[8] glacial periods may provide lower $\delta^{234}U$ values when compared to interglacial and modern ocean signatures. Therefore, the Blanchon-criterion (Blanchon et al. 2009) could be inadequate or misleading for samples of marine glacial carbonates. Considering slightly lower $\delta^{234}U$ initials for glacial periods (Thompson et al. 2003) would support the reliability of the presented U/Th age of the 318 cm sample. However, its remarkable age around 300 ky is pointing to cold-water coral growth at the transition from the late MIS 9 (9.2) interglacial to the early MIS 8 (8.4) glacial period. Due to the difference between U/Th and ^{234}U-excess age and the related range of uncertainty a clear discrimination between both stages cannot be given based on the actual data set.

Independently, the age of sample 178 is reflecting cold-water coral growth at early MIS 6.5 during a slightly cooler glacial phase than the early MIS 8 according the LR04-stack (Lisiecki & Raymo 2005).

This result supports the hypothesis that cold-water coral growth is not restricted only to interglacial periods. Nevertheless, the 178 data does not reflect any indication of lower $\delta^{234}U$ values, which is not supporting the suggestions for glacial periods (Thompson et al. 2003).

Related mound growth rates from U-series dating

The deduced mean growth rate of the Propeller Mound throughout the last 300 ky at the site of core 6730-1 (S-spur of the Propeller Mound) is about 1.1 ± 0.1 cm/ky.

This rate is simply calculated between the shallowest and the deepest data point considered for geochronological interpretation, supported by an average trend through the reliable 6730-1 data set reflecting a slope of 1.1 cm/ky with an R^2 of 0.97. Relative to this general trend, within each data cluster (296 to 176 ky BP; 112 to 99 ky BP, 2 to 5 ky BP) a steepening in growth rate is implied (Fig. S1). A discontinuous accumulation of the mound, most probably related to time intervals of stepwise proceeding cold-water coral growth, is indicated.

Calculating the individual slopes, the steepening effect becomes stronger from 2.4 ± 0.7 cm/ky (calculated from 204 to 176 ky BP) over 3.9 ± 0.6 cm/ky (around 100 ky BP) to 4.5 ± 0.3 cm/ky for the Holocene. This succession could imply a prograding improvement of growth conditions at the Propeller Mound towards younger periods of accumulation. In contrast, this and earlier studies (Dorschel et al. 2005; Rüggeberg et al. 2007) demonstrate a general decline in reef and mound growth for Propeller Mound and the Hovland mounds.

Additionally, the apparent progression described above is most probably influenced by the increasing compression of the carbonate framework with increasing sediment depth and erosion of past interglacial sediments during terminations (Dorschel et al. 2005)

However, the presented results support the hypothesis of heterogeneous accumulation phases depending on exposition to changing current regime, related nutrient supply and particle flux (Dorschel et al. 2005; Rüggeberg et al. 2007). Nevertheless, the apparent discontinuous growth ends up in a site-specific long-term average around 1.1 cm/ky at the S-spur of the Propeller Mound throughout the last 300 thousand years.

Stable oxygen isotope analyses on seawater

Stable oxygen isotope ratios of water samples ($^{18}O/^{16}O$) are given versus VSMOW in the usual δ-notation (Craig 1961). The thermohaline gradient within the water column, internal waves at depth, and different seasons during sampling account for the wider spread of the $\delta^{18}O$ results from water depths of carbonate mounds (Fig. S2). Additionally, due to the small salinity range of DS < 0.3 psu and the concentration of samples from coral reefs, the correlation coefficient is low (Fig. S2). However, GEOSECS data (Schmidt et al. 1999) support our findings.

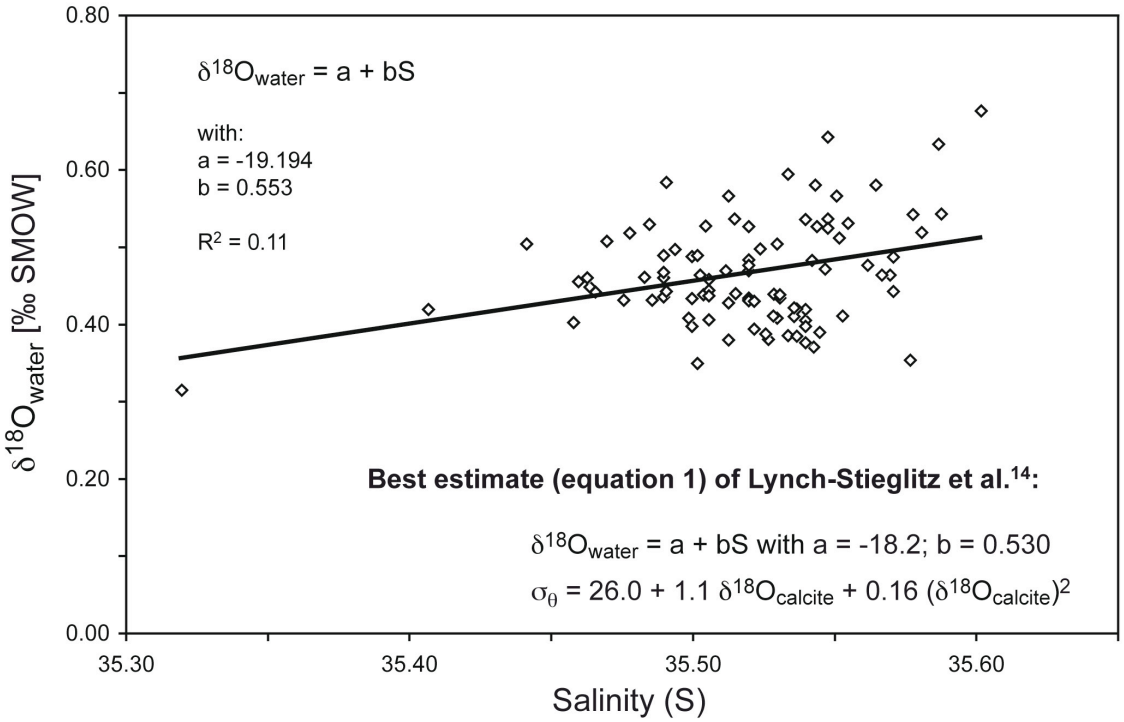

Figure S2: $\delta^{18}O_{water}$–salinity relation of the upper water column (0–1155 m) from water samples collected during cruises M61/1, M61/3, P316 in summer 2004. This $\delta^{18}O_{water}$–salinity relation supported by GEOSECS data (Schmidt et al 1999) justifies the use of equation 1 of Lynch-Stieglitz et al. (1999a).

Stable oxygen and carbon isotope analyses on benthic foraminifera

After cutting the cores of GeoB 6730-1, sediment samples were taken in intervals of 5 cm. Sediment samples of IODP core U1317C were taken every ~10 cm at the IODP Core Repository at Bremen University, Germany (Raddatz et al. 2011).

Previous studies already reported that the stable isotopic ratios of *F. wuellerstorfi* and *C. kullenbergi* are indistinguishable within analytical error (Hodell et al. 2001). In our studied cores of Propeller Mound (Dorschel et al. 2005; Rüggeberg et al. 2007), paired analyses of these species also indicate a 1:1 relation in $\delta^{18}O$ (Fig. S3). The same holds true for *F. wuellerstorfi* and *L. lobatulus* of IODP core U1317C as shown in the downcore record of (Raddatz et al. 2011).

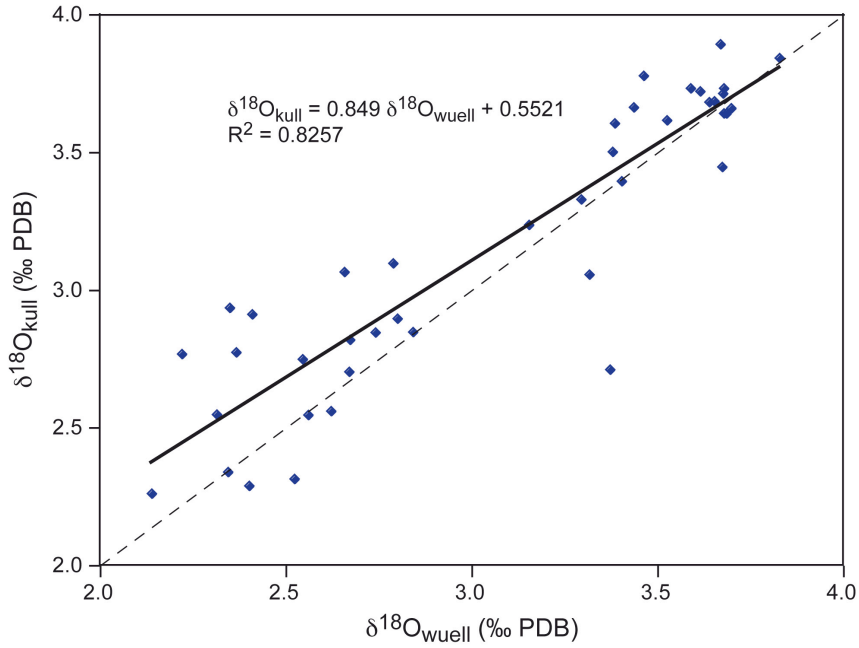

Figure S3: Linear relation between (a) $\delta^{18}O$ of *Cibicidoides kullenbergi* ($\delta^{18}O_{kull}$) and *Fontbotia wuellerstorfi* ($\delta^{18}O_{wuell}$) from GeoB 6730-1 selected from fraction 250 to 500 µm. Dashed line indicates 1:1 relation between the paired $\delta^{18}O$ ratios.

Paleo-seawater density reconstruction

Paleo-seawater densities were reconstructed using $\delta^{18}O$ data from benthic foraminifera derived from cores GeoB 6730-1 and IODP core U1317C. We converted the $\delta^{18}O_{calcite}$ to density using the technique described by Lynch-Stieglitz et al. (1999a). Because the $\delta^{18}O_{calcite}$ in benthic foraminifera reflects not only the temperature but also the $\delta^{18}O$ of the water in which it grew, the $\delta^{18}O_{calcite}$ in foraminifera is an inaccurate paleothermometer without independent knowledge of isotopic composition of the water. The $\delta^{18}O$ of seawater ($\delta^{18}O_{water}$) primarily reflects patterns of evaporation and freshwater influx to the surface of the ocean. Because salinity also reflects these same processes, salinity and $\delta^{18}O_{water}$ are often well correlated in the ocean. Although the exact relationship varies in different areas of the surface ocean (Craig and Gordon 1965; Fairbanks et al. 1992), the vast majority of surface waters in the ocean have a linear salinity and $\delta^{18}O_{water}$ relation (Craig and Gordon 1965; Fairbanks et al. 1992; Broecker 1986). Subsurface waters warmer than 5°C also fall along the surface water trend which hold true for the water masses of Eastern North Atlantic Water (ENAW) and Mediterranean Outflow Water (MOW) within the Porcupine Seabight. The conservative properties of these upper and intermediate water masses reflect the surface water properties at the location of water mass formation, so it is not surprising that they fall along the same regression line as surface waters.

The linear relation between $\delta^{18}O_{water}$ and salinity for the upper water masses of the World Ocean is a consequence of fundamental properties of the ocean-atmosphere system, specifically, the interplay between evaporation/precipitation patterns and the wind-driven ocean circulation. The linear relationship suggests the mixing of seawater with salinity and $\delta^{18}O_{water}$ characteristics of sub-thermocline waters with fresh, low- $\delta^{18}O_{water}$ source.

Since it is not possible to separate the contributions of $\delta^{18}O_{water}$ (related to salinity) and temperature on the $\delta^{18}O_{calcite}$, one still can calculate paleo-densities from the $\delta^{18}O_{calcite}$. In today's ocean, density can be more accurately estimated from $\delta^{18}O_{calcite}$ than temperature. This is because the compensating effects of temperature and salinity on $\delta^{18}O_{calcite}$ and density are very similar. Both, $\delta^{18}O_{calcite}$ and density will increase as a result of increasing salinity or decreasing temperature (Lynch-Stieglitz et al. 1999a).

Chapter IV

Temperature dependence of stable Sr-isotopes, Sr/Ca and Mg/Li in the scleractinian cold-water coral *Lophelia pertusa*

Based on: *Temperature dependence of stable Sr-isotopes, Sr/Ca and Mg/Li in the scleractinian cold-water coral Lophelia pertusa.* Jacek Raddatz, Andre Krabbenhöft, Volker Liebetrau, Andres Rüggeberg, Ed Hathorne, Anton Eisenhauer, Florian Böhm, Hauke Vollstaedt, Jan Fietzke, Matthias López Correa, Paolo Montagna, Andre Freiwald and Wolf-Christian Dullo *(submitted to Earth and Planetary Science Letters).*

Abstract

The aragontic skeletons of scleractian corals serve as valuable archives in paleoceanographic studies. The potential of $\delta^{88/86}$Sr, Sr/Ca and Mg/Li ratios of the cold-water coral *Lophelia pertusa* to record intermediate water mass properties has been investigated using samples from the European continental margin spanning the temperature range 6 to 14°C. Stable strontium isotope measurements were carried out with the recently developed double spike TIMS technique and our results differ from those obtained with less precise methods. In particular we find a weak inverse relationship between $\delta^{88/86}$Sr and temperature from 5.96° to 9.79°C with –0.011 ‰/°C ($r^2 = 0.41$, $p = 0.04$) in contrast to the strong positive relationship of previous studies. Moreover, our data also suggest that this signal can be influenced by seawater carbonate chemistry.

Elemental ratios Sr/Ca, Li/Ca and Mg/Li are significantly related to water temperature and do not correlate with salinity, as found in previous studies. Sr/Ca ratios in *L. pertusa* display the expected inverse correlation with temperature ($r^2 = 0.66$, $p = 0.0007$). However, the scatter in the Sr/Ca data severely limits the fidelity of paleotemperature estimates. Mg/Li ratios in *L. pertusa* are more tightly related to temperature ($r^2 = 0.84$, $p = 0.00001$) and seem to be less

affected by vital effects than Sr/Ca ratios. Mg/Li ratios in *L. pertusa* therefore represent a promising new paleotemperature proxy for intermediate water masses.

4.1. Introduction

The scleractinian cold-water coral *Lophelia pertusa* is widely distributed in the oceans. Along the European continental margin they occur in Norwegian fjords, on the Irish Margin, the Bay of Biscay, the Gulf of Cadiz and a few occurrences are reported from the Mediterranean Sea (Freiwald 2002; Freiwald et al. 2004, 2009; Taviani et al. 2005). Several studies have shown that *L. pertusa* can extend up to 25 mm/yr (Gass and Roberts 2010; Mortensen and Rapp 1998; Orejas et al. 2008) and that each polyp can live several years. The distribution of *L. pertusa* on the European continental margin is controlled by oceanographic conditions such as temperature, current strength, nutrient availability and the density of seawater (e.g. Dullo et al. 2008; Freiwald et al. 2004; Raddatz et al. 2011; Roberts et al. 2006, Rüggeberg et al. 2007). *L. pertusa* occurs at depths from 40 m (Trondheimsfjord, Norway) to >3000 m on the New England seamount chain (Freiwald et al. 2004) and lives in temperatures of 4-14°C and at salinities from 32.0 in Scandinavian fjords to 38.8 in the Mediterranean Sea (Strømgren 1971; Taviani et al. 2005).

Scleractinian cold-water corals archive an array of geochemical tracers in their aragonite skeletons (Sr/Ca, Mg/Li, $\delta^{13}C$, $\delta^{18}O$, $\delta^{88/86}Sr$, etc.), potentially providing vital information about the intermediate and deep oceans of the past (e.g. Adkins et al. 2003; Case et al. 2011, Cohen et al. 2002; Rüggeberg et al. 2008). Significant efforts have been made to identify robust proxies for temperature reconstructions. Coral elemental ratios suggested to be related to water temperature are B/Ca (Sinclair et al. 2006), Mg/Ca (Mitsuguchi et al. 1996), U/Ca (e.g. Shen et al. 1995; Min et al. 1995) and Sr/Ca (e.g. Beck et al. 1992; Shen et al. 1996; Smith et al. 1979). The Sr/Ca ratio of tropical corals is a widely used robust temperature proxy (e.g. Beck et al. 1992; Gagan et al. 1998). However, biological factors known collectively as "vital effects" also influence element incorporation and may be distinctly different between species (Gaetani et al. 2011; Gagnon et al. 2007; Weber and Woodhead, 1972). Other environmental factors can also influence element incorporation. For example, U/Ca ratios in warm- and cold-water corals are more related to carbonate ion concentrations (CO_3^{2-}) and/or pH superimposed on the temperature influence (Anagnostou et al. 2011; Inoue et al. 2011).

The microstructure of *L. pertusa* is characterized by two parts of the skeleton; the early mineralization zones that correspond to the Centres of Calcification (CoC) described by Gladfelter (1982), and the surrounding aragonite fibres. The CoC comprise small, granular, disorganized aragonite crystals, whereas the fibrous skeleton is constructed from fans of aragonite needles (Gladfelter 1982). In comparison to the aragonitic fibres, the CoC have a distinct isotopic composition (δ^7Li, δ^{18}O, δ^{13}C and δ^{11}B) and different elemental ratios (Sr/Ca, Mg/Ca, Mg/Li, U/Ca, etc., Adkins et al. 2003; Blamart et al. 2007; Gagnon et al. 2007; Lutringer et al. 2005; Montagna et al. 2005; Robinson et al. 2004; Rollion-Bard et al. 2009, 2010; Smith et al. 2000, 2002). Accordingly, different strategies have been proposed to avoid and reduce biases from sampling different parts of the skeleton. Smith et al. (2000) developed a method by taking many subsamples in order to extrapolate to the isotopic equilibrium values by using the observed strong linear correlation relationship between δ^{18}O and δ^{13}C. Other studies followed this approach and found a break in the slope for stable isotopes (Adkins et al. 2003) and trace metals in the CoC (Gagnon et al. 2007).

The combination of Li/Ca and Mg/Ca ratios to obtain Mg/Li ratio has been introduced as a potential paleotemperature proxy in benthic foraminifers (Bryan and Marchitto 2008) and cold-water corals (Case et al. 2010). Measurements of *L. pertusa* and other cold-water corals suggest that Mg/Li ratios are primarily controlled by temperature as combining Li/Ca and Mg/Ca ratios removes much of the heterogeneity related to the sampling of the coral micro-structures (Case et al. 2010).

Non-traditional stable isotope analysis of scleractinian corals like $\delta^{44/40}$Ca (Böhm et al. 2006) and $\delta^{88/86}$Sr (Fietzke and Eisenhauer 2006; Rüggeberg et al. 2008) have been introduced as potential paleotemperature proxies in both cold- and warm-water corals. The development of new proxies for reconstructing past intermediate water mass temperature is important for the study of past climates and ocean circulation. To this end we focus on the temperature sensitivity of $\delta^{88/86}$Sr, Sr/Ca and Mg/Li ratios in the scleractinian coral-water coral *L. pertusa*.

4.2 Materials and Methods

Living cold-water coral samples of *L. pertusa* were collected from different locations along the European continental margin (Fig. 1, Tab. 1). Initial $\delta^{88/86}$Sr data for these samples (Galway Mound, Little Galway Mound, Stjernsund, Trondheimsfjord, Trændadjupet, Oslo Fjord; Tab. 1) were previously published (Rüggeberg et al. 2008). In order to extend this

study, additional samples were taken from the Norwegian margin (Lopphavet, Sotbakken, Sula Reef, Oslo Fjord) from two different sites in the Mediterranean Sea (Urania Bank and Santa Maria di Leuca), from the Bay of Biscay (Whittard Canyon, Guilvinec Canyon) as well as from the Gulf of Cadiz (Tab. 1, Fig. 1). Samples were obtained with the manned submersible "JAGO" of IFM-GEOMAR (Kiel), the ROV "QUEST" of MARUM (University of Bremen), the ROV "Genesis" of RCMG (University of Ghent), a video-guided grab (TV-G) and a Van Veen Grab. Water temperatures and salinity were measured via CTD (Conductivity-Temperature-Depth) at the time of sample collection. CTD measurements are only snapshots and do not represent the entire annual variability but we assume that the bathyal temperature variation is generally stable and do not exceed 1.5°C.

About 2 mg of coral powder was drilled from each sample according to Rüggeberg et al. (2008), focusing on the theca and avoiding the CoC. For a heterogeneity tests CoC were specifically targeted in two corals, from the Atlantic (POS-265-499) and the Mediterranean (M70/1-677).

4.2.1 $\delta^{88/86}$Sr measurements

Chemical preparation for $\delta^{88/86}$Sr measurements followed the protocols described by Krabbenhöft et al. (2009, 2010). The $\delta^{88/86}$Sr measurements of Fietzke and Eisenhauer (2006) and Rüggeberg et al. (2008) employed the standard-bracketing technique with multi-collector inductively coupled plasma mass spectrometry (MC-ICP-MS), whereas here we utilize the more precise double spike technique (DS) with thermal ionization mass spectrometry (TIMS). The results of Sr isotope measurements are shown in Table 1. All errors are given as 2 standard deviations (2 SEM) for repeated analyses of the same sample. The long-term external reproducibility of $\delta^{88/86}$Sr for the JCp-1 *Porites* coral reference material (Okai et al. 2002) measured in the course of this study (n = 9) is 0.197 ± 0.019‰ (2sd).

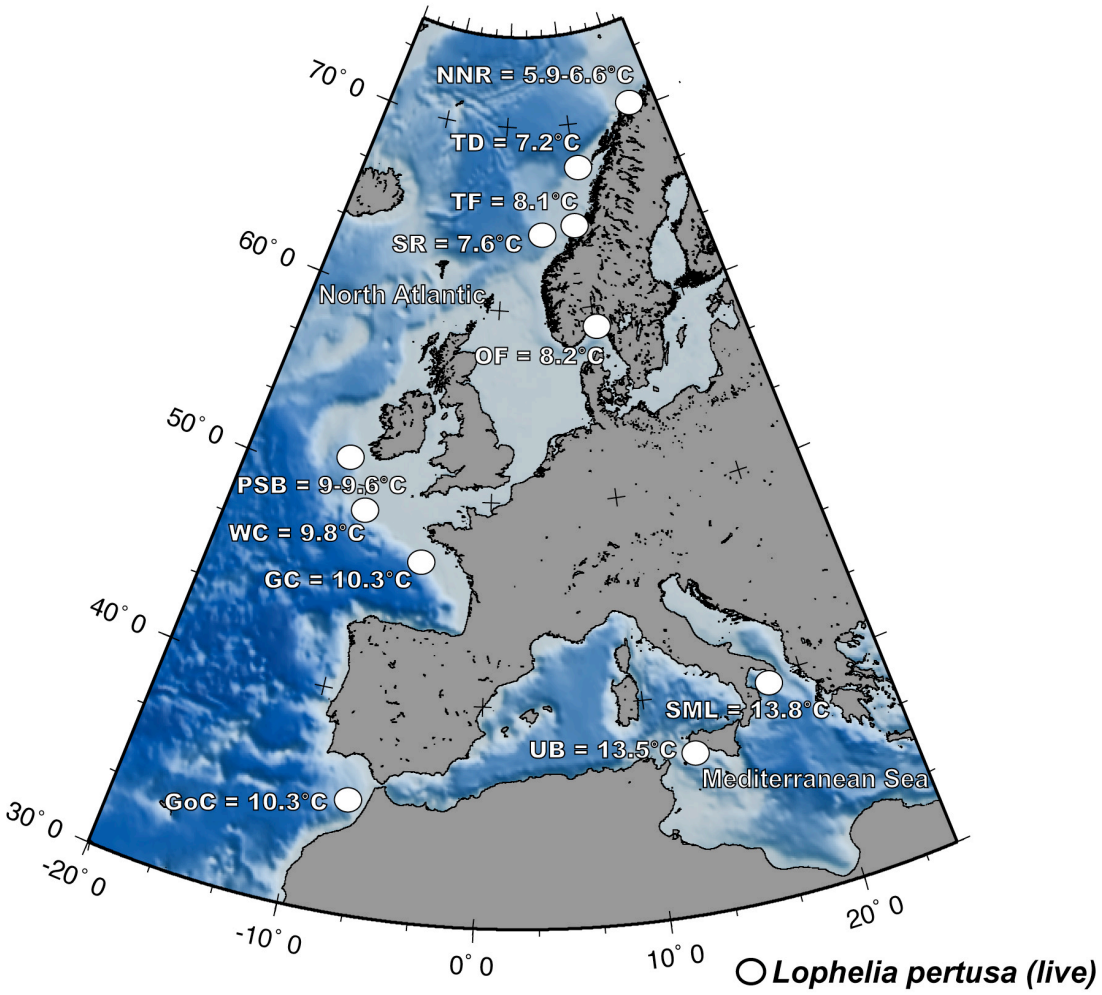

Figure 1: Locations of live-*in situ* sampled scleractinian cold-water coral *Lophelia pertusa* along the European continental margin and average water temperatures. NNR = Northern Norwegian Reefs (Stjernsund, Lopphavet, Sotbakken), TD = Trændadjupet, TF = Trondheimsfjord, SR = Sula Reef, OF = Oslo Fjord, PSB = Porcupine Seabight (Galway Mound, Little Galway Mound, Propeller Mound), WC = Whittard Canyon, GC = Guilvinec Canyon, GoC = Gulf of Cadiz, UB = Urania Bank, SML = Santa Maria di Leuca.

4.2.2 Elemental/Ca measurements

The solutions used for stable strontium isotope measurements were also analyzed for elemental ratios using the ICP-MS (Agilent 7500cs). Elemental/Ca ratios were calculated from the raw counts using the method of Rosenthal et al. (1999). In a first step the Ca concentration was measured and samples were diluted to have ~10 ppm Ca. Six aliquots of *Porites* sp. coral powder reference material JCp-1 (Okai et al. 2002) were treated like samples and the average values obtained during the course of this study (n = 8, including repeated measurements) were Li/Ca 6.15 ± 0.167 mmol/mol, Mg/Ca 4.17 ± 0.026 mmol/mol Sr/Ca

8.76 ± 0.067 mmol/mol and U/Ca 1.190 ± 0.011 mmol/mol. The average Mg/Li ratio was 0.678 ± 0.018 mol/mmol. Based on these results, the reproducibility (2SD) of the analyses was ~1.53 % for Sr, ~1.85 % for U, ~1.25 % for Mg, and 4.07 % for Li and 2.71 % for the Mg/Li ratio. The absolute concentrations measured are within the uncertainties of the recommended values (Okai et al. 2002; Okai et al. 2004).

4.3 Results

Internal variability

One longitudinal mid-plain section of *L. pertusa* (Propeller Mound, POS265-499) was chosen to quantify the range of internal variations of $\delta^{88/86}$Sr and elemental ratios (Sr/Ca, U/Ca, Mg/Li). The test shows an increase in the $\delta^{88/86}$Sr values from 0.166 ± 0.014 ‰ in the inner part (CoC) to 0.203 ± 0.016 ‰ in the outer part of the coral skeleton (Fig. 2). Similarly, the Sr/Ca values of this coral increase from 9.37 ± 0.143 to 9.49 ± 0.145 mmol/mol. Li/Ca and Mg/Ca ratios show a large variability within the skeleton between the theca and the CoC. Li/Ca ratios increase from ~10 to ~17 mmol/mol and Mg/Ca ratios increase from ~3.7 to 5.7 mmol/mol with the highest ratios in the CoC. However, the corresponding Mg/Li ratios show no significant variations (0.315 ± 0.017 mol/mol to 0.333 ± 0.018 mol/mmol; Fig. 2). Four sub-samples within the same *L. pertusa* specimen originating from the Mediterranean Sea (Urania Bank, M70/1-677) show $\delta^{88/86}$Sr values between 0.183 ± 0.011 ‰ and 0.200 ± 0.007 ‰, equal within measurement precision. The mean value of *L. pertusa* from the Mediterranean Sea with 0.193 ± 0.01 ‰ is slightly higher than the mean value of 0.188 ± 0.02‰ for *L. pertusa* from the Porcupine Seabight (Propeller Mound, Fig. 2).

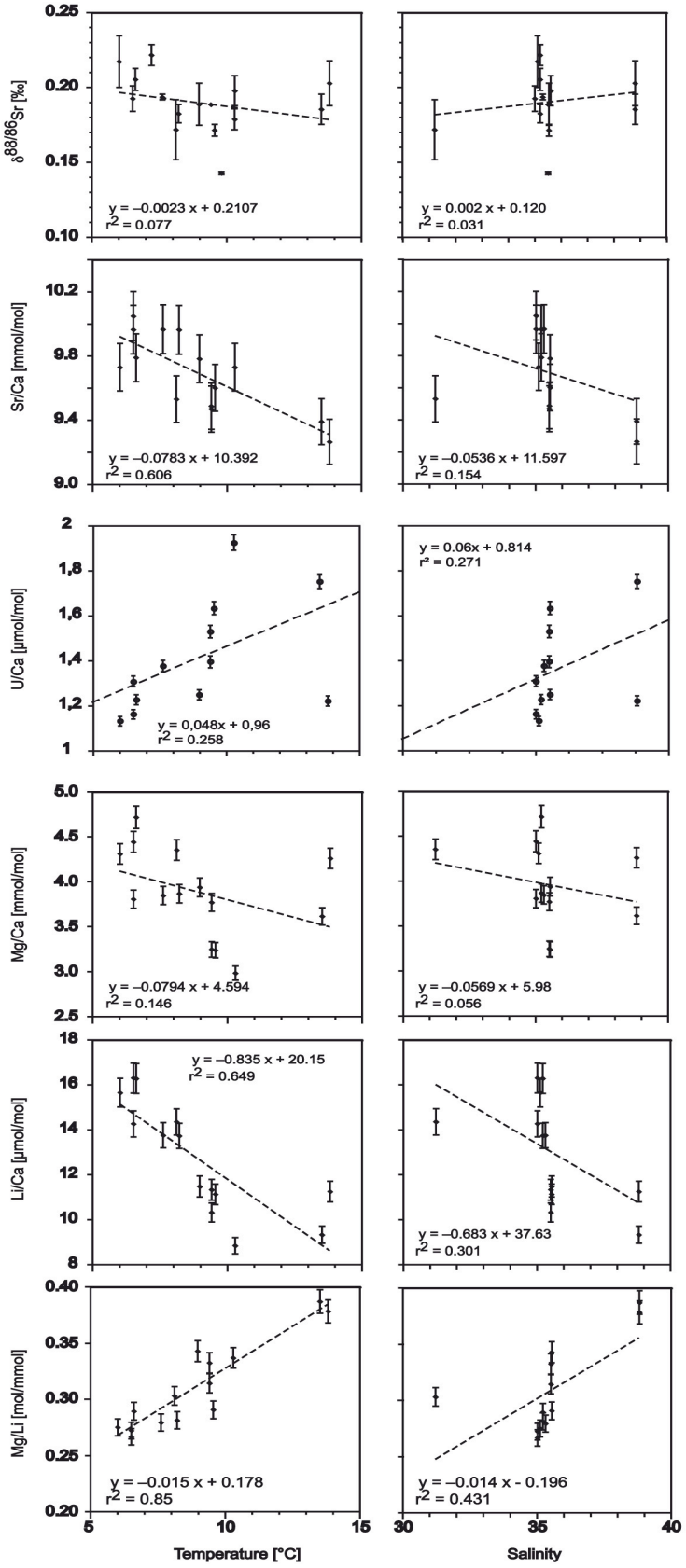

Figure 3: Temperature and salinity dependence of $\delta^{88/86}$Sr, Sr/Ca, Mg/Ca, Li/Ca and Mg/Li ratios in *Lophelia pertusa* indicate that only a weak correlation to salinity exists for Li/Ca ($r^2 = 0.30$) and Mg/Li ($r^2 = 0.43$), while strong correlations to temperature can be found with Sr/Ca ($r^2 = 0.61$), Li/Ca ($r^2 = 0.65$) and Mg/Li ($r^2 = 0.85$).

Temperature

The habitats of *L. pertusa* analyzed in this study cover a large temperature range for cold-water corals, 5.9 °C to 13.8 °C (Fig. 1). Sr/Ca ratios vary from 9.27 mmol/mol at 13.8°C in the Mediterranean Sea to 10.05 mmol/mol at 6.5°C in the northern reefs (Lopphavet). The Sr/Ca ratios show a significant negative linear correlation with temperature ($r^2 = 0.61$, $p = 0.0007$; Fig 3.)

$$\text{Sr/Ca (mmol/mol)} = -0.078 \pm 0.04\ T\ (°C) + 10.39 \pm 0.39 \qquad \text{Eq. (1)}$$

The U/Ca ratios display large variations from 1.06 to 1.92 mmol/mol and are not significantly related to temperature ($r^2 = 0.258$, $p = 0.13$). The Mg/Ca ratios vary from 2.99 to 4.72 (mmol/mol) and also do not have a significant relationship with temperature ($r^2 = 0.146$, $p = 0.18$; Fig. 6). The Li/Ca ratios vary from 8.86 to 16.32 (mmol/mol) and exhibit a significant correlation ($r^2 = 0.65$, $p = 0.005$) with temperature. The Mg/Li ratios were calculated from the measured Li/Ca and Mg/Ca ratios and vary from 0.27 mol/mmol at low temperatures (5.9°C) to 0.39 mol/mmol at the highest temperature at Santa Maria di Leuca (13.8°C). This results in a positive linear correlation with temperature ($r^2 = 0.84$, $p = 0.00001$; Fig. 5) that can be described by the following equation:

$$\text{Mg/Li (mol/mmol)} = 0.015 \pm 0.004\ T\ (°C) + 0.178 \pm 0.04 \qquad \text{Eq. (2)}$$

The stable strontium isotope composition of the entire sample set ranges from 0.143 ± 0.001 ‰ to 0.226 ± 0.006 ‰ (Table 1). Samples from the Stjernsund grew under the lowest temperatures (5.9°C) and have an average $\delta^{88/86}$Sr value of 0.217 ± 0.017 ‰. Samples from the Mediterranean Sea grew at 13.5 to 13.8°C, the highest water temperatures in our sample set, and the $\delta^{88/86}$Sr of these samples is 0.183 ± 0.011 ‰ and 0.203 ± 0.015 ‰. The three samples from the Porcupine Seabight originate from carbonate mounds (Propeller Mound, Galway Mound and Little Galway Mound). They grew at ~9.5 °C and show a mean $\delta^{88/86}$Sr value of 0.190 ± 0.024 ‰. The *L. pertusa* sample from Whittard Canyon at 9.79°C is marked by the lowest $\delta^{88/86}$Sr value of 0.143 ± 0.001‰. A weak ($r^2 = 0.55$, $p = 0.04$), but significant inverse relationship with temperature is found for samples that grew between 5.9 and 9.79°C originating from the North Atlantic by averaging the mean $\delta^{88/86}$Sr value for each location (Fig. 4 and 5):

$$\delta^{88/86}Sr\ [‰] = -0.011 \pm 0.11\ T\ [°C] + 0.282 \pm 0.1 \qquad \text{Eq. (3)}$$

Salinity

The $\delta^{88/86}$Sr, Sr/Ca, U/Ca, Mg/Ca and Li/Ca ratios do not show any significant correlation with salinity (Fig. 3), across the large range from 31.2 in the Trondheimsfjord up to 38.8 in the Mediterranean Sea. The Mg/Li record shows a weak positive correlation with salinity (r^2=0.43, Fig 3), which might be due to the correlation between temperature and salinity (r^2=0.71).

4.4 Discussion

4.4.1 Microscale distribution of $\delta^{88/86}$Sr, Sr/Ca and Mg/Li ratios in *Lophelia pertusa*

In the cross section of the *L. pertusa* skeleton from the Propeller Mound we observe some variability of $\delta^{88/86}$Sr and Sr/Ca (Fig. 2). In particular, the $\delta^{88/86}$Sr values show a trend towards higher values from the inner (older) to the outer (younger) part (Fig. 2). Temperature variations of ~1°C within the coral were calculated from Sr/Ca ratios with the equation of Cohen et al. (2006), which has a sensitivity of 0.18 mmol/mol/C°. Mg/Li ratios also show similar corresponding temperature variations of <1°C (see section 4.4.2).

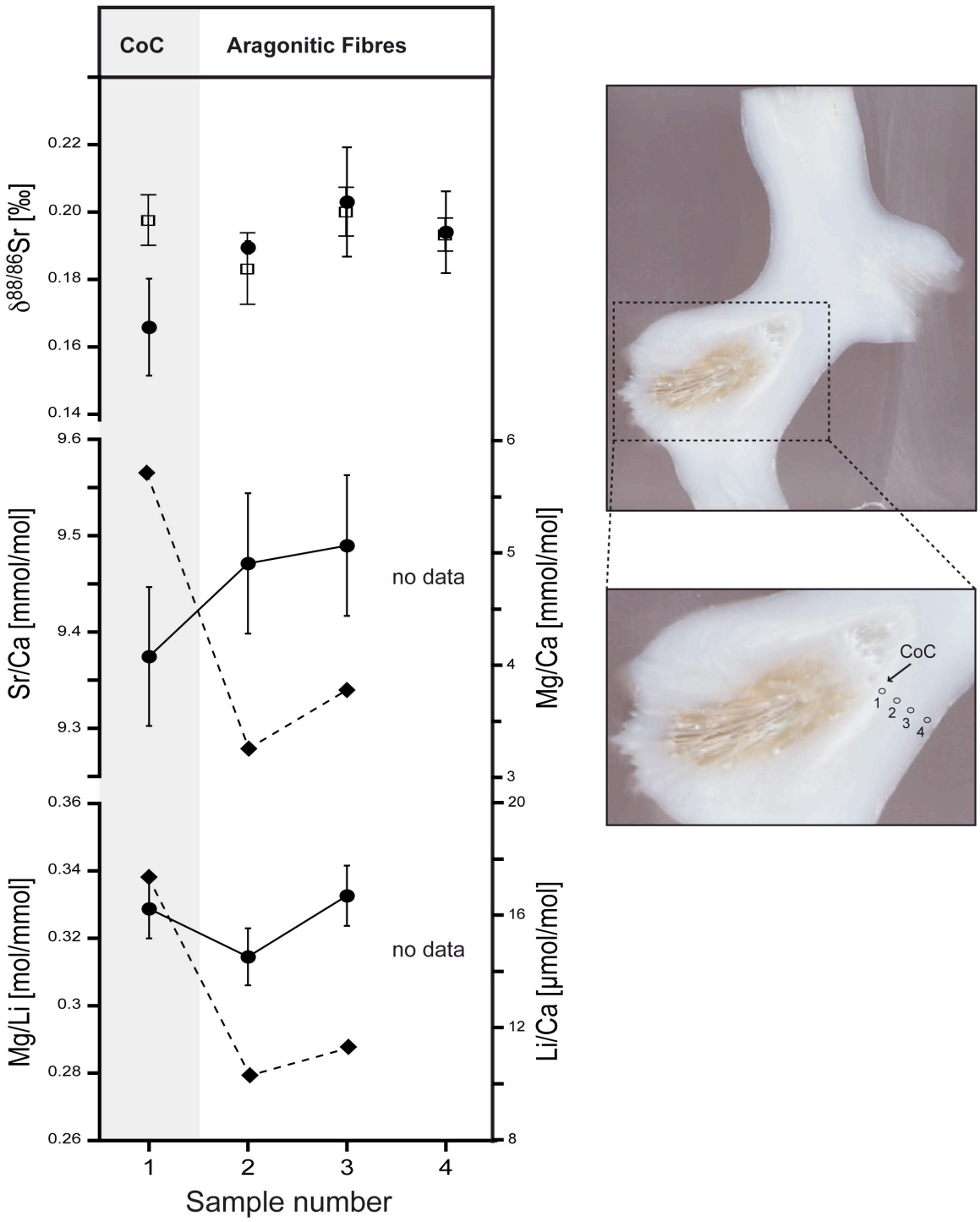

Figure 2: Intra-individual heterogeneity test of $\delta^{88/86}$Sr, Sr/Ca, Mg/Ca, Li/Ca and Mg/Li compositions in a *Lophelia pertusa* specimen from Propeller Mound (open squares in $\delta^{88/86}$Sr from Urania Bank, Mediterranean Sea). The longitudinal section of the Propeller Mound specimen shows the internal architecture of the skeleton. The $\delta^{88/86}$Sr, Mg/Ca and Li/Ca are significantly different at the Centers of Calcification (CoC) compared to the aragonitic theca fibers, whereas Sr/Ca and Mg/Li are equal within measurement uncertainty. Diamonds correspond to Mg/Ca and Li/Ca ratios. Error bars for Mg/Ca and Li/Ca are smaller than the dots. Error bars correspond to 2sem for $\delta^{88/86}$Sr and 2SD for the elemental ratios.

Generally, Sr/Ca ratios measured in the aragonitic fibres apart from the CoC of *Desmophyllum dianthus* correlate with temperature (Gagnon et al. 2007). The same holds true for stable Sr isotopes in *L. pertusa* (Rüggeberg et al. 2008) and Mg/Li ratios in the same species and other scleractinian cold-water corals (Montagna et al. 2008; Case et al. 2010). The apparent temperature variability highlights Sr/Ca and Mg/Li as paleothermometer by comparison with the annual temperature variability of 1.5°C at a water depth of ~800 m in the PSB (Levitus et al. 1994). Stable strontium difference within *L. pertusa* from Propeller Mound may also reflect variations in temperature, considering the temperature sensitivity of 0.026 ‰/C° (Rüggeberg et al. 2008). However, in our study the temperature sensitivity of $\delta^{88/86}$Sr is inverse and weaker than half of the reported positive correlation with -0.011 ‰/C°(see chapter 4.4.2, Fig. 4 and 5). This increases the reconstructed variability to ~3°C, with a tendency towards colder temperatures than expected. However, Mediterranean *L. pertusa* (Urania Bank) do not display a distinct internal-individual variability of $\delta^{88/86}$Sr. This lack in $\delta^{88/86}$Sr variance throughout the inner to the outer theca suggests very low annual temperature variability consistent with the reported annual temperature variability of the Mediterranean Sea intermediate water (Levitus et al. 1994).

Several studies have tried to explain the variability of elemental ratios between the CoC and the aragonitic fibres (Case et al., 2010; Rollion-Bard et al. 2009) by different geochemical models. Case et al. (2010) highlighted that the microscale distribution of Mg and Li is consistent with a Rayleigh fractionation as suggested by (e.g. Cohen et al. 2006; Gaetani & Cohen 2006; Gaetani et al. 2011). By contrast, Rollion-Bard et al. (2010) concluded that Amorphous Calcium Carbonate (ACC) is responsible for the observed variability in elemental ratios. Also our data shows increased Mg/Ca and Li/Ca ratios in the CoC (Figure 2), but nearly constant Mg/Li ratios as seen by Case et al. (2010). However, from our data we cannot exclude or confirm any previously mentioned geochemical models for coral skeletogenesis. But our results indicate that any process that increases the Mg/Ca and Li/Ca ratios is minimized in the Mg/Li ratio.

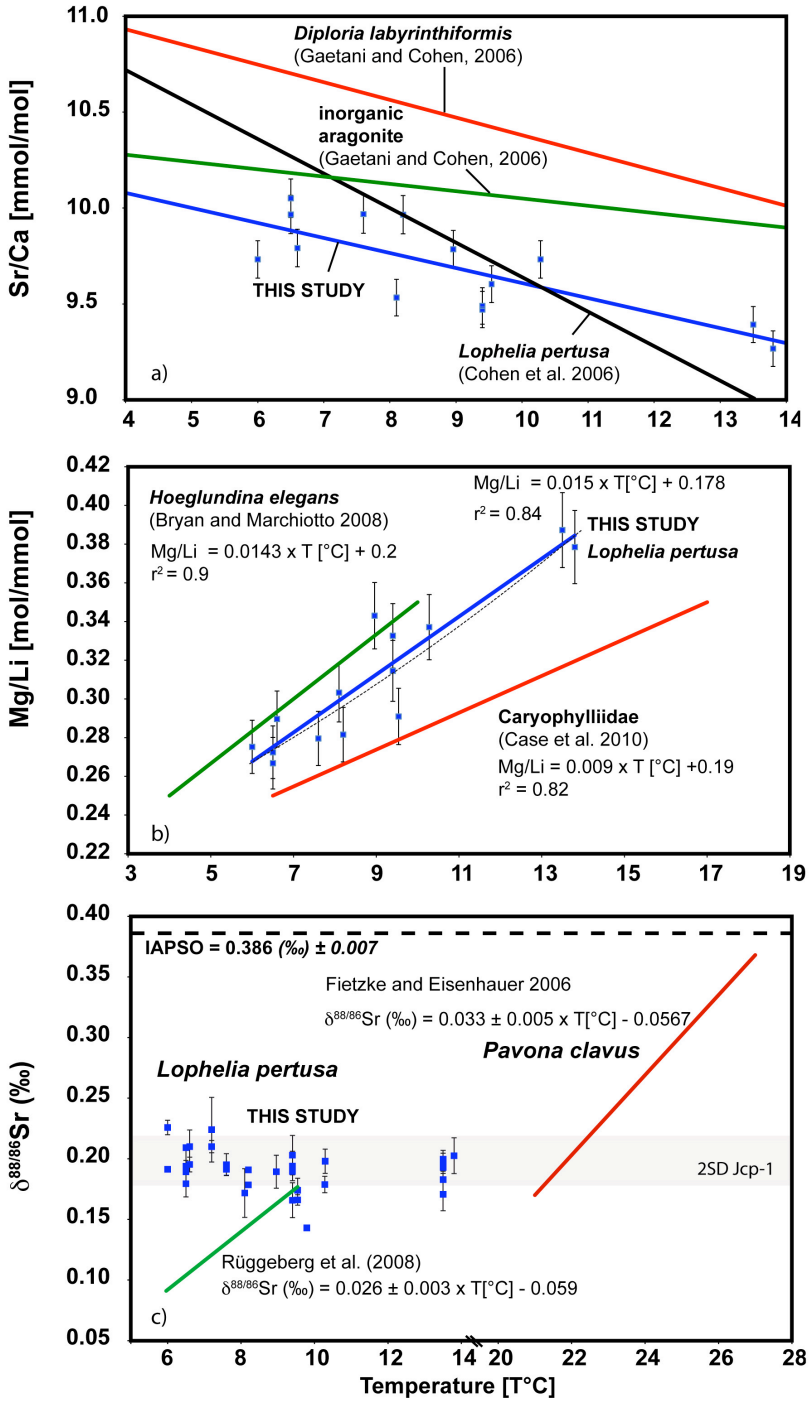

Figure 5: $\delta^{88/86}$Sr, Mg/Li and Sr/Ca ratios measured in scleractinian cold-water coral *Lophelia pertusa* from different Locations with varying water temperatures 6–14°C, *blue squares = Porcupine Seabight, green squares = Norwegian Sea, purple squares = Bay of Biscay, yellow squares = Gulf of Cadiz, red squares = Mediterranean Sea* **a)** Sr/Ca-temperature dependence of this study is compared to *Diploria labyrinthiformis* (Sr/Ca = –0.092 ± 0.001 (T°C) + 11.30 ± 0.03, Gaetani and Cohen 2006) and abiogenic aragonite (Sr/Ca = –0.038 ± 0.004 (T°C) + 10.43 ± 0.19; r^2 = 0.95) and *L. pertusa* (Sr/Ca = –0.18 ± 0.002 (T°C) + 11.44 ± 0.011, r^2 = 0.78, Cohen et al. 2006). Slopes are extrapolated. **b)** Mg/Li ratios of *L. pertusa* lie between the slopes of the aragonitic foraminifera *Hoeglundina elegans* (Bryan and Marchitto 2008) and scleractinian cold-water corals (Case et al. 2010).

Dashed line indicates a possible exponential fit to the data, Mg/Li = $0{,}204e^{0{,}046T}$ (r^2=0,83) c) All $\delta^{88/86}$Sr values determined with the DS-TIMS technique compared to $\delta^{88/86}$Sr measured in scleractinian cold-water coral *L. pertusa* (Rüggeberg et al. 2008) and the tropical coral *Pavona clavus* (Fietzke and Eisenhauer 2006), both determined with the bracketing standard method. IAPSO $\delta^{88/86}$Sr seawater value corresponds to 0.386 ± 0.007 ‰ 2SEM (Liebetrau et al. 2009; Krabbenhöft et al. 2009). The reproducibility of $\delta^{88/86}$Sr for the JCp-1 measured in the course of this study (n = 9) ± 0.019‰ (2SD) is indicated with the grey bar covers more than the half of the entire variations of $\delta^{88/86}$Sr values.

4.4.2 Temperature dependency of geochemical signals in *Lophelia pertusa*

$\delta^{88/86}Sr$

The stable strontium isotope system was introduced by Fietzke & Eisenhauer (2006) as a potential paleothermometer measured in the scleractinian warm-water coral *Pavona clavus*. Subsequently, Rüggeberg et al. (2008) analysed stable strontium isotopes in the cold-water coral *L. pertusa* to develop a potential new proxy for the reconstruction of intermediate ocean water temperatures. They used some of the same *L. pertusa* samples from the European continental margin as this study (Table 1). Here we employ the DS-TIMS method by Krabbenhöft et al. (2009) with a factor of 2–3 improved precision compared to the standard-bracketing MC-ICP-MS method.

The $\delta^{88/86}$Sr values from lower temperature locations on the Norwegian Sea, Irish Margin and Bay of Biscay (6–9.8°C) exhibit on the contrary an inverse correlation to temperature with a slope of -0.011‰/°C ($r^2 = 0.5$ p= 0.04; Fig. 4, Eq.3). This is in direct contrast to the findings of Rüggeberg et al. (2008) who found a strong positive linear relationship of 0.026‰/°C across the temperature range of 5.9 to 9.54°C (Fig. 5) in Atlantic corals between 70°N and 51°N. This discrepancy in the observed stable strontium isotope fractionation in scleractinian cold-water coral *L. pertusa* may be explained by the different measurement methods. On top of the improved precision, the double spike technique also would account for any fractionation during the ion chromatographic Sr separation and the chemical preparation (Krabbenhöft et al. 2009).

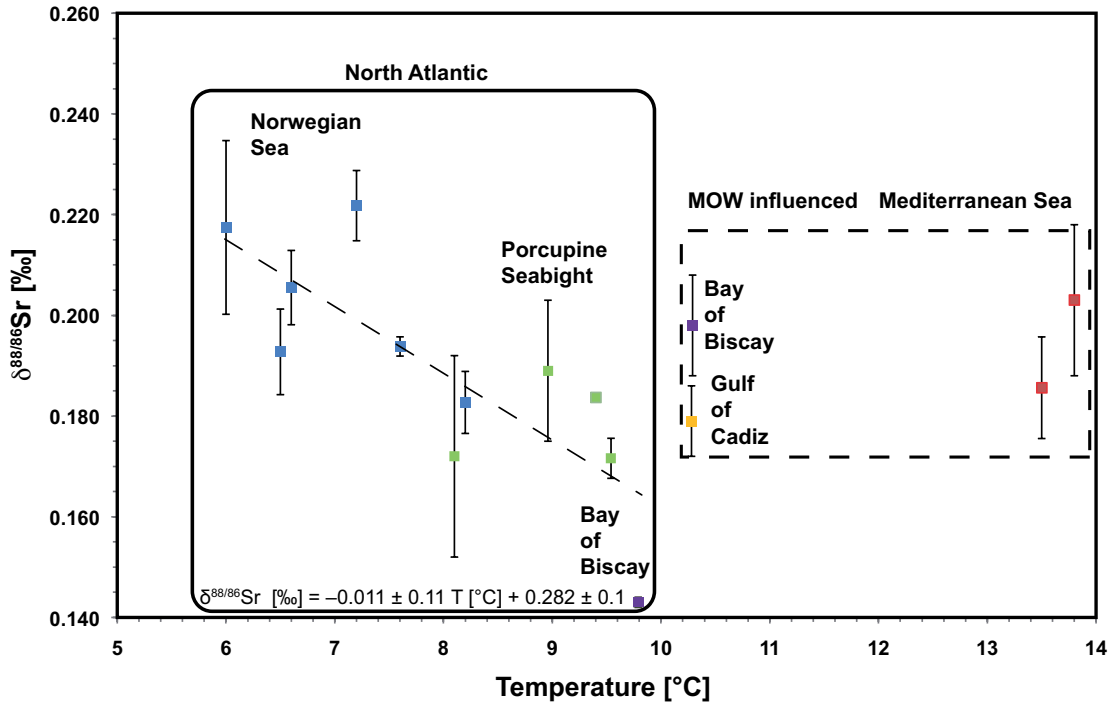

Figure 4: Temperature dependence of weighted mean $\delta^{88/86}$Sr values of each Atlantic location in *Lophelia pertusa* between 6 and 10°C shows a weak but significant correlation (–0.011‰/°C, $r^2 = 0.55$, p= 0.04), whereas weighted mean $\delta^{88/86}$Sr values above 10°C from the Guilvinec Canyon, the Gulf of Cadiz and the Mediterranean Sea show no correlation to temperature.

Additional to Atlantic samples, we also measured *L. pertusa* samples from sites with temperatures >10°C, deriving from the Mediterranean Sea, the Gulf of Cadiz and the Bay of Biscay. These samples show no temperature trend in their isotopic composition compared to the samples from the Irish and Norwegian margins (Fig 4). Possible explanations for this lack in temperature dependence of stable strontium isotope fractionation in *L. pertusa* (>10°C, high salinity) are, 1) differences in growth or calcification rates, 2) diagenetic secondary aragonite or 3) carbonate seawater chemistry. Several studies showed from sites on the Norwegian Margin and the northern North Sea that *L. pertusa* polyps grow and calcify faster in a juvenile than in an adult stage (Gass and Roberts 2010; Maier et al. 2009; Mortensen and Rapp 1998).

Several studies on warm-water corals demonstrated that diagenetic secondary aragonite has a different trace element composition than the primary aragonite with higher Sr and U but lower B, Mg and S contents (Allison et al. 2007; Enmar et al. 2000; Hathorne et al. 2011; Hendy et al. 2007; Lazar et al. 2004). One study found indications of early diagenesis in a sub-recent,

100-200 year old *L. pertusa* (Pons-Branchu et al. 2005). Considering that we exclusively sample theca material of living specimens we can exclude both the presence of secondary precipitates, as well as diagenesis. Strontium has a seawater residence time of ≥4 Ma, this is very long compared to the mixing rate of the oceans (~1000 years) and hence the oceans are well mixed with respect to Sr isotopes (McArthur 1994; Veizer 1989). These findings are supported by first results of Liebetrau et al. (2009) showing that the $\delta^{88/86}$Sr of seawater is homogeneous 0.386 ± 0.007 ‰ at least for the North Atlantic, the Gulf of Cadiz and the Mediterranean.

The $\delta^{88/86}$Sr values of the entire sample set as well as in the internal architecture of *Lophelia* show a significant inverse relationship to the U/Ca ratios (Fig 6). This suggests that U/Ca and $\delta^{88/86}$Sr are controlled by similar processes. Anagnostou et al. (2011) and Inoue et al. (2011) highlighted that the U/Ca ratio in scleractinian corals are primarily controlled by changes in pH and/or carbonate ion concentration of seawater. Coral calcification increases with increasing carbonate ion concentrations (Gattuso et al. 1998). Hence one possible explanation for the obtained U/Ca-$\delta^{88/86}$Sr relationship might be a secondary growth rate effect on the stable strontium isotope fractionation. According to Anagnostou et al. (2010), our U/Ca values result in CO_3^{2-}-seawater concentration between 80 - 130 mmol/kg, which appears to be reasonable. However, the study of Anagnostou et al. (2011) used *Desmophyllum dianthus* for their calibration. Hence we have to consider this relationship with caution. Moreover, the obtained U/Ca-$\delta^{88/86}$Sr relationship here may be multidimensional and should be tested with inorganic precipitation experiments.

However, we suggest that $\delta^{88/86}$Sr in scleractinian cold-water coral *L. pertusa* is only weakly controlled by temperature and internal variations of $\delta^{88/86}$Sr are probably also affected by vital effects. Moreover, we suggest that the stable strontium isotopes in scleractinian cold-water corals are related to carbonate ion concentrations and/or pH of seawater and may hence provide additional and independent constraints on the coral physiology that will be studied in future investigations.

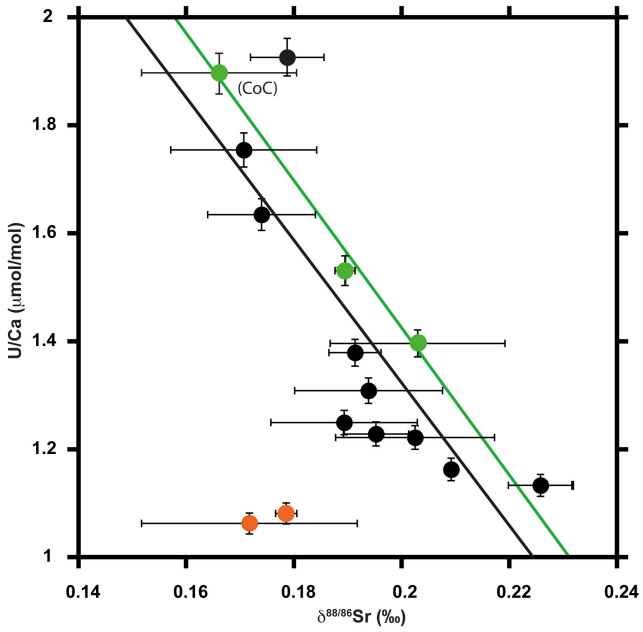

Figure 6: $\delta^{88/86}$Sr and U/Ca of Atlantic and Mediterranean samples (black dots) reveal a significant linear correlation even in the internal microscale of *Lophelia* (green dots), while inshore samples (red dots) from Oslofjord and Trondheimsfjord form outliers. The offset is probably caused by different seawater U/Ca ratios and/or different seawater carbonate chemistry in the fjords. The obtained relationship can be described by the following equation: U/Ca (mmol/mol) = -17.83* $\delta^{88/86}$Sr + 4.882 (r^2 = 0.65).

Sr/Ca ratios

Several studies have shown that the Sr/Ca ratios of inorganic aragonite and aragonitic coral skeletons decrease with increasing water temperature (e.g., Beck et al. 1992; Cohen et al. 2002, Gaetani and Cohen 2006; Kinsman and Holland 1969; Smith et al. 1979). However, the temperature effect on Sr/Ca in biogenic aragonite is up to three times stronger than in inorganic aragonite (Cohen et al. 2006). Cohen et al. (2002) suggested that Sr/Ca ratios measured in azooxanthellate corals are primarily controlled by variations in seawater temperature, whereas the Sr/Ca ratio measured in zooxanthellate corals are largely biologically controlled. Cohen et al. (2006) found a temperature dependency of Sr/Ca in *L. pertusa* grown at 129 m depth at Tisler Reef, Norwegian Margin. However, the observed amplitude of the Sr/Ca variability is too large to be solely explained by temperature (Cohen et al. 2006). These findings are in line with other studies introducing a note of caution by relating Sr/Ca ratios in scleractinian corals to vital or kinetic effects (Montagna et al. 2005; Shirai et al. 2005). Nevertheless, our set of *L. pertusa* samples shows a significant Sr/Ca-temperature relationship (Fig. 5, Eq. 1). This Sr/Ca-temperature relationship exhibits a different slope compared to Cohen et al. (2006). Our data displays that the temperature sensitivity is similar compared to that of the zooxanthellate coral *Diploria labyrinthiformis* (Fig. 5). Therefore, Sr/Ca ratios in *L. pertusa* may serve as a potential proxy for seawater temperatures with an accuracy of ± 1°C.

Mg/Li ratios

In scleractinian corals Mg/Ca ratios are only partly controlled by temperature (Fig. 3) and are strongly affected by coral calcification rates (Cohen et al. 2006). On the other hand, Marriott et al. (2004) demonstrated that Li incorporation in the warm-water coral *Porites* is controlled by temperature. The Mg/Li ratio have been introduced as a potential temperature proxy by Bryan and Marchitto (2008), who showed that Mg/Li ratios in the aragonitic foraminifera *Hoeglundina elegans* are strongly correlated to temperature (Fig. 5). Case et al. (2010) demonstrated a similar temperature-dependency of Mg/Li ratios in scleractinian cold-water corals, whereas Montagna et al. (2008) highlighted an exponential depedendency of Mg/Li ratios in scleractinian corals (Fig. 5).

However, they showed both that neither salinity nor carbonate ion concentration control the Mg/Li ratios. Using traditional sampling techniques Mg/Li correlates with temperature in various scleractinian corals from different ocean basins with $r^2 = 0.62$ for all investigated species and with $r^2 = 0.82$ for the family Caryophylliidae (Case et al. 2010). Our results confirm the potential of Mg/Li ratios as a paleothermometer in cold-water corals. In particular, our dataset is the first extensive examination of *L. pertusa* samples using traditional techniques, revealing a temperature sensitivity of 0.015 mol/mmol/°C for Mg/Li (Eq.2) similar to the Caryophylliidae slope of Case et al. (2010) (0.009 mol/mmol/°C). Although it is important to consider potential differences in calibration between data from two different laboratories (e.g. Greaves et al. 2005) the two coral species for which Mg/Li calibrations now exist display an offset of 0.02 mol/mmol at 5.9°C and 0.06 mol/mmol at 13.8°C, suggesting a potential species dependent offset and/or minimal vital effect. The scatter in the Mg/Li record of *L. pertusa* is smaller compared to the Sr/Ca ratios, but may still restrict temperature reconstructions. Using the temperature dependence of 0.015 ± 0.004 mol/mmol/°C and the precision of 2.71% (2σ) temperature variations larger than ~2°C can be reconstructed with 95% confidence.

4.5 Conclusions

This study investigated the potential of the scleractinian cold-water coral *L. pertusa* to serve as an archive for intermediate water temperatures using geochemical proxies such as $\delta^{88/86}$Sr, Sr/Ca and Mg/Li ratios. Results of earlier studies of $\delta^{88/86}$Sr could not be confirmed and no simple positive linear temperature dependency was found for *L. pertusa*. With the higher precision of the Double-Spike-TIMS technique compared to bracketing standard MC-ICP-MS, it was not possible to confirm the findings of Rüggeberg et al. (2008) by measuring the

isotopic composition of some of the same samples. We found that the $\delta^{88/86}$Sr and temperature is inversely correlated between 5.9 and 9.79°C in the north Atlantic. Moreover, we suggest that $\delta^{88/86}$Sr of cold-water corals is also dependent on seawater carbonate chemistry. However, observed $\delta^{88/86}$Sr variations are close to the measurement precisions and should therefore be interpreted with caution.

Our measurements of elemental ratios such as Sr/Ca and Mg/Li support earlier studies in showing significant temperature relationships that may form the basis for paleotemperature proxies. The scatter in the *L. pertusa* Sr/Ca data, however, severely limits the use as a paleotemperature proxy and further studies are needed to analyse Sr/Ca ratios at micrometre-scale in multiple specimens. In contrast, the scatter of the Mg/Li record in *L. pertusa* is smaller showing the promise of Mg/Li ratios as a more reliable paleotemperature proxy for new perspectives to reconstruct past intermediate water dynamics.

4.6. Acknowledgements

The authors gratefully thank all captains, crews and cruise scientists involved in this study. Claudia Wienberg is gratefully acknowledged for providing some of the coral samples from the Gulf of Cadiz, and Marco Taviani kindly provided the Apulian Bank corals. This work has been made possible thanks to the support from DFG [TRISTAN and ISOLDE (Du 129/37 and Du 129/45 I +II)]. AF and MLC acknowledge funding from the EU-FP VII HERMIONE project (Contract number 226354). Additionally, we would like to thank Folkmar Hauff, Ana Kolevica and Jutta Heinze for their Lab-support.

Chapter V

Control mechanisms of long-term cold-water coral mound growth in the Porcupine Seabight

Based on*: Control mechanisms of long-term cold-water coral mound growth in the Porcupine Seabight***.** Jacek Raddatz, Andres Rüggeberg, Volker Liebetrau, Anneleen Foubert, Ed Hathorne, Anton Eisenhauer, Jan Fietzke, Dirk Nürnberg, and Wolf-Christian Dullo (in preparation for submission)

Abstract

The IODP Expedition 307 made it possible for the first time to investigate the entire sediment body of a 155m high cold-water coral carbonate mound. Here we provide new insights into the long-term history of Challenger Mound on the European continental margin off Ireland. This study is based on age determinations ($^{230}Th/^{234}U$, $^{87}Sr/^{86}Sr$-Strontium Isotope Stratigraphy (SIS)) and geochemical signals from different archives such as scleractinian cold-water corals *Lophelia pertusa* (Mg/Li, Ba/Ca) as well as benthic (*P. ariminensis*) and planktonic (*G. bulloides*) foraminifera (Mg/Ca, $\delta^{13}C$) from IODP Site 1317 in the Porcupine Seabight. Earlier studies revealed that the Challenger Mound is characterized by mainly two different episodes of growth, M1 the fast initial rapid development and M2 the slower episode. Our additional age constraints indicate that mound initiation already occurred at ~3 Ma due to the simultaneous intensification of Mediterranean Outflow Water (MOW). Bottom-Water-Temperatures (BWT) reconstructed with *P.ariminensis* - Mg/Ca ratios and *G.bulloides* - $\delta^{13}C$ ratios indicate that the rapid mound growth in M1 may have benefited from less intense glacial conditions. Moreover these periods were dominated by sea-surface waters from northern origin leading to an increased sea-surface productivity in the Porcupine Seabight. Moreover, paleoceanographic reconstructions based on *Lophelia*-Mg/Li and Ba/Ca ratios reveal that coral growth in the Porcupine Seabight was restricted to a narrow temperature envelope between 7.8-9.3°C and enhanced nutrient supply. We interpret this as an interconnection between growth and the boundary layer between MOW and the Eastern

North Atlantic Water (ENAW). The build up of a stable water mass stratification between ENAW and MOW caused enhanced nutrient supply and facilitated a steady and rapid mound growth between 3.0 and 1.5 Ma. During the late Pleistocene, the last 0.5 Ma, mound growth was restricted to interglacial periods since environmental conditions became obviously unfavourable for cold-water corals to grow during glacials. Finally, from our data we suggest that the demise of Challenger Mound growth is caused by its own growth beyond the range of optimal conditions and a possible long-term lowering of the ENAW/MOW boundary.

5.1 Introduction

During the last two decades significant efforts have been made to explore deep-sea coral ecosystems. In contrast to their tropical counterparts, these scleractinian corals are thriving in deep, cold and nutrient-rich waters. The most common reef-building cold-water coral is the heterotrophic, filter-feeding and azooxanthellate *Lophelia pertusa*. The appearance of *L. pertusa* is controlled by environmental parameters such as temperature, current strength, nutrient availability, and the density of seawater (Dullo et al. 2008; Freiwald et al. 2004, Roberts et al. 2006; Rüggeberg et al. 2007). The continental slopes along the European margin are frequently covered by *Lophelia*-reefs (Roberts et al. 2006; Freiwald et al. 2004). They occur from northern Norway in the Barents Sea (70°N, Lindberg et al. 2007) to NW Africa off Mauritania (16°N, Colman et al. 2005). On the Norwegian margin large flourishing reefs developed after the retreat of the glaciers (Fosså et al. 2005; Freiwald et al. 2004). The margin southwest of Ireland represents one major region of abundant carbonate mounds associated to cold-water coral growth. These mounds tend to cluster in provinces (De Mol et al. 2007; Freiwald et al. 2004) and vary in height from a few meters up to > 380 m (Wheeler et al. 2007). A coral mound can vary strongly in appearance. However, the framework of a vivid coral ecosystem is often dominated by cold-water corals such as *L. pertusa* and *Madrepora oculata* (Foubert et al. 2005).

The Porcupine Seabight (PSB) is characterized by different mound provinces with over 1000 buried and exposed mounds (Huvenne et al. 2007). In particular the Belgica Mound province is one of these five mound provinces (De Mol et al. 2002; Foubert et al. 2005; Wheeler et al. 2011) and the Challenger Mound is one of 66 mounds in this province. Within the Belgica Mound Province, the coral mounds are elongated, subconical structures and occur in depth between 600 and 1000 m corresponding to the transition zone of Eastern North Atlantic Water (ENAW) and the underlying Mediterranean Outflow Water (MOW). The ENAW originates in the Bay of Biscay and the MOW in the Mediterranean Sea, both streaming

poleward into the Porcupine Seabight (Figure 1, Pollard et al. 1996; White 2007). Topographically steered by the slope in the north of this unique amphitheatre shaped embayment, these water masses change into a flow direction to the southwest. Due to the large differences in density between the MOW and ENAW a pycnocline forms at around ~800 m (Dullo et al. 2008). Here, corals benefit from organic matter that settles from the sea surface and from high current velocity of > 15 cm/s. Whereas, the study of Purser et al. (2010) demonstrated that *L. pertusa* polyps capture more efficiently zooplankton under slow flow velocities with about 5 cm/s. However, internal waves might be responsible for a general steady supply of nutrients into the mound regions (White 2007; Kiriakoulakis et al. 2007). These specific hydrodynamic conditions facilitate a region of dense cold-water coral SW of Ireland (De Mol et al. 2002; Kano et al. 2007).

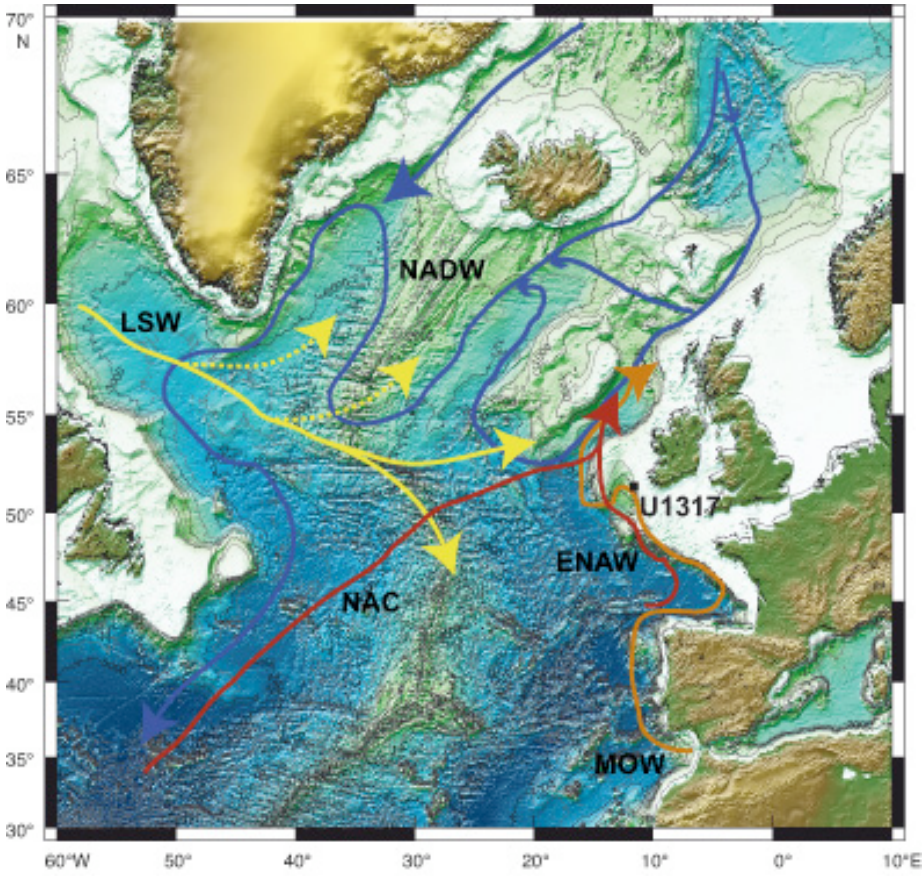

Figure 1: Map showing the North Atlantic with the core location of IODP Site U1317 in the Porcupine Seabight (PSB). The orange arrow indicates the flow of the Mediterranean Outflow Water (MOW), the red arrow of the Eastern North Atlantic Water (ENAW) and the North Atlantic Current (NAC), the yellow arrow marks the flow path of the Labrador Seawater (LSW) and the blue arrows of the North Atlantic Deep Water (NADW).

5.1 The Challenger Mound (IODP Site 1317)

In 2005 the IODP Expedition 307 drilled for the first time complete records through the entire sediment body of the 155 m high Challenger Mound, located in the Porcupine Seabight (52°23'N, 11°43'W; ~ 800 m below sea level, Figure 1). The recovered sediment cores contained mainly the scleractinian cold-water coral *L. pertusa* and only to a minor degree *M. oculata*. The lithic components consist of clay, fine silt and sand near the mound base. The mound is situated on top of an unconformity with a Miocene age of up to 16.58 Ma (Louwye et al. 2007; Kano et al. 2007). The Sedimentary record of the Challenger Mound can be subdivided into the two units: M1 between 155 and 22.98 m below seafloor (mbsf) and M2 between 22.98 and 0 mbsf for Hole 1317 E. The presence of corals throughout the mound sequence made it possible to state that corals played the major role in the initiation of mound growth and further development (Williams et al. 2006, Fig.2). Paleoenvironmental reconstruction clearly showed that carbonate mound growth in the PSB was restricted to interglacial periods for the late Pleistocene (Dorschel et al. 2005; Eisele et al. 2008; Rüggeberg et al. 2007). Regarding the Challenger Mound stratigraphic work carried out by Kano et al. (2007, Strontium Isotope Stratigraphy (SIS)) showed that mound growth initiated at ~ 2.6 Ma, whereas ages based on magnetostratigraphy point to an earlier onset at ~ 2.9Ma (Foubert and Henriet 2009). Nevertheless, both studies recognized a significant hiatus at around 23.6 mbsf in IODP Site 1317 hole E. This major hiatus separates the mound record into a period of fast (2.6–1.7 Ma = M1) and slower mound growth (1.0–0.5 Ma = M2, Figure 2).

First settlement of cold-water coral larvae and mound formation occurred in times of intensified Northern Hemisphere Glaciation (Kleiven et al. 2002) ~ 2.6 Ma ago (Kano et al. 2007). Generally the amplitude in interglacial/glacial cycles amplified during the last 2.6 Ma and climatic conditions and variations between 2.6 and 1.7 Ma were not as extreme as during the last interglacial/glacial cycles (Lisiecki & Raymo 2005). Early development of Challenger Mound during M1 was fast and rather continuous (Mound Booster Stage) and hence may indicate that environmental conditions until 1.7 Ma were favourable for cold-water corals growth (Kano et al. 2007). The period of fast initial mound development in the early Pleistocene was characterized by weak sea-level fluctuations caused by the low-amplitude 41-ka cycle. The most recent interglacial/glacial cycles were affected by a 100-ka cycle, characterized by changes in sea level of ~120 m (Lisiecki & Raymo 2005). Growth of the Challenger Mound therefore seems to have been connected to major global climatic changes, such as the major initiation of Northern Hemisphere Glaciation and the Mid-Pleistocene

Transition (MPT: Muddelsee & Schulz 1997).

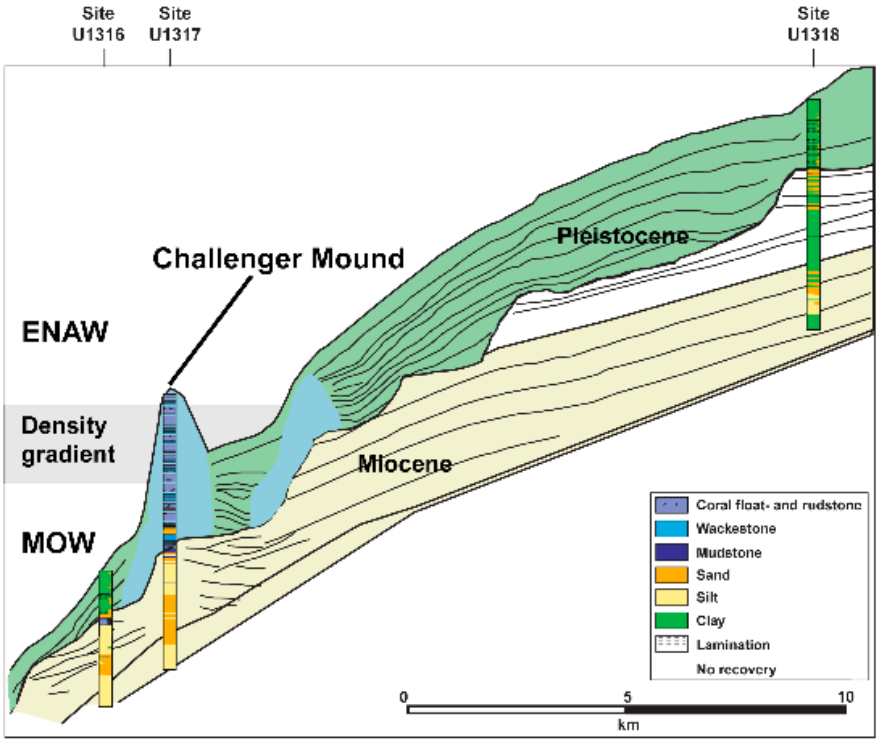

Figure 2: Seismic profile with lithological columns of three drilled sites (U1316–U1318) on interpreted seismic cross section (De Mol et al. 2002). Mound units are displayed in blue. The two main water masses Eastern North Atlantic Water (ENAW) and the Mediterranean Outflow Water (MOW) build a promiment density gradient close to the mound summit.

In addition, Sakai et al. (2009) presented an oxygen isotope stratigraphy of the planktonic foraminifera *Globigerina bulloides* for IODP Site 1317 E and highlighted an even faster development of the Challenger Mound during its initial growth phase. They suggested mound initiation during marine isotope stage 92 (2.24 Ma) and growth until 1.85 Ma, as well as a restart of growth in MIS 19 at 750 ka. However, they did not consider additional unconformities as suggested by Titschack et al. (2009) and Thierens et al. (2010).

This study will contribute to the understanding of the long-term development of Challenger Mound (IODP Site 1317) and its dependency to paleoceanography and paleoclimate. Based on additional age constraints (combined U/Th and $^{87}Sr/^{86}Sr$) and different paleoenvironmental proxies from coral skeleton (Mg/Li, Ba/Ca) and foraminiferal tests ($\delta^{13}C$, Mg/Ca) we show that the mechanisms of intermediate water masses of southern origin and their variability during the Pleistocene have an impact on coral growth and decline along the Irish margin.

5.2 Material and Methods

Sediments from Site U1317 recovered during IODP Expedition 307 with R/V Joides Resolution in 2005 (Expedition 307 Scientists, 2006) were investigated in this study. In order to obtain undamaged half cores, the drill cores were frozen before splitting (Dorschel et al.

2005; Foubert et al. 2007). IODP Site 1317 consists of 5 different holes A, B, C, D and E. In this study we only used samples from hole E and C.

At 147.95 mbsf sediments from hole U1317C are characterized by an unconformity, marked by a sharp colour change from the greenish-grey underlying unit to the grey, coral bearing sediments. Samples were taken every 10 to 20 cm in the interval between 0 and 30 mbsf for stable isotopes and elemental ratio analyses on the foraminiferal tests. All samples were dried at 50 °C, weighed and then wet sieved through a 63-µm sieve.

Clean and well-preserved coral samples were taken from the base of hole E and C (148–115 mbsf) and from 0–30 mbsf of core C with a higher resolution for age determination and elemental ratio analyses. On the basis of X-ray diffraction all coral samples retain in their initial aragonitic skeleton (>99% aragonite). Before analyses corals were cleaned according to Cheng et al. (2000a). Moreover, all samples were drilled according to Rüggeberg et al. (2008) avoiding the centres of calcification, since these parts of the skeleton have different elemental isotopic and elemental compositions compared the rest of skeleton. For comparison all depths were calibrated to IODP Site 1317 hole E (mbsf according to Foubert & Henriet (2009). The mound record in hole E is 155.02 m long and in hole C 147.7 m and hence the mound base is about 7.3 m deeper in hole E. The major hiatus recognized by Foubert & Henriet (2009) and Kano et al. (2007) occurs in hole E at 23.3 mbsf and in hole C at 26.5 mbsf. Further details and tiepoints are shown in Table 1.

Table 1: Correlation table of IODP Site 1317 Hole E and C. Tiepoints are based on the magnetostratigraphy dates and additional tiepoints according to Foubert & Henriet (2009).

1317E		1317C		
depth (mbsf)	Time (TWT)	depth (mbsf)	Time (TWT)	Magnetostratigraphic datings (Foubert & Henriet 2009)
5.00	1.04321	5.93	1.05400	Tiepoint1
17.84	1.06114	14.08	1.06547	Tiepoint2
18.15	1.06147	18.91	1.07281	Brunhes/Matuyama 0.78Ma
23.30	1.06938	26.50	1.08312	Hiatus_TopMatuyama 1.00/1.67Ma
23.78	1.07003	26.83	1.08353	Tiepoint3
27.43	1.0744	29.96	1.08747	Gilsa 1.68Ma
40.54	1.09057	40.15	1.10054	TopOlduvai 1.77Ma
51.52	1.10391	47.80	1.10977	Tiepoint4
57.73	1.11122	63.66	1.12849	BaseOlduvai 1.95Ma
61.36	1.11516	66.50	1.13208	Tiepoint5
68.70	1.12416	74.63	1.14144	Tiepoint6
78.99	1.13675	82.35	1.15112	TopRéunion 2.115Ma
81.63	1.13965	84.79	1.15380	Tiepoint7
99.03	1.15932	99.94	1.17214	BaseRéunio 2.153Ma
107.50	1.16782	112.19	1.18471	Tiepoint8
123.61	1.18563	131.09	1.20581	Tiepoint9
133.90	1.19675	137.50	1.21275	Tiepoint10
151.50	1.21583	-	-	TopGauss 2.58Ma
155.02	1.21958	147.47	1.22387	Moundbase

5.2.1 Strontium Isotope Stratigraphy

Strontium isotope ratios were determined by Thermal Ionization Mass Spectrometry (TIMS, TRITON, ThermoFisher Scientific at IFM-GEOMAR) after chemical separation via cation exchange chromatography using a Sr-specific resin (Eichrom). For Sr isotope measurements about 200 ng of coral Sr was used. All isotope ratios were internally normalized to an $^{88}Sr/^{86}Sr$ ratio of 0.1194. Repeated analysis of the standard NIST SRM 987 in the course of this study yielded an average value of 0.710219 ± 10 (2σ, $n = 15$). For comparison with literature values all $^{87}Sr/^{86}Sr$ were normalized to a value of 0.710248 for the NIST SRM 987. Ages were calculated after the seawater evolution curve (Lookup Table Version 4B-08-04, McArthur and Howarth 2004; MacArthur et al. 2001).

5.2.2 Thorium/Uranium age determinations

The Thorium and Uranium isotope measurements were performed on a VG Elemental AXIOM MC-ICP-MS at IFM-GEOMAR applying the multi-static MIC (multi-ion-counting)-

ICP-MS approach after Fietzke et al. (2005). For isotope dilution measurements a combined $^{233/236}U/^{229}Th$-spike was used, with stock solutions calibrated for concentration using NIST-SRM 3164 (U) and NIST-SRM 3159 (Th) as combi-spike calibrated against CRM-145 uranium standard solution (also known as NBL-112A) for U-isotope composition, and against a secular equilibrium standard (HU-1, uranium ore solution) for determination of $^{230}Th/^{234}U$ activity ratio. Whole procedure blank values of this sample set were around 0.6 fg for ^{230}Th, 2 pg for ^{232}Th and around 2 pg for U, which are in the typical range of this method and laboratory. Element separation procedure was based on Eichrom-UTEVA resin. Calculation of geochronological data and activity ratios is based on the decay constants given by Cheng et al. (2000b).

5.2.3 Elemental ratio determinations

Selected samples of the cold-water coral powders used for Sr and U/Th age determinations measurements were split for additional ICP-QMS measurements (Quadrupole ICP-MS, Agilent 7500 series at IFM-GEOMAR). Element/Ca ratios were calculated from the raw counts using the method of Rosenthal et al. (1999) Calcium concentrations were measured and samples diluted to a Ca concentration of ~10 ppm. Six aliquots of *Porites* sp. coral powder reference material JCp-1 (Okai et al. 2002) were treated like samples and the average values obtained during the course of this study (n = 8, including repeated measurements) for Sr/Ca were 8.76 ± 0.067 mmol/mol, Mg/Ca 4.170 ± 0.026, U/Ca 1.190 ± 0.011 mmol/mol, Li/Ca 6.150 ± 0.167 mmol/mol, Ba/Ca 7.19 ± 0.36 mmol/mol resulting in an average value for Mg/Li ratios of 0.679 ± 0.018 mol/mmol. The reproducibility of the measurements was ~1.54 % for Sr, ~2.64 % for Mg, 1.79 % for U, 10.0 % for Ba, 11.6 % for B and for Li 4.07 % resulting in 5.42 % for the Mg/Li ratio for the JCp-1 (2σ). The absolute concentrations are within the uncertainty of the recommended values (Okai et al. 2002, 2004). The coral Mg/Li ratios were used to calculate the Bottom-Water-Temperature (BWT) after the equation of Raddatz et al. (submitted). The Mg/Li is calculated from the Mg/Ca and Li/Ca ratio. For both it was suggested that the seawater value has been increased by a factor <2 over last 3Ma (Hathorne et al. 2006; Fantle and DePaolo 2006; Coggon et al. 2010). Therefore was assume the seawater Mg/Li ratio to be constant. Moreover, the impact of a variable Mg/Li seawater ratio on the coral Mg/Li ratio is not known. Hence, we do not consider a change in the Mg/Li_{sw} ratio for the temperature reconstructions.

According to Anagnostou et al. (2011) Ba/Ca_{coral} ratios were used to calculate Ba/Ca-seawater ratios after this equation $Ba/Ca_{coral} = 1.4* Ba/CA_{sw} + 0$. We are aware of the fact Anagnostou

et al. (2011) used *Desymophyllum dianthus* for these calibrations and not *L. pertusa*, however, we used these calibrations to reconstruct trends and not absolute values. The Ba/Ca ratio measured in foraminifera was shown to be a proxy to reconstruct ocean circulation and nutrients (Lea & Boyle 1990). Subsequently, Anagnostou et al. (2011) demonstrated that the Ba/Ca ratio in scleractinian cold-water corals also serves as a proxy for the reconstruction of $Ba/Ca_{seawater}$ and hence records variations in nutrient supply.

5.2.4 Stable carbon isotope and Mg/Ca measurements on foraminifers

Planktonic and benthic specimens were selected from the size fraction > 250 μm. Sample material was crushed, mixed and visually divided into two thirds used for Mg/Ca analyses, and one third for the light stable isotope measurements. Isotope measurements were conducted on a Finnigan MAT-253 (at IFM-GEOMAR, Kiel) equipped with a fully automated carbonate preparation device. Results exhibit an analytical precision (± 1σ) better than ± 0.07 ‰ for $\delta^{18}O$ and ± 0.05 ‰ for $\delta^{13}C$. All values are reported relative to Pee Dee Belemnite (PDB, based on calibration directly to National Bureau of Standards (NBS-19)). For Mg/Ca determinations, all samples were cleaned after Barker et al. (2003). Measurements were performed on a simultaneous, radially viewing ICP-OES (IFM-GEOMAR) with an analytical error for the Mg/Ca ratios of ~ 0.1 % (2σ). To monitor contamination by clays or Mn-carbonates Fe/Ca ratios (mean of ~ 0.05 mmol/mol) and Mn/Ca ratios (mean of ~ 0.03 mmol/mol) were carefully evaluated. Benthic foraminiferal tests of *P. ariminensis* were used to calculate Bottom Water Temperatures (BWT) using the equation of Lear et al. (2002) Mg/Ca = 0.911exp (0.062 x BWT). Constraints on the Mg/Ca ratio of seawater over time is in the focus of recent studies (e.g Fantle and DePaolo 2006; Coggon et al. 2010) and a twofold increase has been demonstrated within the last 3 Ma. Again, the impact of a variable Mg/Ca seawater ratio on the foraminiferal Mg/Ca ratio is not known and hence we assume this as negligible.

5.3 Results

5.3.1 Strontium Isotope measurements

Radiogenic strontium isotope measurements were carried out on corals covering the upper (0-30 mbsf) and the lower mound sequence (115-148 mbsf). Overall the $^{87}Sr/^{86}Sr$ isotope ratios vary from 0.709061 ± 0.000010 to 0.709174 ± 0.000010 and show an increasing trend from the lower to the upper mound part. In particular, $^{87}Sr/^{86}Sr$ isotope ratios in the interval between 110-148 mbsf of M1 are similar and vary only between 0.709061 and 0.709081. In

the interval between 0-26 mbsf covering the hiatus at 23 mbsf the $^{87}Sr/^{86}Sr$ isotope ratios display a increase from 0.70910 to 0.70917. Corresponding ages were calculated after the Lookup Table Version 4B-08-04 (McArthur & Howarth 2004; McArthur et al. 2001).

Table 2: Radiogenic strontium isotope ratios measured in cold-water corals fragments.

Lab-code	$^{87}Sr/^{86}Sr$	2σ error	SIS-04 min age Ma	SIS-04 mean age Ma	SIS-04 max age Ma	core depth mbsf	IODP 1317 hole ID
334-09	0.709081	0.000010	1.77	2.15	2.49	116.03	C
335-09	0.709061	0.000010	2.44	3.02	4.29	118.60	C
336-09	0.709078	0.000013	1.72	2.24	2.87	119.88	C
337-09	0.709072	0.000013	1.91	2.43	3.58	135.57	C
337-09	0.709072	0.000010	2.02	2.43	3.23	135.57	C
338-09	0.709063	0.000010	2.37	2.84	4.09	136.59	C
339-09	0.709085	0.000019	1.46	2.01	2.80	136.99	C
340-09	0.709072	0.000010	2.12	2.43	2.87	137.08	C
341-09	0.709074	0.000013	1.83	2.36	3.37	137.18	C
342-09	0.709081	0.000013	1.65	2.15	2.69	137.19	C
343-09	0.709072	0.000010	2.12	2.43	2.87	138.80	C
346-09	0.709082	0.000010	1.74	2.12	2.45	115.20	E
347-09	0.709075	0.000010	1.91	2.33	2.87	116.11	E
348-09	0.709081	0.000019	1.53	2.15	3.23	116.99	E
349-09	0.709083	0.000010	1.77	2.08	2.35	117.18	E
350-09	0.709071	0.000010	2.15	2.46	2.99	132.27	E
351-09	0.709084	0.000010	1.72	2.05	2.35	135.14	E
352-09	0.709062	0.000010	2.34	2.93	4.39	141.19	E
352-09	0.709073	0.000013	1.87	2.39	3.46	141.19	E
353-09	0.709062	0.000010	2.40	2.93	4.19	145.69	E
354-09	0.709082	0.000010	1.80	2.12	2.38	148.42	E
650-10	0.709174	0.000010	0.00	0.01	0.27	0.10	C
648-10	0.709163	0.000010	0.23	0.41	0.61	4.67	C
646-10	0.709161	0.000010	0.28	0.48	0.65	7.75	C
651-10	0.709159	0.000010	0.34	0.55	0.69	10.70	C
652-10	0.709159	0.000010	0.34	0.55	0.69	11.40	C
649-10	0.709103	0.000010	1.39	1.53	1.70	23.24	C
653-10	0.709096	0.000010	1.52	1.67	1.89	28.69	C
897-10	0.709118	0.000010	1.19	1.30	1.41	23.24	C
899-10	0.709114	0.000010	1.25	1.35	1.48	22.74	C
895-10	0.709101	0.000010	1.42	1.57	1.74	26.92	C
903-10	0.709121	0.000010	1.15	1.26	1.36	20.18	C

Note*: 2σ: standard error of the mean. Mean age = Age from the mean isotopic value on the mean age curve, Min age = younger age: Age from the isotopic value 2σ on the upper limit age curve. Max age: Age from the isotopic value 2σ on the lower limit age curve.

Calculated Sr-ages reveal that the mound generally becomes younger from the base to the top of the mound. In particular the mound base shows ages between 3.02 Ma and 2.01 Ma (SIS mean age), whereas the upper mound interval displays ages between 1.67 Ma and subrecent 0.000 - 0.27 Ma (Tab. 2, Fig. 3).

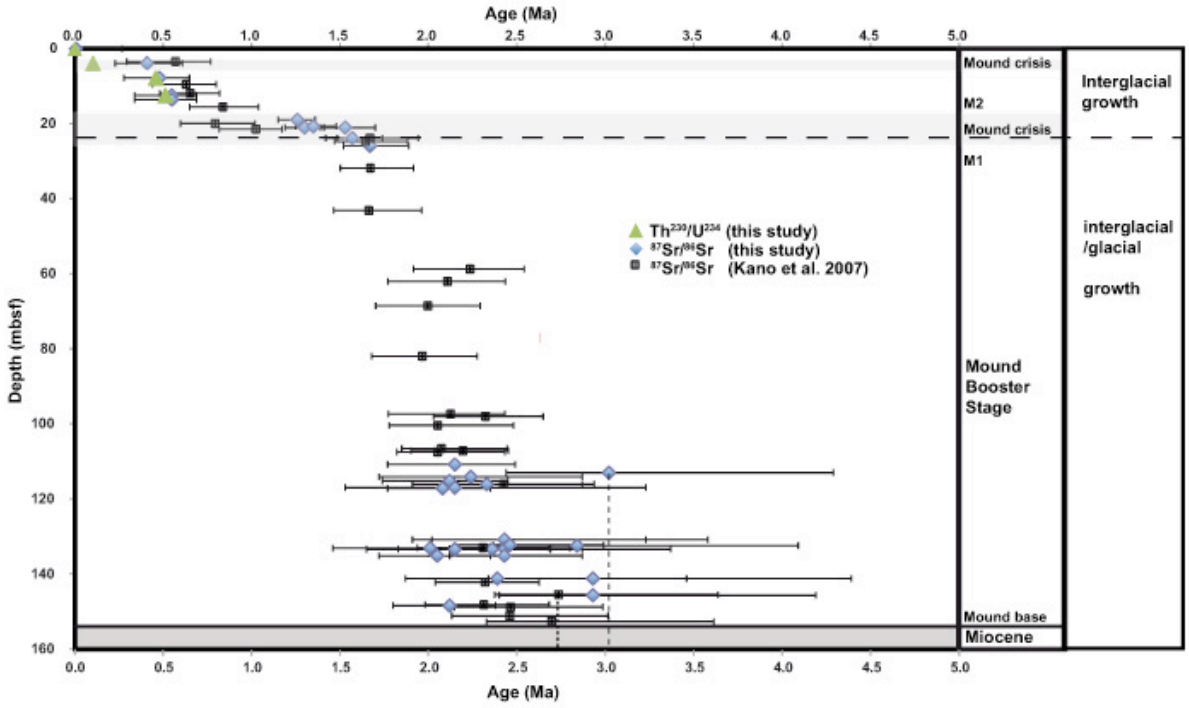

Figure 4: Strontium isotope and U/Th data of IODP Site 1317 are plotted within an age-depth plot. Both age chronometers display similar ages within uncertainty. Core depths of 1317C and E are correlated to core E according to Foubert & Henriet (2009). Black squares show the $^{87}Sr/^{86}Sr$ ages from Kano et al. (2007). Dotted vertical lines indicate potential period of mound initation based on Kano et al. (2007) and this study.

5.3.2 U/Th age determinations

Calculated U-series ages of 16 corals vary from 1.2 ka to 513 ka (Table 3, Fig. 3). The measured ^{232}Th concentrations are small < 2 ng g^{-1} and hence negligible due to the high activity ratio of $^{230}Th/^{232}Th$ of > 1000. However, calculated initial $\delta^{234}U_0$ values vary between 15.6 ± 4.51 and 156.8 ± 3.89 (Fig. 4, Table 2). The $\delta\ ^{234}U_0$ scatter for the samples below 5 mbsf is larger compared to the samples above 5 mbsf probably due to perculating carbonate-rich pore waters leading to an increasing U-series opening (Thompson et al. 2003). In general, coral samples that differ in their initial $\delta^{234}U$ from the modern seawater (149 ‰) are considered to provide unreliable U/Th ages (Stirling et al. 1998). Here, four samples are within the range of 149 ± 10 ‰ (Fig. 4, compare Stirling et al. 1998; Robinson et al. 2004)

and show similar U/Th ages compared to the SIS-ages within uncertainty (Fig. 3). The reliable U/Th ages of 1.2 ka ± 0.02 (MIS 1), 104.7 ± 7 ka (MIS 5) and 513.9 ± 35.2 (MIS 13) identify growth only for interglacial. Glacial coral growth at 460.2 (MIS 12) is indicated for a sample from 7.75 mbsf, but due to the to the large uncertainty 460 ± 63 ka, interglacial growth can not be excluded (Tab. 3). For further geochemical investigations corals were omitted indicating open-system behaviour.

However, corals from the lower mound sequence were not measured for Thorium/Uranium age determination. Here, the quality of coral samples is based XRD measurements and careful visual inspection of thin sections. However, corals analysed for elemental ratios comprise to two different groups M2 (1.2 ka, 0.105 Ma, 0.46 Ma, 0.513 Ma, 1.22 Ma, 1.35 Ma) and M1 (1.53 Ma, 1.67 Ma, 2.12 Ma, 2.46 Ma and 2.93 Ma, Fig. 3). Corals from the interval M1 were only taken for elemental ratio analyses that exceed the range of error bars based on the Sr-isotope ages, except for the 2.93 Ma sample as it represents the deepest in our sample set (151.25 mbsf).

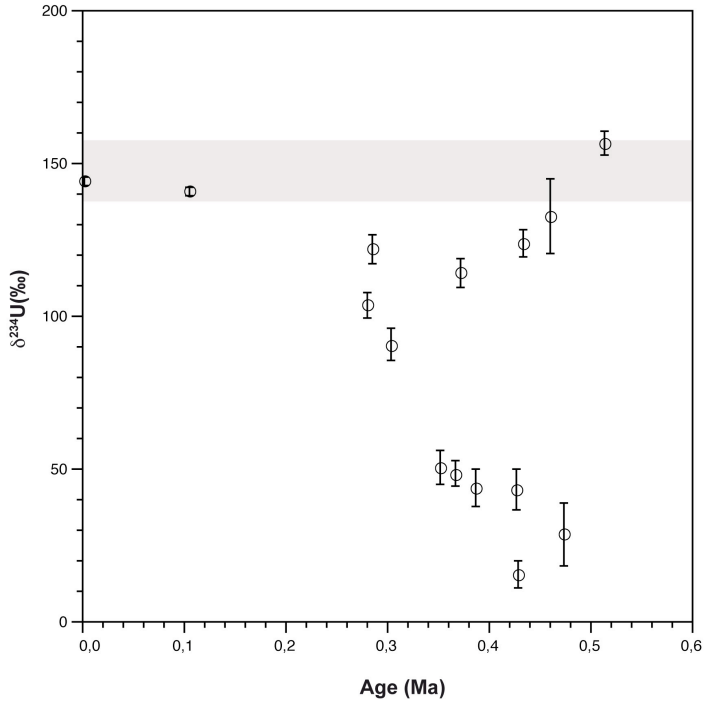

Figure 4: Initial $\delta^{234}U$ of dated corals from the top 30 m of IODP Site U1317 indicates that only four samples lay within the range of modern seawater values of 149 ± 10 ‰ (grey bar; compare also Stirling et al. 1998; Robinson et al. 2004; Wienberg et al. 2011).

Table 3: U and Th isotopes and calculated ages of cold-water coral (*Lophelia pertusa*) fragments from IODP Site 1317.

LAB-ID	Depth. (mbsf)	Weight mg	Age ka	± ka	^{238}U ppm	± ppm	^{232}Th ppb	± ppb	$\delta^{234}U_{(0)}$ ‰	± ‰	$\delta^{234}U_{(T)}$ ‰	± ‰	Reliability
900-09	0.1	36.61	1.24	0.03	4.899	0.004	b.d.l*	-	144	1	144	1	R
908-09	4.67	45.5	433.0	21.7	3.521	0.004	b.d.l*	-	36	1	124	5	n
901-09	4.75	49.21	104.8	0.7	4.628	0.004	48.673	2.076	105	1	141	2	R
898-09	5.55	33.67	371.3	13.3	3.861	0.005	0.217	3.023	40	2	114	5	n
909-09	7.75	15.66	460.2	65.4	3.924	0.009	b.d.l*	-	36	3	133	12	R
907-09	10.7	55.29	513.9	35.3	4.246	0.003	0.272	1.841	37	1	157	4	R
903-09	20.18	40.59	386.4	25.3	2.402	0.004	0.065	2.508	15	2	44	6	n
899-09	22.74	39.18	426.0	37.4	2.596	0.004	1.765	2.598	13	2	43	7	n
897-09	23.24	36.84	351.9	15.3	2.846	0.005	1.644	2.763	19	2	51	6	n
904-09	23.57	53.05	367.6	19.3	2.610	0.003	2.062	1.919	17	2	49	4	n
905-09	25.6	41.82	280.7	10.0	2.750	0.004	b.d.l*	-	47	2	104	4	n
910-09	26.12	33.15	304.0	11.7	2.701	0.004	5.144	3.071	38	2	91	5	n
895-09	26.92	31.39	285.6	6.9	3.254	0.005	17.380	3.243	54	2	122	5	n
906-09	28.41	48.95	427.9	30.2	3.274	0.003	1.456	2.080	5	1	16	5	n
896-09	28.96	30.64	473.8	86.5	2.440	0.005	60.685	3.337	8	3	29	10	n

note: * = below detection limit. Statistical errors are two standard deviations of the mean (2σ). Ages are calculated using the equation:

$(^{230}Th/^{238}U)_{act.}=1-\exp(-\lambda_{230Th}xT)+(\delta_{234}U(0))x0.001(\lambda_{230Th}/(\lambda_{230Th}\lambda_{234U}))x(1\exp((\lambda_{234U}-\lambda_{230Th})xT))$. Decay constants: λ_{234U}: $2.8263x10^{-6}$ yr-1; λ_{238U}:$1.5513x10^{-10}$ yr^{-1}; λ_{230Th}: $9.158x10^{-6}$ yr^{-1} (see Fietzke et al. 2005). Samples are corrected for blanks and inherited ^{230}Th associated with detrital ^{230}Th assuming that the $^{230}Th/^{232}Th$ activity ratio is 0.6 ± 0.2 (Blanchon et al. 2009). Note, in most cases this correction is negligible due to sufficiently high $^{230}Th/^{232}Th$ activity ratios in the carbonates. The measured $(^{234}U/^{238}U)$ activity ratios ($\delta^{234}U_{(0)}$) and ($\delta^{234}U_{(T)}$) are presented as deviation per mil (‰) from the equilibrium value. The $\delta^{234}U_{(0)}$ value represents the originally today measured $(^{234}U/^{238}U)$ activity ratio, given in delta notation ($\delta^{234}U_{(0)} = ((^{234}U_{act}/^{238}U_{act})-1) * 1000$). The $\delta^{234}U_{(T)}$ values reflect age corrected $(^{234}U/^{238}U)$ activity ratios by recalculating the decay of ^{234}U for the time interval T ($\delta^{234}U_{(T)} = \delta^{234}U_{(0)}\exp^{(}\lambda_{234}xT^{)}$), determined from $^{230}Th/^{234}U$ age of each individual sample. Note, due to the generally high ages in this sample set, the impact of age correction on the interpretation of $\delta^{234}U$ values is significant and as criteria for closed system behavior and isotopic reliability of ^{230}Th age data applicable. The $\delta^{234}U_{(T)}$ criterion and related U-Th age reliability can be explained as: n = not reliable (potential diagenetic overprint), R = reliable (passing the 149 ± 10 ‰ $\delta^{234}U_{(T)}$ criterion); SR = strictly reliable (within 146.6 - 149.6 ‰ $\delta^{234}U_{(T)}$ (Blanchon et al. 2009) representing values for modern corals and modern seawater, respectively). However, none of the samples plot within the SR criteria.

5.3.3 Element/Ca ratio determination

Mg/Li

Magnesium/Lithium ratios were calculated from the measured coral-Mg/Ca and coral Li/Ca ratios. Mg/Ca ratios vary from 2.5 to 4.8 mmol/mol and the Li/Ca show corresponding values from 9.4 to 16.0 mmol/mol. But calculated Mg/Li ratios presented here vary from 0.223 to 0.308 mol/mmol with a mean of 0.273 mol/mmol in the entire mound sequence (Fig. 5). The

mean of Mg/Li in M1 is slightly lower to the overall mean with 0.250 ± 0.021 mol/mmol and the mean in M2 slightly higher compared to the overall mean with 0.285 ± 0.019 mol/mmol. In general the Mg/Li ratios display an increasing trend from M1 to M2 from 0.247 to 0.304 mol/mmol. Here we used the temperature relationship of Mg/Li in *L. pertusa* (Raddatz et al. submitted) and calculated the BWT of the ambient seawater in times of coral growth (Fig. 5). Reconstructed BWT show an increasing trend from M1 to M2 from ~ 7.8°C to 9.2°C (Fig. 5). The overall variation only exceeds the precision (± 1) of the method by 0.4°C and therefore should be considered with caution. However, reconstructed mean BWT in M1 show values of 8.2°C and in M2 of 8.9°C (Fig. 5).

Ba/Ca

The coral Ba/Ca record provides an overall mean of 14.71 μmol/mol, displaying a maximum of 41.79 μmol/mol in M1 and a minimum of 7.86 μmol/mol in M2. Generally the interval M1 is characterized by higher $Ba/Ca_{Lophelia}$ values with a mean of 23.23 μmol/mol, whereas the mean of $Ba/Ca_{Lophelia}$ values in M2 is lower with 10.44 μmol/mol. Hence a significant shift of $Ba/Ca_{Lophelia}$ values is observed from M1 to M2. In particular $Ba/Ca_{Lophelia}$ values vary between 7.85 μmol/mol and 16.44 μmol/mol in M2, whereas values appear to be higher in M2 with variations between 12.76 μmol/mol and 41.79 μmol/mol (Fig. 5). Calculated $Ba/Ca_{seawater}$ values show similar pattern and result in lower mean values of in M2 7.46 show the same trend with higher $Ba/Ca_{seawater}$ values in M1 compared to M2 (Fig. 5).

5.3.4 Stable carbon isotope and Mg/Ca measurements on foraminifers

$\delta^{13}C$

The *G. bulloides* stable carbon isotope record ($\delta^{13}C_{planktonic}$) in the mound sequence vary between 0.40 and -3.26 ‰ and display a total mean of -0.81 ‰. Moreover, the $\delta^{13}C_{planktonic}$ record is characterized by a decreasing trend from 155 to 23 mbsf with some gradual changes and an increase of $\delta^{13}C$ from 23 to 0 mbsf (Fig. 6). Generally the $\delta^{13}C_{planktonic}$ values are about 1 ‰ lower in M1 compared to M2. The gradual pattern in M1 of $\delta^{13}C_{planktonic}$ values shows variations between -1.0 ‰ and -2.0 ‰. However, at 24.4 mbsf and 41.9 mbsf sharp drops occur to -3.12 ‰ and -3.26 ‰ respectively. In the upper mound sequence $\delta^{13}C_{planktonic}$ values increase gradually from -1.15 ‰ to a maximum of 0.32 ‰ (Fig 6.)

Mg/Ca

The Mg/Ca ratios measured in the benthic foraminifera *P. ariminensis* vary between 1.87 and 3.68 mmol/mol with a mean of 2.83 mmol/mol (Fig. 6) Overall, the $Mg/Ca_{planulina}$ record displays an increasing trend within the mound sequence M1 from 2.40 mmol/mol to 2.85 mmol/mol and maximum of 3.68 mmol/mol at 41.9 mbsf. $Mg/Ca_{planulina}$ values vary by ~ 1 mmol/mol between from 2.46 mmol/mol to 3.43 mmol/mol in M2, which is lower compared to the variations in M1. Here, $Mg/Ca_{planulina}$ values show variations of 1.4 mmol/mol. Corresponding reconstructed Bottom Water Temperatures (BWT) vary from 7 to 13°C throughout the foraminiferal mound record with a mean of 10.7°C. In M1 BWT reveal a slightly lower mean of 10.3°C compared to M2 with 10.9°C. Moreover, the highest and lowest BWT are recorded in M1 characterized by a BWT variability of ~ 6°C from 7 to 13°C and hence is twice as large as the variability in M2 of ~ 3°C, varying from 9.5 to 12.5°C (Fig. 6).

5.4 Discussion

5.4.1 Age constraints on Challenger Mound

We determined $^{87}Sr/^{86}Sr$ based SIS-age estimates of coral skeletons from the base and of the top of Challenger Mound. Results indicate that coral growth initiated at ~ 3 Ma and continued to grow about 130 m until 1.53 Ma at ~ 21 mbsf, where an abrupt shift occurs (Fig 3.) We observe similar growth pattern for Challenger Mound compared to Kano et al. (2007) and Foubert & Henriet (2009). However, our data indicate a Challenger Mound initiation several 100 ka earlier compared to Kano et al. (2007), but similar to the magnetostratigraphy of Foubert & Henriet (2009, Fig. 3). Challenger mound growth ceased at around 1.53 Ma and reinitiated its growth at around 1.2 Ma. Similar growth behaviour was already identified by other studies (Foubert & Henriet 2009; Kano et al. 2007; Sakai et al. 2009; Titschack et al. 2009). These findings are again supported by the $^{87}Sr/^{86}Sr$ ages presented here revealing that coral growth in this crucial period appeared to be reduced (Fig. 3).

For the top mound part we applied combined age determination by the use of U/Th and $^{87}Sr/^{86}Sr$ systematics. Results indicate that both chronometers are within their uncertainties in good accordance to each other (Fig. 3). From 13 mbsf to the top of the Challenger Mound Sr ages generally become younger again and show ages between 0.5 Ma to 0 Ma. However, mound growth in the upper mound part M2 appears not be as fast as in the lower mound part M1. Based on our results the two growth phases are characterized by a fast growing period

M1 with ~ 8 cm/ka between ~ 3.0 and ~ 1.53 Ma, and a slow growing period M2 with ~ 2 cm/ka between 1.53 and 0 Ma. U/Th ages presented here reveal that Challenger Mound growth in the late Pleistocene occurred during interglacial periods, except for MIS 12. Identified periods of growth are in MIS 1, 5e, and 13 (Fig. 3). Moreover, a significant hiatus is identified at ~ 4 mbsf revealing a period of no deposition and/or erosion of ~0.33 Ma between MIS5 and MIS12. This interpretation is consistent with findings of Titschack et al. (2009) who highlighted that the sedimentary record might be disturbed by several hiatuses. The coral growth implied for MIS 12 could not be identified precise enough to exclude interglacial background, due to the large uncertainty (0.46 ± 0.07 Ma). With these new age constrains the depositional rate of the upper mound section of 23m is reduced to ~ 2 cm/ka (1.2–0.001Ma). Several studies have shown that carbonate mound growth on the Irish margin was restricted to the Holocene and interglacial periods (Dorschel et al. 2005; Eisele et al. 2008; Frank et al. 2005; Frank et al. 2009; Frank et al. 2011; Rüggeberg et al. 2007) with only a few exceptions. Further south in the Bay of Biscay cold-water coral growth tend to occur during interstadials (Schröder-Ritzrau et al. 2005), whereas in the Gulf of Cadiz during glacials (Wienberg et al. 2009, 2011) as well as off Mauritania (Eisele et al. 2011).

Focusing on the very top of the Challenger Mound U/Th age determinations show that mound growth was active during MIS 1 and MIS 5. By contrast Kano et al. (2007) and Ferdelmann et al. (2006) indicated that mound ceased at ~ 0.46 Ma. However, their top mound ages are only based on Sr-isotopes and nannofossil biostratigraphy. Moreover, from our observation we show that the restriction of carbonate mound growth to warmer periods at around 50°N on the Irish Margin is valid for the last ~ 0.5 Ma.

5.4.2 Oceanographic controls on carbonate mound growth

Environmental control mechanisms of cold-water coral reefs and mounds on the European continental margin between 20° and 70°N are under debate of ongoing paleoceanographic research. Recent studies have shown that late Pleistocene distribution of flourishing coral-reefs and mounds oscillated from the NE Atlantic down to the Gulf of Cadiz and off Mauretania in correspondence to interglacial/glacial cycles induced by the expansion and retreat of the Northern-Hemisphere ice-sheets (Dorschel et al. 2005; Eisele et al. 2008; Frank et al. 2005; Frank et al. 2009; Rüggeberg et al. 2007, Wienberg et al. 2009; Wienberg et al. 2011). This biogeographical limitation was caused by changes in sea-surface productivity (Eisele et al. 2011; Wienberg et al. 2011), upwelling (Wienberg et al. 2011) and bottom currents (Huvenne et al. 2009; Rüggeberg et al. 2005), which in turn were affected by

changes in intermediate water mass variability. Strong bottom currents, enhanced sea-surface productivity, temperatures above 4°C, and a prominent strong density gradient between the upper and intermediate water masses favoured coral growth during the last interglacial periods on the Irish Margin (Dorschel et al. 2005; Dullo et al. 2008; Eisele et al. 2008; Frank et al. 2005; Frank et al. 2009; Rüggeberg et al. 2007).

5.4.3 Growth responses to glacial and interglacial variability

We observe large $BWT_{Planulina}$ variations of ~ 6°C in M1 that are clearly in phase with $\delta^{13}C_{Planktonic}$ variations of ~ 1 (‰). These variations may represent continuous growth of the mound through glacial and interglacial periods highlighted already by other studies (Figure 5, Foubert & Henriet 2009; Kano et al. 2007; Sakai et al. 2009). Between 3.0 and 1.5 the global climate was forced by low amplitude 41-kyr cycles and hence glacial/interglacial variations were not as intense as in the late Pleistocene (Lisiecki & Raymo 2005). Sea-level fluctuations were only about 60 m during build-up of the lower part of the mound (Sakai et al. 2009), thus MOW inflow probably prevailed throughout interglacial and glacial periods and reached the mound summit leading to the observed $BWT_{Planulina}$ variations. Moreover, the $\delta^{13}C_{planktonic}$ values vary coincidently with the $BWT_{Planulina}$ values. The use of stable carbon isotopes in the planktonic foraminifera *G. bulloides* may be complicated due to several effects such as upwelling (Kroon and Ganssen 1989) and carbonate ion concentrations (Spero et al. 1997). However, Ganssen and Kroon (2001) have shown that stable carbon isotopes of *G. bulloides* can be used to estimate the nutrient concentration of surface waters in the North Atlantic. According to their findings, our $\delta^{13}C_{planktonic}$ values reveal advances of nutrient enriched sea surface waters during glacial periods, whereas interglacial periods appear to show lower nutrient contents. This is in accordance to other findings. In particular, during the late Pliocene glacial periods the North Atlantic Current (NAC) was reduced and led to advances of colder nutrient-rich polar waters dominating the North Atlantic (Naafs et al. 2010). Moreover, sea surface productivity increased during this time due to amplified winds (Lawrence et al. 2009; Naafs et al. 2010). Therefore, during the late Pliocene/early Pleistocene surface waters in the Porcupine Seabight were characterized by enhanced productivity that probably led to an amplified export productivity.

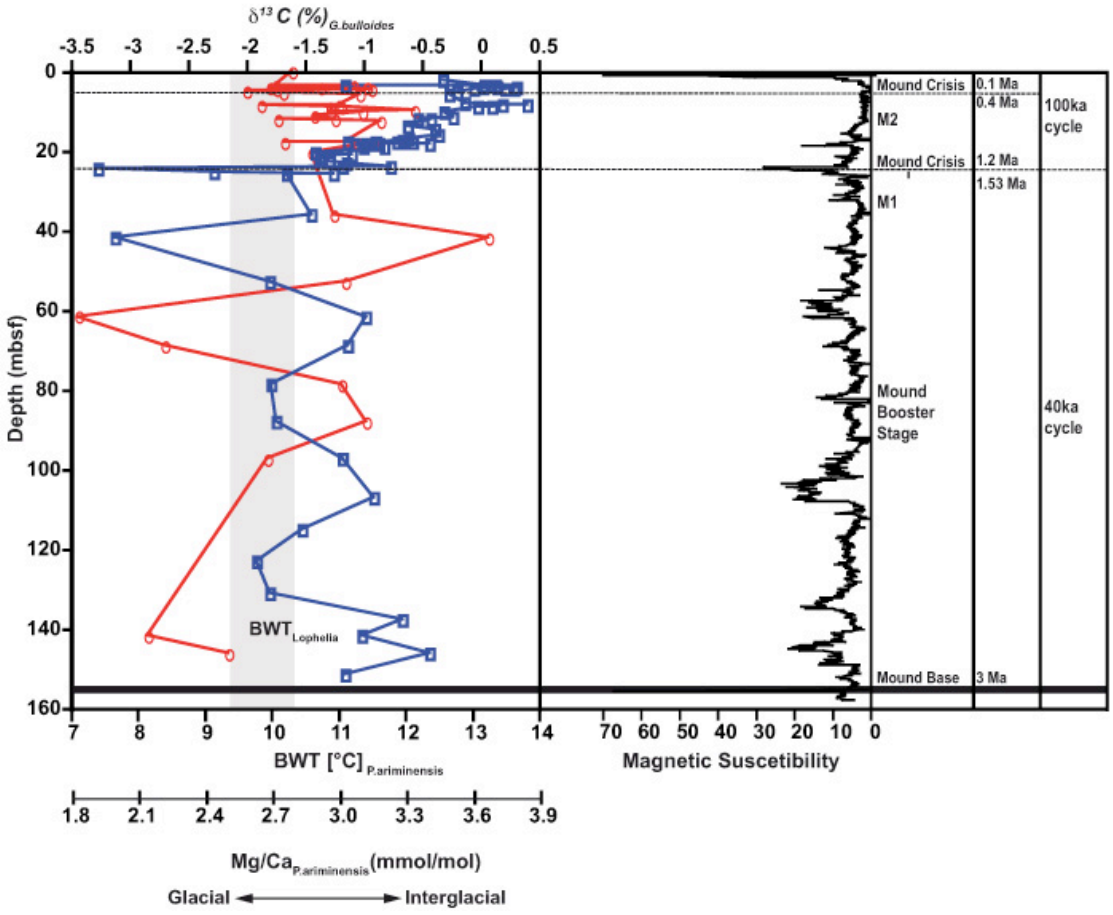

Figure 5: Foraminiferal planktonic stable carbon isotopes and benthic Mg/Ca-temperatures of IODP Site 1317 are plotted against depth. Benthic foraminiferal Mg/Ca-temperatures (red, BTW_{foram}) were calculated after Lear et al. (2002). BWT_{foram} in M1 shows variations of ~ 6°C and a similar pattern as the $\delta^{13}C_{planktonic}$ (blue), whereas in M2 $\delta^{13}C_{planktonic}$ display a gradual increase and BWT only little variations of < 2°C. In good accordance to the $\delta^{13}C_{planktonic}$ are the magnetic susceptibility values (Foubert & Henriet 2009) indicating glacial interglacial variability. Also plotted is the recent seasonal variation of BWT at 800m depth (Levitus et al. 1994).

By contrast to M1 $BWT_{Planulina}$ values in M2 shows only small variations of ~ 2°C indicating that only interglacial conditions have been recorded (Fig. 5 and 6). Glacial periods leave only a little trace in mound records (Dorschel et al. 2005; Rüggeberg et al. 2007) caused by non-depositon and/or erosion of sediment. During glacial periods, when sea-level dropped by ~120m, the MOW was not sufficiently strong enough to reach as far north as the Porcupine Seabight (Schönfeld and Zahn 2000). Moreover, BWT decreased and may have dropped below 4°C (Rüggeberg et al. 2007; Kano et al. 2007) probably due to advances of Glacial North Atlantic Intermediate Water (GNAIW). After these sluggish events sedimentation has

been re-established by the reintroduction of a vigorous MOW (Dorschel et al. 2005). Subsequently, low sea level stands and BWT >4°C have caused mound decline, whereas high sea level stands and relatively high BWT indicate active mound growth.

Therefore, our data support the late Pleistocene (M2) variability of mound growth and shows that this variability occurred since MIS 13. Furthermore, this mound growth pattern of interglacial growth and glacial retreat did not occur during the Late Pliocene/Early Pleistocene phase of Challenger Mound (M1) that in turn favoured a Mound Booster Stage (Henriet et al. 2001).

5.4.4 Interconnectivity between intermediate water mass dynamics, food supply and Challenger Mound growth

North Atlantic carbonate mound growth initiated in several phases since the Pliocene (van Weering et al. 2003; van Rooij et al. 2007). Based on our Strontium Isotope Stratigraphy (SIS) age determinations Challenger Mound initiation coincided with the reintroduction of the MOW in the late Pliocene at ~3 Ma into the Porcupine Seabight (Khélifi et al. 2009). Previously the MOW had already been suggested to be the main carrier of cold-water coral larvae onto the Irish margin (De Mol et al. 2002). Moreover, our $BWT_{Lophelia}$ reconstructions vary between 8-10C° and thus are consistent with the Mg/Ca-based foraminiferal paleotemperatures at DSDP Site 548 by Khelifi et al. (2009) and $\delta^{18}O$-based foraminiferal paleotemperatures by Raddatz et al. (2011, Fig. 4). This highlights that coral growth appear to occur in a narrow temperature envelope of < 2°C. Additionally, reconstructed $BWT_{Lophelia}$ variations are similar to the recent seasonal variations (9.4–10.5°C, Levitus et al. 1994). However, we interpret this rather as a dependency to the inflow of the warm and saline MOW causing a density gradient to the overlying ENAW then to a very narrow tolerated range of temperature. This density gradient favoured the settlement of organic matter and hence the coral community became established. In general cold-water corals are known to thrive in cold and nutrient-rich water that lack large seasonal variability (Roberts et al. 2006) and active mound growth is restricted to specific environmental conditions (Dullo et al. 2008, Fig. 5). Furthermore the Challenger Mound is characterized by two different episodes of growth (Fig. 3). In particular the mound grew to ~ 130 m above the surrounding sea floor and dramatically decreased its growth at ~ 1.53 Ma. Accordingly, we observed a gradual trend in the $BWT_{Lophelia}$ record as well in the $Ba/Ca_{Seawaater}$ values (Fig. 6). We interpret these trends as a change in nutrient supply due to a shifting water mass boundary between the ENAW and

MOW leading to a stronger influence of warmer nutrient depleted ENAW at the core summit (Fig. 5 and 6).

In general, living cold-water reefs and mounds in the North Atlantic occur within a certain density envelope and an associated permanent thermocline (Dullo et al. 2008; White & Dorschel 2010). Moreover, sea-surface productivity is one of the major controlling parameters of cold-water corals growth as corals benefit from organic matter that settles down from the sea-surface (Guinotte et al. 2006). White et al. (2005) investigated the productivity over the Porcupine Bank and concluded that coral growth depends on high sea-surface productivity and high utilization of organic matter due to a dense nutrient rich water mass. We infer that a stable water mass stratification between the ENAW and the MOW formed such a density gradient close to the mound summit and hence provided the coral community with nutrients. The reestablishment of the coral community at around 1.2 Ma was characterized by significant slower growth (Fig. 3). This crucial period corresponds to the Mid-Pleistocene-Transition initiated due to enlarged ice-sheets (Mudelsee & Schulz 1997) and increasing sea-level fluctuations (Lisiecki & Raymo 2005). Subsequently, this was followed by a long-term lowering of the transition zone between ENAW and MOW that in turn caused gradual decreasing nutrient supply to the mound summit (Fig. 6).

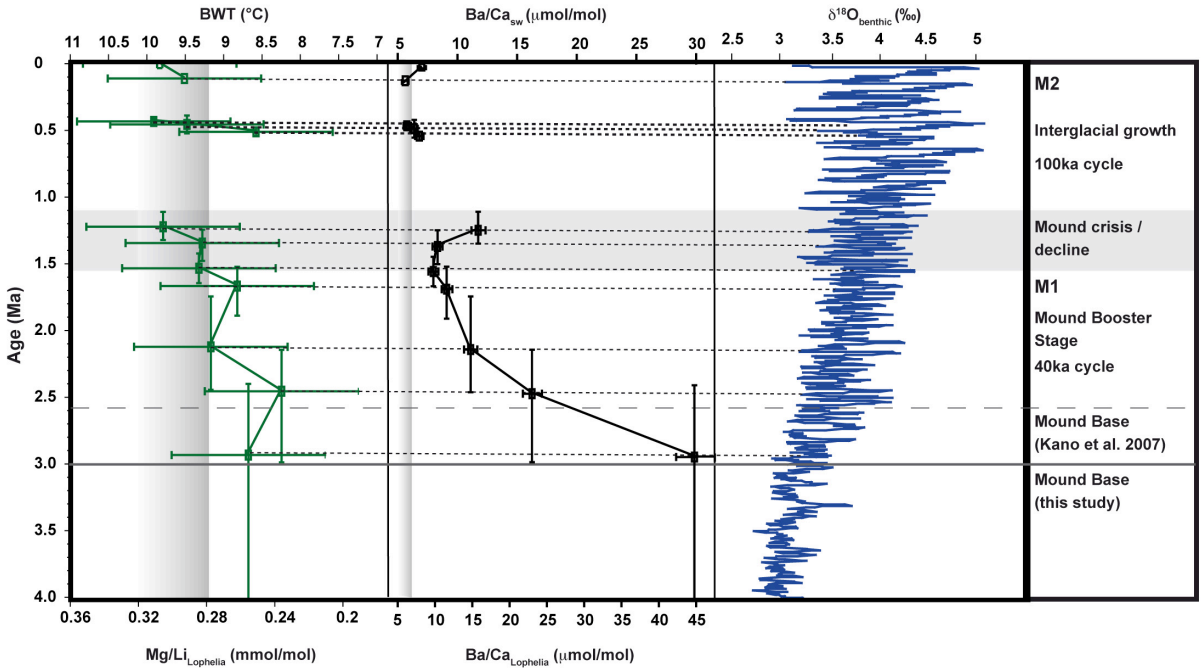

Figure 6: Paleoceanographic reconstruction based on U/Th, and $^{87}Sr/^{86}Sr$ dates corals. Elemtental ratioswere measured in scleractinian cold-water corals *Lophelia pertusa*. Mg/Li were transferred into temperature after the equation of Raddatz et al. (submitted) showing that corals thrived in a narrow temperature envelope comparable to recent seasonal variation (shaded envelope, taken from Levitus et al. 1994). The Ba/Ca$_{Lophelia}$ were transferred into Ba/Ca of seawater based on the study of Anagnostou et al. (2011) showing a clear shift towards lower values from lower to the upper part of mound. The Ba/Ca envelope illustrates the recent Ba/Ca values from the Irish Margin. Also plotted is the benthic LR04 stack of Lisiecki & Raymo (2005).

In the most recent glacial periods MOW was restricted south of 40°N (Schönfeld and Zahn 2000) and therefore the build-up of the recent water mass stratification was not possible leading to insufficient nutrient and food supply. Today the Porcupine Seabight oceanography reveals that the "dead" top of Challenger Mound is situated well over the boundary layer between the ENAW and the MOW, whereas other vivid mounds appear to occur deeper (Huvenne et al. 2003). This implies that corals on the top of the Challenger Mound are not sufficiently provided with nutrients and food which in turn lead to the recently observed decline of Challenger Mound.

Finally, we suggest that coral growth on the one hand benefited from a complex oceanographic setting that supported an enhanced nutrient and food supply, but in turn on the other hand mound growth also suffered from its own fast growth and enhanced sea-level fluctuations as well as long-term lowering of the boundary layer between ENAW and MOW over the last 1.2 Ma.

5.5. Conclusion

The IODP Expedition 307 drilled the Challenger Mound through its entire sediment body. Paleoceanographic reconstructions revealed seawater characteristics since the onset of mound growth. Reconstructions are based on calcareous organisms such as benthic and planktonic foraminifera ($\delta^{13}C$ and Mg/Ca) as well as the scleractinian cold-water coral *Lophelia pertusa* (Mg/Li and Ba/Ca).

Our age constraints indicate that Challenger Mound already initiated at 3.0 Ma coincidently with the Mediterranean Outflow Water (MOW) intensification. Foraminiferal $\delta^{13}C$ and Mg/Ca values indicate a continuous Challenger Mound growth between 3.0 and 1.5 Ma. This implies that corals have overcome low amplitude interglacial/glacial cycles (41 kyr). Late Pliocene sea level changes were not severe enough to affect Challenger Mound growth. Moreover, paleoceanographic reconstructions by *Lophelia*-Mg/Li and Ba/Ca ratios reveal that coral growth was restricted to specific oceanographic settings. The reintroduction of MOW into the Porcupine Seabight at 3 Ma initiated the recent water mass stratification an in turn established the necessary density gradient for enhanced nutrient supply between the Eastern North Atlantic Water (ENAW) and MOW at the mound summit. Between 1.53–1.2 Ma mound development was interrupted coincidently with the Mid-Pleistocene-Transition, a period of global climate change when the high amplitude interglacial/glacial cycles (100 ka) initiated and glacial conditions became unfavourable for corals in the Porcupine Seabight. In particular during last glacial periods no MOW entered the Porcupine Seabight as the sea-level dropped by about 120 m and hence coral mound growth only occurred in interglacial periods.

Finally this study underlines that cold-water coral communities are restricted to specific environmental conditions and hence climate change may cause a dramatic decline in cold-water coral mound growth on the European continental margin as previously suggested by Guinotte et al. (2006).

5.6. Acknowledgements

We are gratefully thankful to the Captain and crew of the IODP Exp. 307 as well as to the Scientific Party. Samples were kindly provided by IODP. Thanks to Walter Hale helping with the core sampling at the IODP Core Repository, MARUM, Bremen. This work was funded by the DFG Project ISOLDE 1 and 2 (Du 129/45-1 and Du 129/45-3). Folkmar Hauff, Nadine Gehre, Ana Kolevica and Lulzim Haxhiaj are acknowledged for lab support. AR acknowledges funding from DFG project TRISTAN (Du 129/37).

Chapter VI

Summary and outlook

6. Summary and outlook

This study focused on the environmental control of cold-water coral and mound growth in the North Atlantic. For this purpose, geochemical signals from the scleractinian cold-water corals *Lophelia pertusa* as well as benthic and planktonic foraminifera have been analysed from the Challenger Mound IODP Site 1317 in the Porcupine Seabight. In summary, new insights were shown into the environmental control on carbonate mound initiation, the use of cold-water corals as paleo-archives and the long-term history of coral growth since the onset on the European continental margin at around 3 Ma.

High resolutions records of stable carbon and oxygen isotopes in benthic foraminifera such as *Discanomalina coronata, Planulina ariminensis*, *Lobatula antartica, Fontbotia wuellerstorfi* and *Lobatula lobatula* as well as the planktonic foraminifera *Globigerina bulloides* and grain sizes analyses revealed the paleoenvironmental conditions in times of Challenger Mound initiation. These records showed the presence of an extended hiatus between the Middle Miocene and Late Pliocene/Early Pleistocene at the mound base. Moreover, reconstructed Bottom Water Temperature (BWT) estimations using foraminiferal $\delta^{18}O$ indicate values in the range of tolerance of the reef-building cold-water coral *Lophelia pertusa* (7-11°). Challenger Mound initiation was affected by vertical movements of Mediterranean Outflow Water comparable to the recent glacial/interglacial cycles that in turn was probably replaced by advances of Southern Component Water. However, foraminiferal $\delta^{13}C$ in carbonate mound can be overprinted by diagenetic processes and may therefore have to be carefully evaluated. According to recent oceanographic studies, $\delta^{18}O$ analyses of benthic foraminifers also showed that active mounds thrive always within a density envelope of sigma-theta (σ_Θ) = 27.35–27.55 kg m^3. This confirms that seawater density appears to be one of the main controlling environmental parameters favoring coral growth.

The temperature dependency of $\delta^{88/86}Sr$, Mg/Li and Sr/Ca was investigated to test the use of the main framework builder, the scleractinian cold-water coral *L. pertusa*, as a paleoceanographic archive for temperature reconstructions. For this purpose *L. pertusa* from contrasting seawater temperatures (5.9°–13.65°C) along the European continental margin

originating from the Norwegian margin, Porcupine Seabight, Bay of Biscay, Gulf of Cadiz and the Mediterranean Sea was investigated. Results are contrary to earlier findings that $\delta^{88/86}$Sr in *Lophelia* skeleton is positively correlated with temperature. Stable strontium isotope ratios measured with the Double Spike-TIMS technique show that it is rather inversely correlated with temperature between 5.9–9.5°C in the Atlantic sector. However, this temperature effect appears to be superimposed by changes in the ocean carbonate system. Elemental ratios such as Mg/Li and Sr/Ca clearly show a temperature dependency. Especially Mg/Li appears to be less vitally affected and may serve as a potential temperature proxy in future studies.

Paleoceanographic reconstructions revealed the control mechanisms of Challenger Mound growth in the Porcupine Seabight. Using both archives scleractinian corals (Mg/Li, Ba/Ca, Sr^{87}/Sr^{86}, U/Th) and calcitic foraminifera (Mg/Ca, $\delta^{13}C$) results indicate that mound initiation occurred coincidently with the reintroduction of the Mediterranean Outflow Water (MOW) at ~ 3Ma. Subsequently, this led to similar water mass stratification as today between the Eastern North Atlantic Water (ENAW) and MOW.

Early mound development prevailed throughout glacial and interglacial periods in the late Pliocene/early Pleistocene period, whereas the recent mound decline was caused by high amplitude excursions of the last interglacial/glacial cycles. Between 1.53–1.2 Ma mound development was interrupted coincidently with the Mid-Pleistocene-Transition, a period of global climate change when the high amplitude interglacial/glacial cycles (100 ka) initiated and glacial conditions became unfavourable for corals in the Porcupine Seabight. Overall, coral growth appears to occur within a temperature envelope between 8 to 10°C. However, besides temperature nutrient supply appears to be one of the main controlling mechanisms for cold-water coral mound growth. In the late Pleistocene variations of intermediate water masses such as the MOW and the Eastern North Atlantic Water (ENAW) and hence triggered mound growth and decline in the Porcupine Seabight. Whereas prior to the mid-Pleistocene rapid coral and mound growth benefited from high organic matter and nutrient concentrations due to a stable boundary layer between the MOW and ENAW.

Finally, this study highlights that cold-water coral ecosystems need specific environmental conditions and hence the recent climate change may cause a dramatic decline and shifts of the biogeographical distribution of cold-water coral reefs in the North Atlantic.

Outlook

Further investigation will be carried out in the DFG research project ECHO (Interm**E**diate water mass history at a **C**old-water coral **H**abitat in the N**O**rth Atlantic: Geochemical signals from IODP Site 1317) Main aim of this study is the reconstruction of inflowing intermediate water masses, such as the Mediterranean Outflow Water (MOW) into the Porcupine Seabight. Here, cold-water coral *Lophelia pertusa* from IODP Site 1317 will serve as an archive for neodymium isotopes of the past water masses in the Porcupine Seabight. Additionally, benthic foraminifera will be used in selected time intervals where no corals are recorded in order to establish a most complete variability of intermediate water masses through time. These investigations will improve our understanding of the role and trigger mechanisms of intermediate water mass dynamics, circulation, and potential admixture (MOW, Bay of Biscay) in relation to the colonization of cold-water corals in the Porcupine Seabight around 3 Ma, as well as during the Pleistocene and Holocene during the further development of carbonate mounds.

Three major questions for this research are:

• Was mound initiation and further development controlled by the reintroduction of MOW?

• Are the different stages of mound growth affected by the variability of intermediate water masses and or/vertical movements of MOW?

• How does MOW interact with the ENAW? Are both water masses ambient at the site of coral growth throughout the time of mound growth or have their been shifts in their relative proportions?

References

Adkins, J.F., Boyle, E.A., 1997. Changing atmospheric $\Delta^{14}C$ and the record of deep water paleoventilation ages. *Paleoceanography,* 12, 3, 337-344.

Adkins, J.F., Cheng, H., Boyle, E.A., Druffel, E.R.M. and Edwards, R.L., 1998. Deep-sea coral evidence for rapid changes in ventilation of the deep North Atlantic at 15.4 ka. *Science*, 280, 725-728.

Adkins, J.F., Boyle, E.A., Curry, W.B., Lutringer A., 2003. Stable isotopes in deep-sea corals and a new mechanism for "vital effects". *Geochimica et Cosmochimica Acta*, 67, 1129–1143.

Allison, N., Finch, A.A., 2007. High temporal resolution Mg/Ca and Ba/Ca records in modern *Porites lobata* corals. *Geochemistry, Geophysics, Geosystems*, 8, 5, pp. Q05001.

Anagnostou, E., Sherrell R. M., Gagnon A., LaVigne M., Field M. P., McDonough W. F., 2011. Seawater nutrient and carbonate ion concentrations recorded as P/Ca, Ba/Ca, and U/Ca in the deep-sea coral Desmophyllum dianthus. *Gecochimica et Cosmochimica Acta*, 75, 2529-2543, doi:10.1016/j.gca.2011.02.019

Barker, S., Greaves, M., Elderfield, H., 2003. A study of cleaning procedures used for foraminiferal Mg/Ca paleothermometry. *Geochemistry, Geophysics, Geosystems*, 4, doi: 10.1029/2003GC000559.

Bauch, D., Erlenkeuser, H., Andersen, N, 2005. Water mass processes on Arctic shelves as revealed from $\delta^{18}O$ of H_2O. *Global and Planetary Change,* 48, 165–174.

Beck, J.W., Edwards, R.L., Ito, E., Taylor, F.W., Recy, J., Rougerie, F., Joannot, P., Henin, C., 1992. Sea-Surface Temperature from Coral Skeletal Strontium Calcium Ratios. *Science*, 257, 5070, 644-647.

Becker, J., Lourens, L.L., Raymo, M.E., 2006. High-frequency climate linkages between the North Atlantic and the Mediterranean during marine oxygen isotope stage 100 (MIS100). *Paleoceanography*, 21, PA3002, doi 10.1029/2005PA001168.

Böhm, F., Gussone, N., Eisenhauer, A., Dullo, W-Chr., Reynaud, S., Paytan, A., 2006. Calcium isotope fractionation in modern scleractinian corals. *Geochimica et Cosmochimica Acta*, 70, 17, 4452-4462.

Blamart, D., Rollion-Bard, C., Meibom, A., Cuif, J.-P., Juillet-Leclerc, A., Dauphin, Y., 2007. Correlation of boron isotopic composition with ultrastructure in the deep-sea coral Lophelia pertusa: implications for biomineralization and paleopH. *Geochemistry*

Geophysics Geosystems, 8, Q12001. doi:10.1029/ 2007GC001686.

Blanchon, P., Eisenhauer, A., Fietzke, J., Liebetrau, V, 2009. Rapid sea-level rise and reef back-stepping at the close of the last interglacial highstand. *Nature,* 458, 881–884.

Broecker, W.S., 1986. Oxygen isotope constraints on surface ocean temperatures. *Quaternary Research*, 26, 121–134.

Bryan, S. P., Marchitto, T.M., 2008. Mg/Ca-temperature proxy in benthic foraminifera: new calibrations from the Florida Straits and a hypothesis regarding Mg/Li. *Paleoceanograph*y, 23, PA2220.

Case, D., Robinson, L.F., Auro, M.E., Gagnon, A.C., 2010. Environmental controls on Mg and Li in deep-sea scleractinian corals. *Earth and Planetary Science Letters*, 300, 3-4, 215-225.

Cheng, H., Adkins, J.F., Edwards, R.L., Boyle, E.A., 2000a. U–Th dating of deep-sea corals. *Geochimica et Cosmochimica Acta,* 64, 2401–2416.

Cheng, H., Edwards, R.L., Hoff, J., Gallup, C.D., Richards, D.A., Asmerson, Y., 2000b. The half-lives of uranium-234 and thorium-230. *Chemical Geology* 169, 17–33.

Coggon, R. M., D. A. Teagle, C. E. Smith‐Duque, J. C. Alt, and M. J. Cooper, 2010. Reconstructing past seawater Mg/Ca and Sr/Ca from mid‐ocean ridge flank calcium carbonate veins, *Science*, 327, 1114–1117, doi:10.1126/science.1182252.

Cohen, A.L., Owens, K.E., Layne, G.D., Shimizu, N., 2002. The effect of algal symbionts on the accuracy of Sr/Ca paleo-temperatures from corals. *Science*, 296, 331–333.

Cohen, A.L., Gaetani, G.A., Lundalv, T., Corliss, B.H., George, R.Y., 2006. Compositional variability in a cold-water scleractinian, Lophelia pertusa: New insights into "vital effects". *Geochemistry Geophysics Geosystems*, 7, Q12004, doi:10.1029/2006GC001354.

Colman, J.G., Gordon, D.M., Lane, A.P., Forde, M.J., Fitzpatrick, J., 2005. Carbonate mounds off Mauritania, Northwest Africa: status of deep-water corals and implications for management of fishing and oil exploration activities. In: Freiwald, A., Roberts, J.M. (Eds.), Cold-water Corals and Ecosystems. *Springer*, Heidelberg, pp. 417–441.

Craig, H., 1961. Standard for reporting concentrations of deuterium and oxygen 18 in naturals waters. *Science,* 133, 1833–1834.

Craig, H., Gordon, L. I., 1965. *Proceedings of the Third Spoleto Conference*, Spoleto, Italy, (ed. Tongiori, E.) 9–130 (Sischi and Figli, Pisa, Italy).

Davies, A. J., Wisshak, M., Orr, J. C., Roberts, J. M., 2008. Predicting suitable habitat for the

cold-water coral Lophelia pertusa (Scleractinia). Deep-Sea Research I, 55, 1048–1062.

De Cock, K., 2005. 3D-seismiche studie van koralbaanken aan de oostelijke rand van het Porcupine bekken, unpublished M.Sc. thesis, Ghent University, Belgium.

Delanghe, D., Bard, E., Hamelin, B., 2002. New TIMS constraints on the uranium-238 and uranium-234 in seawaters from the main ocean basins and the Mediterranean Sea. *Marine Chemistry,* 80, 79–93.

De Haas, H., Mienis, F., Frank, N., Richter, T.O., Steinbacher, R., de Stigter, H., van der Land, C., van Weering, T.C.E., 2009. Morphology and sedimentology of (clustered) cold-water coral mounds at the south Rockall Trough margins, NE Atlantic Ocean. *Facies*, 55, 1–26.

De Mol, B., Van Rensbergen, P., Pillen, S., Van Herreweghe, K., Van Rooji, D., McDonnell, A., Huvenne, V., Ivanov, M., Swennen, R., Henriet, J. P., 2002. Large deep-water coral banks in the Porcupine Basin, southwest of Ireland. *Marine Geology*, 188, 193-231.

De Mol, B., Kozachenko, M., Wheeler, A., Alvares, H., Henriet, J.-P., Olu-Le Roy, K., 2007. Thérèse Mound: a case study of coral bank development in the Belgica Mound Province, Porcupine Seabight. *International Journal of Earth Sciences*, 96, 103-120.

Dodds, L.A., J.M. Roberts, A.C. Taylor, and F. Marubini. 2007. Metabolic tolerance of the coldwater coral Lophelia pertusa (Scleractinia) to temperature and dissolved oxygen change. *Journal of Experimental Marine Biology and Ecology*, 349, 205–214.

Dorschel, B., Hebbeln, D., Rüggeberg, A., Dullo, W.-C., Freiwald, A., 2005. Growth and erosion of a cold-water coral covered carbonate mound in the Northeast Atlantic during Late Pleistocene and Holocene. *Earth and Planetary Science Letters*, 233, 33-44.

Dorschel, B., Hebbeln, D., Rüggeberg, A., Dullo, C., 2007a. Carbonate budget of a cold-water coral carbonate mound: Propeller Mound, Porcupine Seabight. *International Journal of Earth Sciences*, 96, 73-83.

Dorschel, B., Hebbeln, D., Foubert, A., White, M., Wheeler, A.J., 2007b. Hydrodynamics and cold-water coral facies distribution related to recent sedimentary processes at Galway Mound west of Ireland. *Marine Geology*, 244, 184-195.

Dullo, W.-C., Flögel, S., Rüggeberg, A., 2008. Cold-water coral growth in relation to the hydrography of the Celtic and Nordic European continental margin. *Marine Ecology Progress Series*, 371, 165-176.

Duplessy, J.C. , Lalou, C., Vinot, A.C., 1970. Differential isotopic fractionation in benthic foraminifera and paleotemperatures reassessed. *Science*, 168, 250-251.

Edwards, R. L., Chen, J. H., Wasserburg, G. J., 1986. ^{238}U–^{234}U–^{230}Th–^{232}Th systematics and the precise measurement of time over the past 500,000 years. *Earth and Planetary Science Letters*, 81, 175–192.

Eisele, M., Hebbeln, D., Wienberg, C., 2008. Growth history of a cold-water coral covered carbonate mound - Galway Mound, Porcupine Seabight, NE-Atlantic. *Marine Geology*, 253, 160-169.

Eisele, M., Frank. N., Wienberg, C., Hebbeln, D., López-Correa, M., Douville, E., Freiwald, A., 2011. Productivity controlled cold-water coral growth periods during the last glacial off Mauritania. *Marine Geology*, 280, 1-4, 143-149.

Emiliani, C., 1955. Pleistocene temperatures. *Journal of Geology*, 63, 538-578.

Enmar, R., M. Stein, M. Bar-Matthews, E. Sass, A. Katz, B. Lazar, 2000. Diagenesis in live corals from the Gulf of Aqaba. I. The effect on paleo-oceanography tracers, *Geochimica et Cosmochimica Acta*, 64, 3123-3132.

Erez, J., Luz, B., 1983. Experimental paleotemperature equation for planktonic foraminifera. *Geochimica et Cosmochimica Acta*, 47, 1025-1031.

European Commission, 2007. The Deep-Sea Frontier: Science Challenges for a Sustainable Future, *Luxembourg: Office for Official Publications of the European Communities*, pp. 53. ISBN 92-79-05266-8.

Expedition Scientists, 2005. Modern carbonate mounds: Porcupine drilling. *IODP Preliminary Report*, 307. doi:10.2204/iodp.pr.307.2005

Expedition 307 Scientists, 2006. Site U1317. In Ferdelman, T.G., Kano, A., Williams, T., Henriet, J.-P., and the Expedition 307 Scientists, 2006. *Proceedings of the Integrated Ocean Drilling Program, 307*: Washington, DC, *Integrated Ocean Drilling Program Management International, Inc.*, doi:10.2204/iodp.proc.307.104.2006

Fantle, M. S., DePaolo, D.J., 2006. Sr isotopes and pore fluid chemistry in carbonate sediment of the Ontong Java Plateau: Calcite recrystallization rates and evidence for a rapid rise in seawater Mg over the last 10 million years, *Geochimica et Cosmochimica Acta*, 70, 3883–3904, doi:10.1016/j.gca.2006.06.009.

Fairbanks, R. G., Charles, C. D., Wright, J. D., 1992. in Four Decades of Radiocarbon: An Interdisciplinary Approach (eds Long A. & Kra, R.) 473−500 (Springer).

Ferdelman, T.G., Kano, A., Williams, T., Henriet, J.-P., and the IODP Expedition 307 Scientists, 2006, Modern carbonate mounds: Porcupine Drilling, *Proceedings of the*

Integrated Ocean Drilling Program, Volume 307: College Station, Texas, *Integrated Ocean Drilling Program Management International, Inc.*, doi: 10.2204/iodp.proc.307.2006.

Fietzke, J., Liebetrau, v., Eisenhauer, A., W-Chr., Dullo, 2005. Determination of uranium isotope ratios by multi-static MIC-ICP-MS: method and implementation for precise U- and Th-series isotope measurements, *Journal of Analytical Atomic Spectrometry*, 20, 395-401. Doi: 10.1039/B415958F

Fietzke, J., Eisenhauer, A., 2006. Determination of temperature-dependent stable strontium isotope ($^{88}Sr/^{86}Sr$) fractionation via bracketing standard MC-ICP-MS. *Geochemistry Geophysics Geosystems*, 7, Q08009, doi:10.1029/2006GC001243

Fine, M., Tchernov, D., 2007. Scleractinian coral species survive and recover from decalcification. *Science*, 315, 5820, 1811. DOI: *10.1126/science.1137094*

Flower, B., Kennett, J.P., 1994. The middle Miocene climatic transition: East Antarctic ice sheet development, deep ocean circulation and global carbon cycling. *Palaeogeography, Palaeoclimatology, Palaeoecology*, 108, 537-555.

Flemming, J., 1846. On the recent Scottish Madrepores, with remakrs on the climatic character of the extinct races. Proceedings of the Royal Society, Edinburgh, 2,82-83.

Fosså, J.H., Lindberg, B., Christensen, O., Lundälv, T., Svellingen, I., Mortensen, P.B., Alvsvåg, J., 2005. Mapping of Lophelia reefs in Norway: experiences and survey methods. In: Freiwald, A., Roberts, J.M. (Eds.), Cold-water Corals and Ecosystems, *Springer*, Berlin Heidelberg, pp. 359-391.

Foubert, A., Beck, T., Wheeler, A.J., Opderbecke, J., Grehan, A., Klages, M., Thiede, J., Henriet, J.-P., Polarstern ARK-XIX/3a Shipboard Party, 2005. New View of the Belgica Mounds, Porcupine, NE Atlantic: preliminary results from the Polarstern ARK-XIX/3a ROV cruise. In: Freiwald, A., Roberts, J.M. (Eds.), Cold-Water Corals and Ecosystems. *Springer*, Berlin Heidelberg, pp. 403-415.

Foubert, A., Van Rooij, D., Blamart, D., Henriet, J.-P., 2007. X-ray imagery and physical core logging as a proxy of the content of sediment cores in cold-water coral mound provinces: a case study from Porcupine Seabight, SW of Ireland. *International Journal of Earth Sciences*, 96, 141-158.

Foubert, A., Henriet, J.-P., 2009. Nature and significance of the Recent Carbonate Mound Record. Lecture Notes in Earth Sciences 126, *Springer-Verlag*, Berlin, pp. 298.

Frank, N., Paterne, M., Ayliffe, L., van Weering, T.C.E., Henriet, J.-P., Blamart, D., 2004. Eastern North Atlantic deep-sea corals: tracing upper intermediate water Δ14C during

the Holocene. *Earth Planetary Science Letters*, 219, 297–309.

Frank, N., Lutringer, A., Paterne, M., Blamart, D., Henriet, J.-P., van Rooij, D., van Weering, T.C.E., 2005. Deep-water corals of the northeastern Atlantic margin: carbonate mound evolution and upper intermediate water ventilation during the Holocene. In: Freiwald, A., Roberts, J.M. (Eds.), Cold-water Corals and Ecosystems. *Springer*, Heidelberg, pp. 113–133.

Frank, N., Turpin, L., Cabioch, G., Blamart, D., Tressens-Fedou, M., Colin, C., Jean-Baptiste, P., 2006. Open system U-series ages of corals from a subsiding reef in New Caledonia: implications for sea level changes, and subsidence rate. *Earth Planetary Science Letters*, 249, 274–289.

Frank, N., Ricard, E., Lutringer-Paque, A., van der Land, C., Colin, C., Blamart, D., Foubert, A., Van Rooij, D., Henriet, J.-P., de Haas, H., van Weering, T.C.E., 2009. The Holocene occurrence of cold-water corals in the NE Atlantic: implications for coral carbonate mound evolution. *Marine Geology*, 266, 129–142.

Frank, N., Freiwald, A., Correa M.L., Wienberg, C., Eisele,M., Hebbeln, D., Van Rooij, D., Henriet, J.P., Colin, C., van Weering, T., de Haas, H., Buhl-Mortensen, P., Roberts, J.M., De Mol., B., Douville, E., Blamart, D., Hatte, C., 2011. Northastern Atlantic cold-water coral reefs and climate. *Geology*, 39, 8 ,743-746. doi:10.1130/G31825.1

Frederiksen, R., Jensen A., and Westerberg H., 1992. The distribution of the scleractinian coral Lophelia pertusa around the Faroe islands and the relation to internal tidal mixing. *Sarsia*, 77, 157-171.

Freiwald, A., 2002. Reef-forming cold-water corals. In: Wefer, G., Billet, D., Hebbeln D., Jorgensen, B.B., Schlüter, M., Van Weering, T., (Eds.), Ocean Margin Systems. *Springer-Verlag*, Heidelberg, pp. 365-385.

Freiwald, A., Fosså, J.H., Grehan, A., Koslow, T., Roberts, J.M., 2004. Cold-water coral reefs. UNEP-WCMC Biodiversity Series, 22. UNEP-WCMC, Cambridge, pp. 84.

Freiwald, A., Beuck, L., Rüggeberg, A., Taviani, M., Hebbeln, D., R/V Meteor Cruise M70-1 participants, 2009. The White Coral Community in the Central Mediterranean Sea revealed by ROV surveys. *Oceanography*, 22, 1, 58-74.

Gaetani, G.A., Cohen A.L., 2006. Element partitioning during precipitation of aragonite from seawater: A framework for understanding paleoproxies, *Geochimica et Cosmochimica Acta*, 70, 4617–4634.

Gaetani, G.A., Cohen, A.L., Wang, Z., Crusius, J., 2011. Rayleigh-based, multi-element coral thermometry: A biomineralization approach to developing climate proxies.

Geochimica et Cosmochimica Acta, 75, 1920-1932.

Gagan, M.K., Ayliffe, L.K., Hopley, D., Cali, J. A., Mortimer, G.E., Chappell, J., McCulloch, M., Head, M.J., 1998. Temperature and surface ocean water balance of the mid-Holocene tropical western Pacific, *Science*, 279, 1014–1018.

Gagnon, A.C., Adkins, J.F., Fernandez, D.P., Robinson, L.F., 2007. Sr/Ca and Mg/Ca vital effects correlated with skeletal architecture in a scleractinian deep-sea coral and the role of Rayleigh fractionation. *Earth Planetary Science Letters*, 261, 280–295.

Ganssen, G., Kroon, D., 2000. The isotopic signature of planktonic foraminifera from the NE Atlantic surface sediments: implications for the reconstruction of past oceanic conditions. *Journal of the Geological Society of London*, 157, 693–699.

Gattuso, J.P., Frankignoulle, M., Bourge, I., Romaine, S., Buddemeier, R.W., 1998. Effect of calcium carbonate saturation of seawater on coral calcification. *Global Planetary Change*, 18, 37–46.

Gass, S.E., Roberts, J.M., 2011. Growth and branching patterns of Lophelia pertusa (Scleractinia) from the North Sea. *Journal of Marine Biological Association of the United Kingdom*, 91, 831-835.

Gladfelter, E.H., 1982. Skeletal development in Acropora cervicornis: I. Patterns of calcium carbonate accretion in the axial corallite. *Coral Reefs*, 1, 45–51.

Goldstein, S.J., Lea, D.E., Chakraborty S., Kashgarian M., Murrell M.T., 2001. Uranium-series and radiocarbon geochronology of deep-sea corals: implications for southern ocean ventilation rates and the oceanic carbon cycle. *Earth and Planetary Science Letters*, 193, 167–182.

Graham, D.W., Corliss, B.H., Bender, M.L., Keigwin Jr., L.D., 1981. Carbon and oxygen isotopic disequilibria of recent deep-sea benthic foraminifera. *Marine Micropaleontology*, 6, 5-6, 483-497.

Greaves, M., Barker, S., Daunt, C., and Elderfield, H., 2005. Accuracy, standardization, and interlaboratory calibration standards for foraminiferal Mg/Ca thermometry, *Geochemistry Geophysics Geosystems*, 6, Q02D13, doi:10.1029/2004GC000790

Guinotte, J.M., Orr, J., Cairns, S., Freiwald, A., Morgan, L., George, R., 2006. Will human-induced changes in sewater chemistry alter the distribution of deep-sea scleractinian corals? *Frontiers in Ecology and Environment*, 4, 3, 141-146.

Gunnerus, J.E., 1768. Om nogle Norske Coraller. *Konglige Norske Videnskabers Selskabs Skrifter*, 38-73.

Hargreaves, P.M., 1984. The distribution of Decapoda (Crustacea) in open ocean near bottom

over an adjacent slope in the Nothern North-east Atlantic Ocean during autumn 1979. *Journal of the Marine Biological Association of the United Kingdom*, 64, 829–857.

Hathorne, E., James, R.H., 2006. Temperoal record of lithium in seawater: a tracer for silicate weathering? *Earth and Planetray Science Letters*, 246, 393-406.

Hathorne, E., Felis, T., James, R.H., Thomas, A., 2011. Laser ablation ICP-MS screening for coral diagenetically affected areas applied to Tahiti coral from the last deglaciation. *Geochimica Et Cosmochimica Acta*, 75, 1490–1506.

Haug, G.H., Tiedemann, R., 1998. Effect of the formation of the Isthmus of Panama on Atlantic Ocean thermohaline circulation. *Nature* 393, 673–676.

Henderson, G.M., Anderson, R.F., 2003. The U-series Toolbox for Paleoceanography. *Reviews in Mineralogy and Geochemistry,* 52, 493–531.

Hendy, E.J., Gagan, M.K., Lough, J.M., McCulloch, M. T., de Menocal, P. B., 2007. Impact of skeletal dissolution and secondary aragonite on trace element and isotopic climate proxies in Porites corals, *Paleoceanography*, 22, PA4101, doi:4110.1029/2007PA001462.

Henriet, J.-P., De Mol, B., Pillen, S., Vanneste, M., Van Rooij, D., Versteeg, W., Croker, P.F., Shannon, P.M., Unnithan, V., Bouriak, S., Chachkine, P., 1998. Gas hydrate crystals may help build reefs. *Nature,* 391, 648-649.

Henriet, J.-P., De Mol, B., Vanneste, M., Huvenne, V., Van Rooij, D., the Porcupine-Belgica 97, 98, and 99 Shipboard Parties, 2001. Carbonate mounds and slope failures in the Porcupine Basin: a development model involving fluid venting. In: Shannon, P.M., Haughton, P., and Corcoran, D. (eds.) Petroleum Exploration of Ireland's Offshore Basins. *Geological Society Special Publications*, 188, 375–383.

Hodell, D. A., Curtis, J. H., Sierro, F. J., Raymo, M. E., 2001. Correlation of late Miocene to early Pliocene sequences between the Mediterranean and North Atlantic. *Paleoceanography*, 16, 2, 164–178.

Hooper, P.W.P., Funnell, B.M., 1986. Late Pliocene to Recent planktonic foraminifera from the North Atlantic DSDP Site 552A: quantitative palaeotemperature analysis. *Geological Society Special Publication*, 21, 181-90.

Hovland, M., Croker, P.F., Martin, M., 1994. Fault-associated seabed mounds (carbonate knolls?) off western Ireland and north-west Australia. *Marine and Petroleum Geology*, 11, 232-246.

Hovland, M., Mortensen, P.B., Brattegard, T., Strass, P., Rokengen, K., 1998. Ahermatypic coral banks off mid-Norway: evidence for a link with seepage of light hydrocarbons.

Palaios, 13, 189–200.

Huvenne, V.A.I., De Mol, B., Henriet, J.-P., 2003, A 3D seismic study of the morphology and spatial distribution of buried coral banks in the Porcupine Basin, SW of Ireland, *Marine Geology*, 198, 5 – 25, doi:10.1016/S0025-3227(03)00092-6.

Huvenne, V.A.I., Beyer, A., de Haas, H., Dekindt, K., Henriet, J.P., Kozachenko, M., Olu-Le Roy, K., Wheeler, A.J., the TOBI/Pelagia 197 and CARACOLE cruise participants, 2005. The seabed appearance of different coral bank provinces in the Porcupine Seabight, NE Atlantic: results from sidescan sonar and ROV seabed mapping. In: Freiwald, A., Roberts, J.M. (Eds.), Cold-water corals and ecosystems. *Springer-Verlag*, Heidelberg, pp. 535-569.

Huvenne, V.A.I., Bailey, W.R., Shannon, P., Naeth, J., di Primio, R., Henriet, J.P., Horsfield, B., de Haas, H., Wheeler, A., Olu-Le Roy, K., 2007. The Magellan mound province in the Porcupine Basin. *International Journal of Earth Sciences*, 96, 85-101.

Huvenne, V.A.I., Van Rooij, D., De Mol, B., Thierens, M., O'Donnell, R., Foubert, A., 2009. Sediment dynamics and palaeo-environmental context at key stages in the Challenger cold-water coral mound formation: Clues from sediment deposits at the mound base, *Deep Sea Research I,* 56,12, 2263-2280.

Imbrie, J., Hays, J.D., Martinson, D.G., McIntyre, A., Mix, A.C., Morley, J.J., Pisias, N.G., Prell, W.L., and Shackleton, N.J., 1984. in: Milankovitch and Climate, Part I. The orbital theory of Pleistocene climate: Support from a revised chronology of marine $\delta^{18}O$ record. (eds. Berger, A. L.) 269–305 (*Hingham, Mass*.)

Inoue, M., R. Suwa, A. Suzuki, K. Sakai, Kawahata, H. 2011. Effects of seawater pH on growth and skeletal U/Ca ratios of Acropora digitifera coral polyps. *Geophysical Resesearch Letters*, 38, L12809; doi:10.1029/2011GL047786.

Kano, A., Ferdelman, T.G., Williams, T., Henriet, J.-P., Ishikawa, T., Kawagoe, N., Takashima, C., Kakizaki, Y., Abe, K., Sakai, S., Browning, E.L., Li, X., IODP Expedition 307 Scientists, 2007. Age constrains on the origin and growth history of a deep-water coral mound in the northeast Atlantic drilled during Integrated Ocean Drilling Program Expedition 307. *Geology*, 35, 1051-1054.

Keller, G., Barron, J.A., 1983. Paleoceanographic implications of Miocene deep-sea hiatuses. *Geological Society of America Bulletin*, 94, 590-613.

Kenyon, N.H., Akhmetzhanov, A.M., Wheeler, A., van Weering, T.C.E., de Haas, H., Ivanov, M.K., 2003. Giant carbonate mud mounds in the southern Rockall Trough. *Marine Geology*, 195, 5-30.

Khélifi, N., Sarnthein, M., Andersen, N., Blanz, T., Frank, M., Garbe-Schönberg, D., Haley, B.A., Stumpf, R., Weinelt, M., 2009. A major and long-term Pliocene intensification of the Mediterranean Outflow (3.4–3.3). *Geology*, 37, 9, 811-814.

Kinsman, D. J. J., H. D. Holland, 1969. The co-precipitation of cations with $CaCO_3$–IV. The co-precipitation of Sr^{2+} with aragonite between 16°C and 96°C, *Geochimica et Cosmochimica Acta*, 33, 1–17.

Kiriakoulakis, K., Freiwald, A., Fischer, E., Wolff, G. A., 2007. Organic matter quality and supply to deep-water coral/mound systems of the NW European Continental Margin. *International Journal of Earth Sciences,* 96, 159–170.

Kleiven, H.F., Jansen, E., Fronval, T., Smith, T.M., 2002. Intensification of Northern Hemisphere glaciations in the circum Atlantic region (3.5–2.4 Ma) — ice-rafted detritus evidence. *Palaeogeography Palaeoclimatology Palaeoecology*, 184, 3–4, 213–223.

Krabbenhöft, A., Fietzke, J., Eisenhauer, A., Liebetrau, V., Böhm, F., Vollstaedt, H., 2009. Determination of radiogenic and stable strontium isotope ratios ($^{87}Sr/^{86}Sr$/ $\delta^{88/86}Sr$) by thermal ionization mass spectrometry applying an $^{87}Sr/^{84}Sr$ double spike. *Journal of Analyical Atomic Spectrometry*, 24, 1267–1271.

Krabbenhöft, A., Eisenhauer, A., Böhm, F., Vollstaedt, H., Fietzke, J., Liebetrau, V., Augustin, N., Peucker-Ehrenbrink, B., Müller, M.N., Horn, C., Hansen, B.T., Nolte, N., Wallmann, K., 2010. Constraining the marine strontium budget with natural strontium isotope fractionations ($^{87}Sr/^{86}Sr^*$, $\delta^{88/86}Sr$) of carbonates, hydrothermal solutions and river waters. *Geochimica et Cosmochimica Acta*, 74, 14, 4097-4109.

Kroon, D., Ganssen, G., 1989. Northern Indian Ocean upwelling cells and the stable isotope composition of living planktonic foraminferas, *Deep Sea Research I*, 36, 1219-1236.

Lawrence, K.T., Herbert, T.D., Brown, C.M., Raymo, M.E., Haywood, A.M., 2009. Highamplitude variations in North Atlantic sea surface temperature during the early Pliocene warm period. *Paleoceanography*, 24, PA2218 doi:2210.1029/2008pa001669

Lazar, B., Enmar, R., Schossberger, M., Bar-Matthews, M., Halicz, L., Stein, M., 2004. Diagenetic effects on the distribution of uranium in live and Holocene corals from the Gulf of Aqaba, *Geochimica et Cosmochimica Acta*, 68, 4583-4593.

Lea, D.W. Boyle, E.A., 1990. A 210,000-year record of barium variability in the deep northwest Atlantic Ocean. *Nature*, 347, 269-272

Lear, C.H., Rosenthal, Y., Slowey, N., 2002. Benthic foraminiferal Mg/Ca-paleothermometry: A revised core-top calibration, *Geochimica et Cosmochimica Acta*,

66, 3375- 3387.

Le Danois, E., 1948. Les profondeurs de la mer. Payot, Paris, pp. 303.

Levitus, S., T. Boyer, 1994: World Ocean Atlas 1994, Vol. 4: Temperature. *NOAA Atlas NESDIS 4, U.S. Gov. Printing Office*, Washington, D. C., 117 pp.

Liebetrau, V., Eisenhauer, A., Krabbenhöft, A., Fietzke, J., Böhm, F., Rüggeberg, A., Guers, K., 2009. New perspectives on the marine Sr-isotope record: $\delta^{88/86}Sr$, $^{87}Sr/^{86}Sr^*$ and $\delta^{44/40}Ca$ signatures of aragonitic molluscs throughout the last 27 Ma. *Geochimica et Cosmochimica Acta*, 73, A762.

Liebetrau, V., Eisenhauer, A., Linke, P., 2010. Cold seep carbonates and associated cold-water corals at the Hikurangi Margin, New Zealand: New insights into fluid pathways, growth structures and geochronology. *Marine Geology*, 272, 307-318, doi:10.1016/j.margeo.2010.01.003

Lindberg, B., Berndt, C., Mienert, J., 2007. The Fugløy Reef at 70°N; acoustic signature, geologic, geomorphologic and oceanographic setting. *International Journal of Earth Sciences*, 96, 201–213.

Linnaeus, C., 1758. Systema naturae, 10th edn, vol. 1. Stockholm: L. Salvii.

Lisiecki, L.E., Raymo, M.E., 2005. A Pliocene-Pleistocene stack of 57 globally distributed benthic $\delta^{18}O$ records. *Paloeceanography*, 20, PA1003, doi 10.1029/2004PA001071.

Loeblich, A.R., Tappan, H., 1988. Foraminiferal Genera and their Classification. *Van Nostrand Reinhold*, New York, 2 volumes.

Louwye, S., Foubert, A., Mertens, K., Van Rooij, D., IODP Expedition 307 Scientific Party, 2007. Integrated stratigraphy and palaeoecology of the Lower and Middle Miocene of the Porcupine Basin. *Geological Magazine*, 145, 1-24.

Lutringer, A., Blamart, D., Frank, N., Labeyrie, L., 2005. Paleotemperatures from deep-sea corals: scale effects. In: Freiwald, A., Roberts, J.M. (Eds.), Cold-water Corals and Ecosystems. *Springer-Verlag*, pp. 1081–1096.

Lutze, G.F., Thiel, H., 1987. Cibicidoides wuellerstorfi and Planulina ariminensis, elevated epibenthic Foraminifera. Report N., 6. Sonderforschungsbereich 313, *Universität Kiel*.

Lynch-Stieglitz, J., Curry, W.B., Slowey, N., 1999a. A Geostrophic Transport Estimate for the Florida Current from the Oxygen Isotope Composition of Benthic Foraminifera. *Paleoceanography*, 14, 3, 360-373.

Lynch-Stieglitz, J., Curry, W. B., Slowey, N., 1999b. Weaker Gulf Stream in the Florida Straits during the Last Glacial Maximum. *Nature,* 402, 644–648.

Mackensen, A., Bickert, T., 1999. Stable carbon isotopes in benthic foraminifera: proxies for

deep and bottom water circulation and new production. In: Fisher, G., Wefer, G. (Eds.), Use of Proxies in Paleoceanography: Examples from the south Atlantic. *Springer*, Berlin, pp. 229-254.

Mackensen, A., Schumacher, S., Radke, J., Schmidt, D.N., 2000. Microhabitat preferences and stable carbon isotopes of endobenthic foraminifera: Clue to quantitative reconstruction of oceanic new production. *Marine Micropaleontology*, 40, 233- 258.

Maier, C., Hegeman, J., Weinbauer, M. G., Gattuso, J. P., 2009. Calcification of the cold-water coral Lophelia pertusa under ambient and reduced pH. *Biogeosciences*, 6, 8, 1671-1680.

Margreth, S., Rüggeberg, A., Spezzaferri, S., 2009. Benthic foraminifera as bioindicator for cold-water coral reef ecosystems along the Irish margin. *Deep-Sea Research I*, 56, 12, 2216–2234.

Marriott, C.S., Henderson, G.M., Belshaw, N.S., Tudhope, A.W., 2004. Temperature dependence of δ^7Li, δ^{44}Ca and Li/Ca during growth of calcium carbonate. *Earth Planetary Science Letters*, 222, 615–624.

McArthur, J.M., 1994. Recent Trends in Strontium Isotope Stratigraphy. *Terra Nova*, 6, 4, 331-358.

McArthur, J.M., Howarth, R.J., Bailey, T.R., 2001, Strontium isotope stratigraphy: LOWESS Version 3. Best-fit line to the marine Sr-isotope curve for 0 to 509 Ma and accompanying look-up table for deriving numerical age (look-up table version 4B: 08-04). *The Journal of Geology*, v. 109, p. 155–169, doi: 10.1086/319243

McArthur, J.M., Howarth, R.J., 2004. Sr-isotope stratigraphy: The Phanerozoic 87/86Sr-curve and explanatory notes. In: Gradstein, F., Ogg, J. & Smith, A. G. eds. A Geological Timescale. *Cambridge University Press*, New York, 96–104.

McCave, I.N., Manighetti, B., Robinson, S.G., 1995. Sortable silt and fine sediment size/composition slicing: Parameters for paleocurrent speed and paleoceanography. *Paleoceanography*, 10, 563-610.

McCorkle, D.C., Keigwin, L.D., Corliss, B.H., Emerson, S., 1990. The influence of microhabitats on the carbon isotopic composition of deep-sea benthic foraminifera. *Paleoceanography*, 5, 161-185.

McCulloch, M., Taviani, M., Montagna, P., López Correa, M., Remia, R. & Mortimer, G., 2010. Proliferation and demise of deep-sea corals in the Mediterranean during the Younger Dryas. *Earth and Planetary Science Letters*, 298, 1/2, 143-152; doi:10.1016/j.epsl.2010.07.036.

Mienis, F., van Weering, T., de Haas, H., de Stigter, H., Huvenne, V., Wheeler, A., 2006. Carbonate mound development at the SW Rockall Trough margin based on high resolution TOBI and seismic recording. *Marine Geology*, 233, 1-19.

Mienis, F., de Stigter, H.C., White, M., Duineveld, G., de Haas, H., van Weering, T., 2007. Hydrodynamic controls on cold-water coral growth and carbonate-mound 29 development at the SW and SE Rockall Trough Margin, NE Atlantic Ocean. *Deep Sea Research*, I, 54, 9, 1655-1674.

Mienis, F., van der Land, C., de Stigter, H.C., van de Vorstenbosch, M., de Haas, H., Richter, T., van Weering, T.C.E., 2009. Sediment accumulation on a cold- water carbonate mound at the Sothwest Rockal Trough margin. *Marine Geology*, 265, 40-50.

Miller, K.G., Fairbanks, R.G., 1983. Evidence for Oligocene-Middle Miocene abyssal circulation changes in the western North Atlantic. *Nature*, 306, 250-253.

Min, G.R., Edwards L.R., Taylor F.W., Recy J., Gallup C.D., Beck W.J., 1995. Annual cycles of U/Ca in coral skeletons and U/Ca thermometry. *Geochimica et Cosmochimica Acta*, 59, 2025– 2042.

Mitsuguchi, T., Matsumoto, E., Abe, O., Uchida, T., Isdale, P.J., 1996. Mg/Ca thermometry in coral-skeletons. *Science*, 274, 5289, 961-963.

Moen, T.L., 2006. A translation of Bishop Gunnerus' description of the species Hydroides norvegicus with comments on his Serpula triqvetra. *Scientia Marina*, 70, S3, 115-123.

Montagna, P., McCulloch, M., Taviani, M., Remia, A., Rouse, G., 2005. High-resolution trace and minor element compositions in deep-water scleractinian corals (Desmophyllum dianthus) from the Mediterranean Sea and the Great Australian Bight. In: Freiwald, A., Roberts, J.M. (Eds.), Cold-water Corals and Ecosystems. *Springer-Verlag*, pp. 1109–1126.

Montagna, P., McCulloch, M., Taviani, M., Mazzoli, C., Vendrell, B., 2006. Phosphorus in cold-water corals as a proxy forseawater nutrient chemistry. *Science*, 312, 1788–1791.

Montagna, P., López Correa, M., Rüggeberg, A., McCulloch, M., Rodolfo-Metalpa, R., Dullo, W.-Chr., Ferrier-Pagès, C., Freiwald, A., Henderson, G.M., Mazzoli, C., Russo, S., Silenzi, S., Taviani, M. 2008. Coral Li/Ca in micro-structural domains as a temperature proxy. *Geochimica et Cosmochimica Acta*, 72: A645.

Mortensen, P.B., Rapp, H.T. 1998. Oxygen and carbon isotope ratios related to growth line patterns in skeletons of *Lophelia pertusa* (L) (Anthozoa, Scleractinia): Implications for determination of linear extension rates. *Sarsia* 83, 5, 433-446.

Mortensen, P. B., 2001. Aquarium observations on the deepwater coral Lophelia pertusa (L.,

1758) (Scleractinaria) and selected associated invertebrates. *Ophelia*, 54, 83–104.

Mortlock, R.A., Fairbanks, R.G., Chiu, T.-C., and Rubenstone, J., 2005, $^{230}Th/^{234}U/^{238}U$ and $^{231}Pa/^{235}U$ ages from a single fossil coral fragment by multicollector magnetic-sector inductively coupled plasma mass spectrometry. *Geochimica et Cosmochimica Acta*, 69, 649–657, doi:10.1016/j .gca.2004.06.033.

Muddelsee, M., Schulz, M., 1997. The Mid-Pleistocene climate transition: onset of 100ka cycle lags ice volume build by 280ka. *Earth and Planetray Science Letters*, 151, 1-2,117-123.

Müller, A., M. K. Gagan, and M. T. McCulloch, 2001. Early marine diagenesis in corals and geochemical consequences for paleoceanographic reconstructions, *Geophysical Research Letters*, 28, 4471-4474.

Naafs, B.D.A., Stein, R., Hefter, J., Khélifi, N., De Schepper, S., Haug, G.H., 2010. Late Pliocene changes in the North Atlantic Current. *Earth and Planetary Science Letters*, 298, 434-442.

Naidu, D.P., 2004. Isotopic evidences of past upwelling intensity in the Arabian Sea. *Global and Planetary Change*, 40, 285-293.

Naidu, D.P., Niitsuma, N., 2004. Atypical $\delta^{13}C$ signature in Globigerina bulloides at the ODP Site 732A (Arabian Sea): implications of environmental changes caused by upwelling. *Marine Micropaleontology*, 53, 1-10.

Nikolaev, S.D., Oskina, N.S., Blyum, N.S., Bubenshchikova, N.V., 1998. Neogen-Quaternary variations of the 'pole-equator' temperature gradient of the surface oceanic waters in the North Atlantic and North Pacific. *Global and Planetary Change*, 18, 85-111.

Okai, T., Suzuki, A., Kawahata, H., Terashima, S., Imai, N., 2002. Preparation of a new Geological Survey of Japan geochemical reference material: coral JCp-1, *Geostandards Newsletter*, 26, 95-99.

Okai, T., A. Suzuki, S. Terashima, M. Inoue, M. Nohara, H. Kawahata, and N. Imai, 2004. Collaborative analysis of GSJ/AIST geochemical reference materials JCp-1 (Coral) and JCt-(Giant Clam), *Chikyukagaku (Geochemistry),* 38, 281-286.

O'Neil, J.R., Clayton, R.N., Mayeda, T.K., 1969. Oxygen isotope fractionation in divalent metal carbonates. *Journal of Chemical Physics* , 51, 12, 5547-5558.

Orejas, C., Gori, A., Gili, J.M. 2008. Growth rates of live Lophelia pertusa and Madrepora oculata from the Mediterranean Sea maintained in aquaria. *Coral Reefs*, 27, 2, 255.

Pagani, M., Arthur, M.A., Freeman, K.H., 1999. Miocene evolution of atmospheric carbon dioxide. *Paleoceanography*, 14, 273-292.

Pearson, I., Jenkins, D.G., 1986. Unconformities in the Cenozoic of the North-East Atlantic. In: Summerhayes, C.P., Shackleton, N.J. (Eds.), North Atlantic Palaeoceanography. *Geological Society*, London, Special Publication 21, 79-86.

Peck, V. L., Hall, I.R., Zahn, R., Scourse, J.D., 2007. Progressive reduction in NE Atlantic intermediate water ventilation prior to Heinrich events: Response to NW European ice sheet instabilities? *Geochemistry Geophysics Geosystems*, 8, Q01N10, doi:10.1029/2006GC001321.

Pirlet, H., Wehrmann, L.M., Brunner, B., Frank, N., DeWanckele, J., Van Rooij, D., Foubert, A., Swennen, R., Naudts, L., Boone, M., Cnudde, V., Henriet, J.-P., 2010. Diagenetic formation of gypsum and dolomite in a cold-water coral mound in the Porcupine Seabight, off Ireland. *Sedimentology*, 57, 786-805.

Pons-Branchu, E., Hillaire-Marcel, C., Deschamps, P., Ghaleb, B., Sinclair, D,J., 2005. Early diagensis impact on precise U-series dating of deep-sea corals: Example of a 100-200-year old Lophelia pertusa sample from the northeast Atlantic. *Geochimica Et Cosmochimica Acta*, 69, 20, 4865-4879.

Pontoppidan, E., 1755. The natural history of Norway: containing, a particular and accurate account of the temperature of the air, the different soils, waters, vegetables, metals, minerals, stones, beasts, birds, and fishes; together with the dispositions, customs, and manner of living of the inhabitants; interspersed with physiological notes from eminent writers, and translations of academies. In two parts. Translated from the Danish original. *A. Linde*, London, 206 pp.

Pollard, R.T., Griffiths, M.J., Cunningham, S.A., Read, J.F., Perez, F.F., Rios, A.F., 1996. Vivaldi 1991 – A study of the formation, circulation and ventilation of 14 Eastern North Atlantic Central Water. *Progress In Oceanography*, 37, 2, 167-172.

Purser, A., Larsson, A.I., Thomsen, L., Van Oevelen, D., 2010. The influence of flow velocity and food concentrations on Lophelia pertusa (Scleractinian) zooplankton capture rates. *Journal of Experimental Marine Biology*, 395, 55-62.

Raddatz, J., Rüggeberg, A., Margreth, S. und Dullo, W. C., IODP Expedition 307 Scientific Party, 2011. Paleoenvironmental reconstruction of Challenger Mound initiation in the Porcupine Seabight, NE Atlantic. *Marine Geology*, 282, 79-90. doi:10.1016/j.margeo.2010.10.019.

Raymo, M.E., Ruddiman, W.F., Backman, J., Clement, B.M., Martinson, D.G., 1989. Late Pliocene variation in Northern Hemisphere ice sheets and North Atlantic deep water circulation. *Paleoceanography*, 4, 413–446 doi:410.1029/PA1004i1004p00413.

Raymo, M.E., Hodell, D., Jansen, E., 1992. Response of deep ocean circulation to initiation of Northern Hemisphere Glaciation (3–2 MA). *Paleoceanography*, 7, 645–672 doi:610.1029/1092pa01609.

Ribaud-Laurenti, A., Hamelin, B., Montaggioni, L., Cardinal, D., 2001. Diagenesis and its impact on Sr/Ca ratios in Acropora corals, *Geologische Rundschau*, 90, 438 - 451, doi:10.1007/s005310000168.

Rice, A.L., Billet, D.S.M., Thurston, M.H., Lampitt, R.S., 1991. The Institute of Oceanographic Sciences biology programme in the Porcupine Seabight: background and general introduction, *Journal of the Marine Biological Association of the United Kingdom*, 71, pp. 281-310.

Roberts, J.M., Wheeler, A.J., Freiwald, A., 2006. Reefs of the deep: the biology and geology of cold-water coral ecosystems. *Science*, 312, 543-547.

Roberts, J.M., Wheeler, A., Freiwald, A., Cairns, S.D., Cold water corals, The Biology and Geology of Deep Sea Coral habitats, 2009. *Cambridge University Press*, pp. 352.

Robinson, L.F., Belshaw, N.S., Henderson, G.M., 2004. U and Th concentrations and isotope ratios in modern carbonates and waters from the Bahamas. *Geochimica et Cosmochimica Acta*, 98, 8, 1777-1789.

Rollion-Bard, C., Vigier N., Meibom A., Blamart D., Reynaud S., Rodolfo-Metalpa R., Martin, S., Gattuso J.-P., 2009. Effect of environmental conditions and skeletal ultrastructure on the Li isotopic composition of scleractinian corals. *Earth Planetary Science Letters*, 286, 63–70.

Rollion-Bard, C., Blamart, D., Cuif, J.-P., Dauphin Y., 2010. In situ measurements of oxygen isotopic composition in deep-sea coral, Lophelia pertusa: re-examination of the current geochemical models of biomineralization. *Geochimica et Cosmochimica Acta*, 74, 1338–1349.

Rosenthal, Y., Field, M.P., Sherrell, R.M., 1999. Precise determination of element/calcium ratios in calcareous samples using sector field inductively coupled plasma mass spectrometry. *Analytical Chemistry*, 71, 15, 3248-3253.

Rüggeberg, A., Dorschel, B., Dullo, C., Hebbeln, D., 2005. Sedimentary patterns in the vicinity of a carbonate mound in the Hovland Mound Province, northern Porcupine Seabight. In: Freiwald, A., Roberts, J.M. (Eds.), Cold-water Corals and Ecosystems. *Springer Verlag*, Berlin Heidelberg, pp. 87-112.

Rüggeberg, A., Dullo, C., Dorschel, B., Hebbeln, D., 2007. Environmental changes and growth history of a cold-water carbonate mound (Propeller Mound, Porcupine

Seabight). *International Journal of Earth Sciences*, 96, 57-72.

Rüggeberg, A., Fietzke, J., Liebetrau, V., Eisenhauer, A., Dullo, W-Chr., Freiwald, A., 2008. Stable Strontium Isotopes ($\delta^{88/86}$Sr) in Cold-Water Corals - A new Proxy for Reconstruction of Intermediate Ocean Water Temperatures. *Earth and Planetary Science Letters*, 269, 3-4, 569-574.

Sakai, S., Kano, A., Abe, K., 2009. Origin, glacial-interglacial responses, and controlling factors of a cold-water coral mound in NE Atlantic, *Paleoceanography*, 24, PA2213, doi:10.1029/2008PA001695.

Sarnthein, M., Winn, K., Jung, S.J.A., Duplessy, J.-C., Labeyrie, L., Erlenkeuser, H., Ganssen, G., 1994. Changes in East Atlantic Deepwater Circulation Over the Last 30,000 years: Eight Time Slice Reconstructions. *Paleoceanography*, 9, 2, 209-267.

Savin, S. M., 1977. The history of the Earth's surface temperature during the past 100 million years. *Annual Review of Earth and Planetary Sciences*, 5, 319-355.

Schmidt, G. A., Bigg, G. R., Rohling, E. J., 1999. Global Seawater Oxygen-18 Database, http://data.giss.nasa.gov/o18data/.

Schönfeld, J. and Zahn, R., 2000. Late Glacial to Holocene history of the Mediterranean Outflow. Evidence from benthic foraminiferal assemblages and stable isotopes at the Portuguese Margin. *Palaeogeography Palaeoclimatology Palaeoecology*, 159, 85-111.

Schröder-Ritzrau, A., Freiwald, A., Mangini, A., 2005. U/Th-dating of deep-water corals from the eastern North Atlantic and the western Mediterranean Sea. In: Freiwald, A., Roberts, J.M. (Eds.), Cold-water Corals and Ecosystems. Springer, Heidelberg, pp. 691–700.

Shackleton, N. J., 1974. Attainment of isotopic equilibrium between ocean water and the benthonic foraminifera genus Uvigerina: Isotopic changes in the ocean during the last glacial. *Colloquium International CNRS*, 219, 203-225.

Shen, G. T., and R. B. Dunbar, 1995. Environmental controls on uranium in reef corals, *Geochimica et Cosmochimica Acta*, 59, 2009-2024.

Shen, C.C., Lee, T., Chen, C.-Y,. Wang, C-H., Dai,C.-F., Li,L.-A., 1996. The calibration of D[Sr/Ca] versus sea surface temperature relationship for Porites corals, Geochimica et Cosmochimica Acta, 60, 3849-3858.

Shevenell, A.E., Kennett, J.P., Lea, D.W., 2004. Middle Miocene Southern Ocean cooling and Antarctic cryosphere expansion. *Science*, 305, 1766-1770.

Shirai, K., Kusakabe, M., Nakai, S., Ishii, T.,Watanabe, T., Hiyagon, H., Sano, Y., 2005.

Deep sea coral geochemistry: implication for the vital effect. *Chemical Geology*, 224, 212–222.

Sinclair, D. J., Williams, B., and Risk, M., 2006. A biological origin for climate signals in corals - Trace element "vital effects" are ubiquitous in Scleractinian coral skeletons. *Geophysical Research Letters*, 33, L17707, doi:10.1029/2006GL027183.

Smith, S.V., Buddemeier, R.W., Redalje, R.C., Houck J.E., 1979. Strontium-Calcium Thermometry in Coral Skeletons. Science, 204, 4391, 404-407.

Smith, J.E., Schwarcz, H.P., Risk, M.J., McConnaughey, T.A., Keller, N., 2000. Paleotemperatures from deep-sea corals: overcoming 'vital effects'. *Palaios,* 15, 25–32.

Smith, J.E., Schwarcz, H.P., Risk, M.J., 2002. Patterns of isotopic disequilibria in azooxanhtellate coral skeletons. *Hydrobiologia*, 471, 111–115.

Soria, J.M., Caracuel, J.E., Corbi, H., Dinares-Turell, J., Lancis C., Tent-Manclus J.E., Viseras C., Yebenes, A., 2008. The Messinian-early Pliocene stratigraphic record in the southern Bajo Segura Basin (Betic Cordillera, Spain): Implications for the Mediterranean salinity crisis. *Sedimentary Geology*, 203, 3-4, 267-288.

Spero, H.J., Bijma, J., Lea, D.W., Bemis, B.E., 1997. Effect of seawater carbonate concentration on foraminiferal carbon andoxygen isotopes. *Nature*, 390, 497–500.

Stirling, C.H., Esat, T.M., Lambeck, K., McCulloch, M.T., 1998. Timing and duration of the Last Interglacial: evidence for a restricted interval of widespread coral reef growth. *Earth Planetary Science Letters*, 160, 745–762.

Stoker, M. S., Nielsen, T., van Weering, T. C. E., Kuijpers, A, 2002. Towards an understanding of the Neogene tectonostratigraphic framework of the NE Atlantic margin between Ireland and the Faroe Islands. *Marine Geology,* 188, 233–248.

Stromgren, T., 1971. The vertical and horizontal distribution of Lophelia pertusa (linné) in Trondheimsfjorden on the west coast of Norway. *K norske Vidensk Selsk Skr.* 6, 1-9.

Taviani, M., Remia, A., Corselli, C., Freiwald, A., Malinverno, E., Mastrototaro, F., Savini, A., Tursi, A., 2005. First geo-marine survey of living cold-water Lophelia reefs in the Ionian Sea (Mediterranean basin). *Facies*, 50, 3-4, 409-417.

Thierens, M., Titschack, J., Dorschel, B., Huvenne, V.A.I., Wheeler, A.J., Stuut, J.-B., O'Donnel, R., 2010. The 2.6 Ma depositional sequence from the Challenger cold-water coral carbonate mound (IODP Exp. 307): Sediments contributors and hydrodynamic paleo-environments. *Marine Geology*, 271, 260-277.

Thompson, W.G., Spiegelman, M.W., Goldstein, S.L., Speed, R.C., 2003. An open-system

model for U-series age determinations of fossil corals. *Earth Planetary Sciences Letters,* 210, 365–381.

Thomson, C.W., Carpenter, W.B., Jeffreys, J.G., 1873. The depths of the sea: an account of the general results of the dredging cruises of H.M.SS. 'Porcupine' and 'Lightning' during the summers of 1868, 1869, and 1870. London: *Macmillan & Co*., pp. 527.

Titschack, J., Thierens, M., Dorschel, B., Schulbert, C., Freiwald, A. Kano, A., C. Takashima, C., Kawagoe, N., Li X., IODP Expedition 307 Scientific Party, 2009, Carbonate budget of a cold-water coral mound (Challenger Mound, IODP Exp. 307*), Marine Geology*, 259, 1-4, 36-46.

Van de Flierdt, T., Robinson, L.F., Adkins, J.F., 2010. Deep-sea coral aragonite as a recorder for the neodymium isotopic composition of seawater, *Geochimica et Cosmochimica Acta*, 74, 6014-6032.

Van Rooij, D., Blamart, D., Richter T.O., Wheeler, A.J., Kozachenko, M., Henriet, J.-P., 2007. Quaternary sediment dynamics in the Belgica mound province, Porcupine Seabight: ice-rafting events and contour current processes. *International Journal of Earth Sciences*, 96, 1, 121-140.

Van Weering, T.C.E., De Haas, H., De Stigter, H.C., Lykke-Andersen, H., Kouvaev, I., 2003. Structure and development of giant carbonate mounds at the SW and SE Rockall Trough margins, NE Atlantic Ocean. *Marine Geology*, 198, 1–2, 67-81.

Veizer, J., 1989. Strontium isotopes in seawater through time. *Annual Review of Earth Planetary Sciences*, 17, 141–167.

Vincent, E., Killingley, J.S., 1985. Oxygen and carbon isotope record for the early and middle Miocene in the central Equatorial Pacific (Leg 85) and paleoceanographic implictations. In: Mayer, L., Theyer, F. (Eds). *Initial Reports of the Deeps Sea Drilling Project* , 85, 749-769.

Weber, J.N., Woodhead, P.M., 1972. Temperature Dependence of Oxygen-18 Concentration in Reef Coral Carbonates. *Journal of Geophysical Research*, 77, 3, 463-473.

Wedepohl, K.H., 1995. The composition of the continental crust. *Geochimica et Cosmochimica Acta,* 59 (7), 1217–1232.

Wheeler, A., Kozachenko, M., Beyer, A., Foubert, A., Huvenne, V., Klages, M., Masson, D.G., Olu-Le Roy, K., Thiede, J., 2005a. Sedimentary processes and carbonate mounds in the Belgica Mound province, Porcupine Seabight, NE Atlantic. In: Freiwald, A., Roberts, J.M. (Eds), Cold-Water Corals and Ecosystems. *Springer*, Berlin Heidelberg, pp. 571-603.

Wheeler, A., Beck, T., Thiede, J., Klages, M., Grehan, A., Monteys F.X., and the Polarstern ARK XIX73a Shipboard Party, 2005b. Deep-water coral mounds on the Porcupine Bank, Irish Margin: preliminary results from the Polarstern ARK-XIX/3a ROV cruise. In: Freiwald, A., Roberts, J.M. (Eds), Cold-Water Corals and Ecosystems. *Springer*, Berlin Heidelberg, pp. 393-402.

Wheeler, A., Beyer, A., Freiwald, A., de Haas, H., 2007. Morphology and environment of cold-water coral carbonate mounds on the NW European margin. International Journal of Earth Sciences, 96, 1, 37-56.

Wheeler, A., Kozachenko, M., Henry, L.-A., Foubert, A., de Haas, H., Huvenne, V.A.I., Masson, D.G., Olu, K., 2011. The Moira Mounds, small cold-water coral banks in the Porcupine Seabight, NE Atlantic: Part A--an early stage growth phase for future coral carbonate mounds? *Marine Geology*, 282, 1-2, 53-64.

White, M., Bowyer, P., 1997. The shelf edge current northwest of Ireland. *Annales Geophysicae*, 15, 1076–1083. doi:10.1007/s00585-997-1076-0

White, M., Mohn, C., de Stigter, H., Mottran, G., 2005. Deep-water coral development as a function of hydrodynamics and surface productivity around the submarine banks of the Rockall Trough, NE Atlantic. In: Freiwald A., Roberts, J.M. (Eds.), Cold-Water Corals and Ecosystems. *Springer*, Berlin, pp. 503-514.

White, M., 2007. Benthic dynamics at the carbonate mound regions of the Porcupine Sea Bight continental margin. *International Journal of Earth Sciences*, 96, 1-9.

White, M., Dorschel, B., 2010. The importance of the permanent thermocline to the cold-water coral mound distribution in the North Atlantic. *Earth and Planetray Science Letters*, 296, 395-402.

Wienberg, C., Beuck L., Heidkamp, S., Hebbeln, D., Freiwald, A., Pfannkuche, O., Monteys, X., 2008. Franken Mound: facies and biocoenoses on a newly-discovered “carbonate mound” on the western Rockall Bank, NE Atlantic. *Facies*, 54, 1, 1-24.

Wienberg, C., Hebbeln, D., Fink, H.G., Mienis, F., Dorschel, B., Vertino, A., López Correa, M., Freiwald, A., 2009. Scleractinian cold-water corals in the Gulf of Cádiz – first clues about their spatial and temporal distribution. *Deep Sea Research I*, 56, 1873–1893.

Wienberg, C., Frank, N., Mertens, N, K., Stuut, J.B., Marchant, M., Fietzke, J., Mienis, F., Hebbeln, D., 2011. Glacial cold-water coral growth in the Gulf of Cádiz: Implications of increased palaeo-productivity. *Earth and Planetary Science Letters*, 298, 405- 416.

Williams, T., Kano, A., Ferdelman, T., Henriet, J.-P., Abe, K., Andres, M.S., Bjerager, M.,

Browning, E.L., Cragg, B.A., De Mol, B., Dorschel, B., Foubert, A., Frank, T.D., Fuwa, Y., Gaillot, P., Gharib, J., Gregg, J.M., Huvenne, V.A.I., Léonide, P., Mangelsdorf, K., Tanaka, A., Monteys, X., Novosel, I., Sakai, S., Samarkin, V.A., Sasaki, K., Spivack, A.J., Takashima, C., Titschack, J., 2006. Cold-water coral mounds revealed. *EOS Transactions AGU*, 87, 525-526.

Wilson-Finelli, A., Chandler, G.T., Spero, H.J., 1998. Stable isotope behavior in paleoceanography important benthic foraminifera: results from microcosm culture experiments. *Journal of Foraminiferal Research*, 28, 4, 312-320.

Wood, R., Reef Evolution, 1999. *Oxford University Press*, Oxford, New York, pp. 414.

Wright, J.D., Miller, K.G., Fairbanks, R.G., 1992. Early and middle Miocene stable isotopes: Implications for deepwater circulation and climate. *Paleoceanography*, 7, 3, 357-389.

Zachos, J., Pagani, M., Sloan, L., Thomas, E., Billups, K., 2001. Trends, rhythms, and aberrations in global climate change 65 Ma to present. *Science*, 292, 686-693.

Zahn, R., Sarnthein, M., Erlenkeuser, H., 1987. Benthic isotope evidence for changes of the mediterrranean outflow during the late Quaternary. *Paleoceanography*, 2 (6), 543-559.

Zahn, R., Schönfeld, J., Kudrass, H.-R., Pflaumann, U., Sinha, D.K., Park, M.-H., Erlenkeuser, H., 1997. Thermohaline instability in the North Atlantic during Heinrich Events: stable isotope and faunal records from core SO75-26KL. Portuguese margin. *Paleoceanography*, 12, 696-710.

Supplements

Bioluminescence in deep-sea isidid gorgonians from the Cape Verde archipelago

Based on: Jacek Raddatz, Matthias López Correa, Andres Rüggeberg, Thor Hansteen, Wolf-Christian Dullo, 2011. *Bioluminescence in deep-sea isidid gorgonians from the Cape Verde archipelago*. Coral Reefs, 30:579. DOI:10.1007/s00338-011-0743-5

Cold-water corals, and in particular numerous gorgonian species, occur abundantly on the deep slopes of the Cape Verde archipelago (Fig. 1a). Among them, the isidid gorgonian genus Keratoisis occurred frequently. A living Keratoisis sp. was ROV collected (KIEL 6000) from 3,052 m (16°42.3'N, 25°34.9'W) in the Charles Darwin Volcanic Field (1b) durin METEOR cruise M80/3. A strong luminescence was accidentally observed when this bamboo coralarrived on deck in the early evening hours just before sunset. The entire stem and branch tissue showed a dull blue luminescence. Additionally, when touched, it emitted a very strong blue light (Fig. 1c) that persisted for a few seconds. Coral tissue lit up strongest and flash like at the point of stimulation, and the illumination spread in a wave across the coenenchyme of the distal branches. The most intense light emission originated from the non-retractile sclerite-rich feeding polyps and remained visible for several minutes before it slowly faded. This phenomenon could be reproduced several times within hours. Luminescence in octocorals has been observed in the alcyonarian *Anthomastus sp.,* as well as in isidid gorgonians (*Isidella, Keratoisis, and Lepidisis*), primnoid gorgonians (*Primnoisis* and *Thouarella*), and in *Iridigorgia* and *Acanthogorgia* (Herring 1987). Muzik (1978) documented bioluminescence in the isidid gorgonian *Lepidisis olapa* off Hawaii, and Etnoyer (2008) mentioned luminescent capabilities for *Isidella tentaculum* from the northeast Pacific. Just recently, bioluminescence was reported for *Keratoisis flexibilis* and for the zoanthid *Gerardia sp.* from the Gulf of Mexico (http://oceanexplorer.noaa.gov/explorations/09bioluminescence/). Likely due to the scarce availability of direct deep-sea sampling and observation, there are no further Atlantic records for bioluminescence in the *Keratoisidinae* outside the

Gulf of Mexico. Our additional observations support that bioluminescence in *Keratoisis* and in other deep-sea gorgonians is rather common and deserves detailed in situ observations.

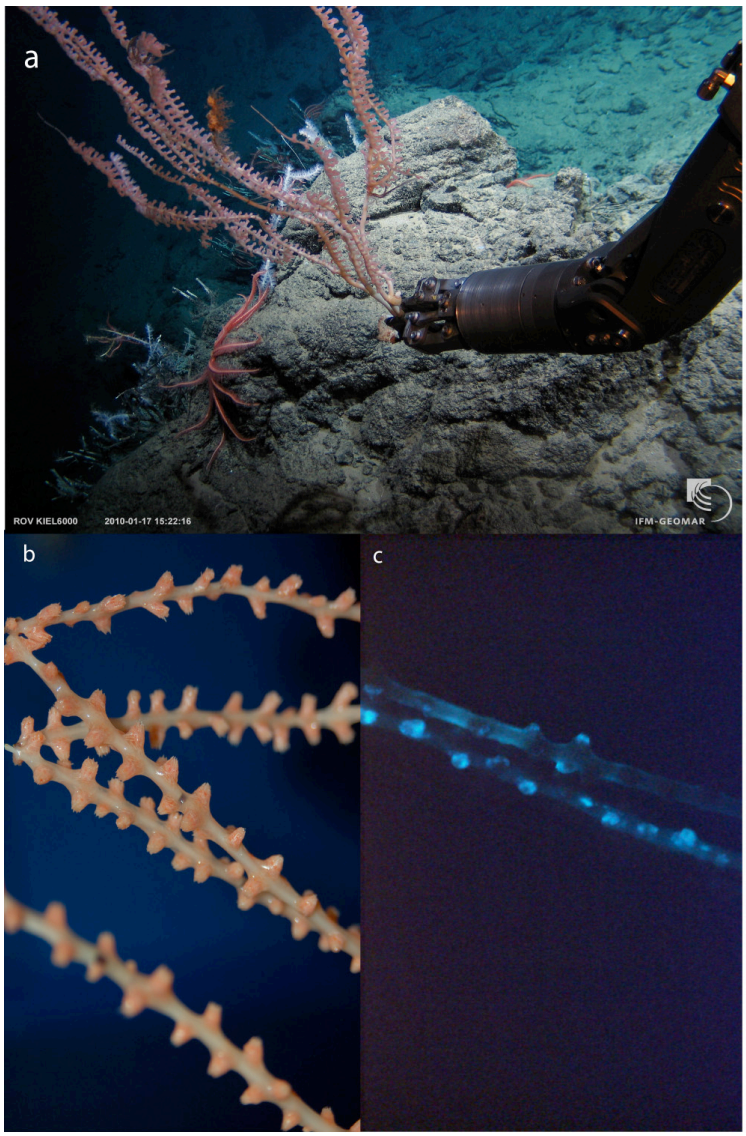

Figure 1: a) ROV sampling of *Keratoisis sp*. ~3,052 m depth in the Cape Verde archipelago. b) Distal branch of *Keratoisis sp*. in plain light. c) Distal branch of the same colony emitting a strong blue bioluminescence after physical stimulation.

References

Etnoyer, P., 2008. A new species of *Isidella* bamboo coral (Octocorallia: Alcyonacea: Isididae) from northeast Pacific seamounts. Proceedings of the Biological Society of Washington, 121:541–553.

Herring, P.J., 1987. Systematic distribution of bioluminescence in living organisms. Journal of Bioluminnescence and Chemiluminescence 1:147–163.

Muzik, K., 1978. A bioluminescent gorgonian, *Lepidisis olapa*, new species (Coelenterata: Octocorallia) from Hawaii. Bulletin of Marine Science 28:735–741.

Chapter II

Table 1: Sortable silt, stable oxygen and carbon isotopes of different benthic and planktonic foraminifera of IODP SITE 1317 C

Depth (mbsf)	Grain-Sizes mean ss (µm)	*G.bulloides* $\delta^{18}O$ (‰)	$\delta^{13}C$ (‰)	*L.lobatula* $\delta^{18}O$ (‰)	$\delta^{13}C$ (‰)	*C.wuellerstorfi* $\delta^{18}O$ (‰)	$\delta^{13}C$ (‰)	*D.Coronata* $\delta^{18}O$ (‰)	$\delta^{13}C$ (‰)	*P.Ariminensis* $\delta^{18}O$ (‰)	$\delta^{13}C$ (‰)	*L.Antartica* $\delta^{18}O$ (‰)	$\delta^{13}C$ (‰)
141,00													
141,18	21,127	0,996	-0,836	1,882	0,295			2,040	-0,83	2,150	0,44	1,827	0,348
141,28	23,157	0,930	-0,782	1,792	0,496					2,230	0,34	1,783	0,207
141,38	24,210	1,054	-1,158	1,800	0,365			1,86	-0,78			1,847	0,303
141,48	23,730	1,140	-0,817	1,831	0,340			1,97	-0,28			1,759	0,049
141,58	23,510	1,136	-0,915	1,847	0,490			2,16	-1,43	2,080	0,750	1,670	0,507
141,68	22,957	1,150	-0,638	1,685	0,316			1,77	-0,76			1,833	0,669
141,78	23,253	1,111	-0,494	1,856	0,512			2,45	-1,23			1,812	0,390
141,88	23,293	1,347	-0,242	1,803	0,187			1,89	-1,16	2,170	0,940	1,826	0,282
141,98	24,050	1,149	-0,779	1,737	0,350			1,84	-1,01			1,755	0,368
142,08	25,693	0,943	-0,975	1,807	0,186			2,26	-0,83	1,950	0,87	1,727	0,764
142,18	22,430	0,932	-1,211	1,999	0,576			1,98	-1,04	2,140	0,98	1,936	0,598
142,28	26,033	1,315	-0,715	1,807	0,364			2,22	-1,41	2,150	0,67	2,085	0,281
142,42	24,957	1,534	-0,382	1,891	0,198			1,84	-0,99	1,990	0,71	1,540	0,195
142,52	24,803	1,753	-0,230	1,949	0,411			2,30	-0,72	1,980	0,81		
142,62	24,430	1,554	-0,460	2,022	0,399	0,643	0,840	2,21	-1,56	2,190	0,85		
142,72	23,073	1,840	-0,053	2,173	0,473			1,27	-0,97	2,120	0,98		
142,82	23,970	1,608	-0,421	2,109	0,413	2,109	-0,500	2,27	-0,82				
142,92	23,393	1,385	-0,431	2,222	0,516			2,300	-0,90	1,730	1,080		
143,02	23,620	1,804	-0,436	2,142	0,448			2,200	-0,900				
143,15	22,820	1,347	-0,889	2,519	0,460								
143,25	21,400	1,485	-1,435	2,479	0,673								
143,34	25,763	1,906	-0,591	2,229	0,027	2,010	-0,090	1,980	-1,490	2,020	0,460	2,000	0,230
143,44	23,430	1,794	-0,703	2,013	0,196	2,077	0,223	2,084	-1,500	1,946	0,547	2,057	0,097
143,54	20,940	1,233	-1,336	1,875	0,393	2,082	-0,757	2,250	-2,269	2,103	-0,206	2,249	-0,850
143,64	22,713	1,262	-1,452	2,103	-0,524	1,947	0,208	2,036	-1,947	1,858	0,328	2,106	-0,148

Depth (mbsf)	Grain-Sizes mean ss (µm)	*G.bulloides* $\delta^{18}O$ (‰)	$\delta^{13}C$ (‰)	*L.lobatula* $\delta^{18}O$ (‰)	$\delta^{13}C$ (‰)	*C.wuellerstorfi* $\delta^{18}O$ (‰)	$\delta^{13}C$ (‰)	*D.Coronata* $\delta^{18}O$ (‰)	$\delta^{13}C$ (‰)	*P.Ariminensis* $\delta^{18}O$ (‰)	$\delta^{13}C$ (‰)	*L.Antartica* $\delta^{18}O$ (‰)	$\delta^{13}C$ (‰)
143,74	22,467	1,657	-1,467	1,917	-0,208	2,076	0,260	2,006	-1,780	1,971	0,590	2,048	0,065
143,84	21,610	1,364	-1,232	2,003	-0,123								
143,94	21,620	0,707	-1,074	2,026	0,397	2,047	0,750	1,390	-2,56	2,090	0,910	1,990	0,336
144,04	21,407	1,618	-0,680	1,454	0,964			1,730	-1,47	2,130	0,83	2,020	-0,081
144,14	21,660	1,421	-0,618	2,063	0,062	2,009	0,247	1,890	-1,30	2,140	0,78	1,970	0,188
144,24	22,857			2,036	0,250	1,964	0,357	1,530	-1,34	2,130	0,69	2,000	-0,008
144,34	22,950	1,483	-0,686	1,887	0,147	1,844	0,229	1,600	-1,58	2,220	0,45	1,640	-0,189
144,44	22,663	1,717	-1,435	1,771	0,163			1,440	-1,53	2,080	0,70	1,940	0,034
144,55	21,940	1,476	-2,299	1,945	-0,186	2,055	0,153	2,229	-1,754	1,918	0,429	1,994	-0,053
144,65	21,400	2,087	-2,835	1,862	-0,383	2,041	0,010	1,840	-1,920	2,180	0,660	1,980	-0,473
144,75	22,240	1,855	-3,431	1,808	-1,161	2,132	-0,635	2,092	-2,439	2,104	-0,726	2,125	-0,642
144,85	23,017	2,031	-3,040							2,010	-0,040	2,025	-0,954
144,95	22,247	1,864	-2,237	2,232	-1,469	2,160	-0,500	2,180	-2,54	2,730	0,000	2,156	-1,297
145,05	22,733	1,511	-0,859	2,278	-0,714	2,000	-2,390	2,080	-2,17	2,530	-0,320	2,328	-1,117
145,15	23,077	1,002	-1,029	1,872	0,258			2,200	-1,26	2,390	0,220	2,092	0,033
145,25	23,597	1,880	-0,236	1,887	-0,077	1,000	0,350	1,890	-1,83	2,280	0,920	1,870	0,150
145,35	22,840	1,387	-0,312	1,841	-0,011	1,860	0,080	1,720	-1,12				
145,45	25,643	1,157	-0,706	1,954	0,436	1,940	0,700	1,870	-1,31			1,830	0,250
145,55	21,473	1,605	-0,412	1,767	-0,325	2,020	-0,190	1,790	-1,78				
145,65	23,410	1,551	-0,612	1,954	0,436	2,230	0,380	1,430	-1,88				
145,78	23,973	1,597	-0,667	2,139	0,597	2,180	0,610	2,020	-1,27	2,190	0,500		
145,85	23,793	1,824	-0,210	1,849	0,106			2,060	-1,33	2,040	0,780		
145,92	24,763			1,898	0,200	1,520	0,300	1,880	-1,20				
145,99	26,790	1,478	-0,515	2,049	0,541	1,974	0,270	2,120	-1,42				
146,06	25,447	1,767	-0,673	1,923	0,282	1,600	0,640	2,190	-0,88				
146,13	26,653	1,684	-0,511			2,233	-0,270	2,140	-0,85	2,450	0,610		

Depth (mbsf)	Grain-Sizes mean ss (µm)	*G.bulloides* $\delta^{18}O$ (‰)	$\delta^{13}C$ (‰)	*L.lobatula* $\delta^{18}O$ (‰)	$\delta^{13}C$ (‰)	*C.wuellerstorfi* $\delta^{18}O$ (‰)	$\delta^{13}C$ (‰)	*D.Coronata* $\delta^{18}O$ (‰)	$\delta^{13}C$ (‰)	*P.Ariminensis* $\delta^{18}O$ (‰)	$\delta^{13}C$ (‰)	*L.Antartica* $\delta^{18}O$ (‰)	$\delta^{13}C$ (‰)
146,20	25,707	1,517	-0,978	2,289	0,132	1,961	0,170						
146,27	24,867	1,919	-0,282	2,163	0,329	2,287	0,720	1,930	-1,61				
146,33	27,200	2,041	-0,334	2,301	0,491	2,177	0,240	2,290	-0,76				
146,39	26,240							1,120	-1,93			2,290	0,181
146,45	25,037												
146,55	24,427					2,079	0,680	1,980	-1,22			2,080	0,274
146,62	24,217					2,046	0,170	1,540	-1,69			1,950	0,169
146,69	24,253			2,003	-0,100								
146,76	24,453	1,350	-0,717	1,963	0,237			1,730	-1,66			1,950	0,170
146,83	23,087	1,914	-0,360	2,101	0,088	1,838	0,350	1,940	-1,68			2,020	0,150
146,90	23,517	1,676	-0,783	1,971	0,359								
147,01	23,270	1,813	-0,376	1,941	0,220	2,090	0,050	2,120	-2,08			2,380	0,070
147,08	23,067	1,628	-0,671	1,981	-0,123								
147,14	23,277	2,057	-1,448	1,927	0,077			2,070	-0,69				
147,20	22,570	1,992	-2,369	2,061	-0,130	2,220	0,710	2,150	-0,890				
147,26	23,010	1,850	-1,967	2,230	-0,780	2,080	0,870	2,180	0,500			1,970	0,550
147,33	23,613	1,850	-1,967	2,171	-0,722	2,258	0,610						
147,40	23,930	1,767	-1,810	2,152	-0,218	2,129	0,604	1,928	-1,540	2,110	0,849	2,264	0,600
147,47	23,973	1,750	0,028	1,929	0,334	2,200	0,670	1,890	-1,380			2,130	0,390
147,54	24,353	1,268	-0,324	2,082	0,372	2,191	0,582	1,718	-1,882	1,899	0,812	2,183	0,751
147,61	24,540	1,846	-0,267	2,141	0,468	2,276	0,738			1,988	0,746	2,234	0,604
147,68	23,503	1,820	-0,714	1,912	-0,224			2,030	-1,110				
147,75	24,733	2,075	0,154	2,144	0,450								
147,82	24,340	1,986	-0,229	2,107	0,648								
147,88	24,747	2,218	0,159	2,112	0,357								
147,95	20,790	0,174	0,486										

Depth (mbsf)	Grain-Sizes mean ss (µm)	*G.bulloides* $\delta^{18}O$ (‰)	$\delta^{13}C$ (‰)	*L.lobatula* $\delta^{18}O$ (‰)	$\delta^{13}C$ (‰)	*C.wuellerstorfi* $\delta^{18}O$ (‰)	$\delta^{13}C$ (‰)	*D.Coronata* $\delta^{18}O$ (‰)	$\delta^{13}C$ (‰)	*P.Ariminensis* $\delta^{18}O$ (‰)	$\delta^{13}C$ (‰)	*L.Antartica* $\delta^{18}O$ (‰)	$\delta^{13}C$ (‰)
148,02	20,183	0,865	-1,079	0,127	1,361								
148,09	21,197	-1,187	0,845	0,078	1,235								
148,19	20,610	-0,533	0,793	0,230	1,501								
148,29	18,800	-0,569	1,183	0,126	1,093								
148,39	19,100	-0,715	1,736										
148,49	19,800	-1,074	2,125	0,175	0,995								
148,59	18,613	-0,796	2,263	0,099	1,346								
148,69	19,007	-0,560	1,688	0,164	1,137								
148,79	19,640	-0,592	1,445	0,428	1,239								
148,89	19,363	-0,978	1,489	-0,170	1,662								
149,00	19,867	-0,311	1,539	0,034	1,108								
149,09	20,050	1,835	-1,387	0,222	1,442								
149,19	19,723	-1,500	1,181	0,132	1,248								
149,29	21,210	-1,104	2,323	0,028	1,552								
149,45	19,633	-0,796	1,445	0,012	1,602								
149,55	19,740	-0,815	1,623	0,189	1,283								
149,65	19,433	-0,182	0,703	-0,022	1,177								
149,75	17,533	-0,185	1,309	0,113	1,241								
149,85	20,033	-0,430	1,510	0,149	1,475								
149,95	18,237	-0,817	1,714	0,077	1,424								
150,05	18,313	-0,831	2,202	0,112	1,493								
150,15	21,717	-0,870	1,712	0,260	1,612								
150,25	20,247	-0,636	1,230										
150,35	21,027	-0,784	1,633	0,080	1,681								
150,45	19,830			0,196	1,427								
150,55	20,573	-0,725	1,839	-0,146	1,184								
150,65	19,320	-0,573	1,296	0,187	1,116								
150,75	18,967	-0,266	1,156	0,203	1,059								

Chapter III

Table 1: U and Th isotopes and calculated ages of cold-water coral fragments from core GeoB 6730-1 (MIS = Marine Isotope Stage).

sample ident (GeoB core / depth in cm)	applied MS (U/Th)	Weight (g)	^{238}U-conc. (µg/g)	^{232}Th conc. (µg/g)	^{230}Th (pg/g)	^{230}Th/^{232}Th act. ratio	^{230}Th/^{234}U act. ratio	$\delta^{234}U_{(0)}$ (‰)	$\delta^{234}U_{(T)}$	**U-Th age (ky BP)**	+/- (‰)	$\delta^{234}U_{(T)}$ criterion	**MIS**
6730-1/3	Triton/Axiom	0.224	4.15 ± *0.02*	14.6 ± *0.1*	1.4 ± *0.1*	17.7 ± *0.8*	0.017 ± *0.001*	147.3 ± *1.8*	148.1 ± *1.8*	**1.9 ± *0.1***	*4.7*	SR	**1**
6730-1/18	Triton/Axiom	0.243	4.64 ± *0.02*	53.3 ± *0.3*	4.3 ± *0.1*	15.0 ± *0.2*	0.047 ± *0.001*	145.0 ± *2.7*	147.2 ± *2.7*	**5.2 ± *0.1***	*2.1*	SR	**1**
6730-1/58	Triton/Axiom1	0.320	4.78 ± *0.02*	12.3 ± *0.1*	52.8 ± *0.3*	802.3 ± 6.5	0.603 ± *0.005*	116.7 ± *4.3*	154.2 ± *5.1*	**99 ± *1***	*1.4*	R (SR)	**5.3**
6730-1/68	Triton/Axiom	0.273	4.57 ± *0.02*	79.2 ± *0.4*	49.6 ± *0.3*	117.3 ± *0.9*	0.595 ± *0.004*	106.4 ± *1.7*	139.9 ± *2.2*	**97 ± *1***	*1.1*	n (R)	**5.3**
6730-1/108	Mat262/Axiom2	0.192	3.94 ± *0.02*	1.05 ± *0.1*	46.5 ± *0.2*	8327 ± 57.3	0.650 ± *0.005*	108.9 ± *5.1*	149.4 ± *6.0*	**112 ± *2***	*1.3*	SR	**5.5**
6730-1/108	Triton/Axiom1	0.192	3.94 ± *0.02*	1.30 ± *0.1*	46.5 ± *0.3*	6696 ± 53.6	0.651 ± *0.005*	106.0 ± *1.9*	145.6 ± *2.6*	**112 ± *1***	*1.2*	R (SR)	**5.5**
6730-1/108	Axiom/Axiom2	0.192	3.98 ± *0.02*	1.05 ± *0.1*	46.5 ± *0.2*	8327 ± 57.3	0.647 ± *0.004*	104.0 ± 3.2	142.3 ± 3.9	**111 ± *1***	*1.2*	R	**5.5**
6730-1/108	mean *	0.192	3.95 ± *0.03*	1.20 ± *0.3*	46.5 ± *0.04*	7512 ± *1631*	0.649 ± *0.003*	106.3 ± *2.86*	145.8 ± *4.14*	**112 ± *1***	*0.7*	R (SR)	**5.5**
6730-1/178	Triton/Axiom	0.148	2.91 ± *0.01*	58.4 ± *0.3*	42.6 ± *031*	136.5 ± *1.1*	0.815 ± *0.006*	91.1 ± *2.0*	149.8 ± *3.4*	**176 ± *3***	*1.8*	R (SR)	**6.5**
6730-1/213	Triton/Axiom	0.169	2.86 ± *0.01*	26.4 ± *0.1*	45.1 ± *0.2*	320.5 ± 2.3	0.881 ± *0.006*	88.5 ± *2.0*	163.7 ± *4.2*	**218 ± *4***	*2.1*	n	***
6730-1/238	Triton/Axiom	0.566	3.68 ± *0.02*	1.13 ± *0.1*	56.1 ± *0.3*	9272 ± *63.0*	0.860 ± *0.007*	82.0 ± *4.8*	145.8 ± *7.0*	**204 ± *5***	*2.2*	R (SR)	**7.2**
6730-1/273	Axiom/Axiom	0.186	3.94 ± *0.02*	14.7 ± *0.1*	62.8 ± *0.3*	798.0 ± 5.6	0.905 ± *0.006*	73.3 ± *2.3*	144.4 ± *4.8*	**240 ± *6***	*2.4*	R (SR)	**7.5**
6730-1/318 **	Axiom/Axiom	0.298	3.34 ± *0.01*	390 ± *2.4*	56.6 ± *0.4*	27.2 ± *0.3*	0.950 ± *0.012*	60.0 ± *2.6*	139.4 ± *9.9*	**296 ± *18***	*6.1*	n (SR)	**8.5 - 9.1**
6730-1/353	Axiom/Axiom	0.018	4.65 ± *0.02*	31.6 ± *0.2*	73.9 ± *0.4*	438.8 ± *3.9*	0.916 ± *0.007*	57.8 ± *2.1*	118.7 ± *4.9*	**254 ± *8***	*3.1*	n	***

Table 1: NOTE: All uncertainties are based on 2 SEM level of the isotope measurements. U-Th measurements of the sample set were performed on a Finnigan MAT 262 RPQ+ (Mat262, U) and a Thermo-Finnigan Triton-RPQ (Triton, U) thermal ionisation mass spectrometer (TIMS) and a VG Axiom multi collector - inductively coupled plasma - mass spectrometer (MC-ICP-MS, including multi ion counting (MIC) set-up). The $\delta^{234}U_{(0)}$ value represents the originally today measured ($^{234}U/^{238}U$) activity ratio, given in delta notation ($\delta^{234}U_{(0)} = ((^{234}U_{act}/^{238}U_{act})-1) * 1000$). Displayed $\delta^{234}U_{(T)}$ values reflect age corrected ($^{234}U/^{238}U$) activity ratios by recalculating the decay of ^{234}U for the time interval T ($\delta^{234}U_{(T)} = \delta^{234}U_{(0)}\exp^{(\lambda 234T)}$), determined from $^{230}Th/^{234}U$ age of each individual sample. Note, due to the generally high ages in this sample set, the impact of age correction on the interpretation of $\delta^{234}U$ values is significant and criteria for isotopic reliability of ^{230}Th age data may applied. Recent reef forming cold-water corals showed within their uncertainties similar $\delta^{234}U_{(0)}$ values of 145.5 ± 2.3 ‰ and 146.3 ± 3.9 ‰, supporting the application of the $\delta^{234}U_{(T)}$ reliability criterion presented for tropical corals. $\delta^{234}U_{(T)}$ criterion and related U-Th age quality code: n = not reliable (potential diagentic overprint), R = reliable (passing the 149 ± 8 ‰ $\delta^{234}U_{(T)}$ criterion); SR = strictly reliable (within 146.6 - 149.6 ‰ $\delta^{234}U_{(T)}$, representing values for modern corals and modern seawater, respectively). First order classification is disregarding the individual analytical uncertainty, avoiding preference to less precise measurements. Maximum quality level reached within range of analytical uncertainty is indicated in brackets.

* Mean values reflect reproducibility and robustness of applied methods. Uncertainties of mean values are given as 2 SEM. ** Nevertheless, despite precise isotope measurements, for sample 318 enlarged age uncertainty and less age reliability must be deduced due to high Th concentrations (> 100 ng/g) and the related uncertainty of correction for potential detrital impact. *** No reasonable classification possible.

Table 2: CTD-salinity data and $\delta^{18}O_{water}$ measurements of samples from the upper water column (0–1155 m) collected during cruises M61/1, M61/3, P316 in summer 2004.

Cruise*	Station	Lat (°N)	Long (°E)	Water depth (m)	Salinity (psu)	$\delta^{18}O$ (‰ SMOW)
M61/3	588	52°09.343	12°45.949	790	35.51	0.46
M61/3	589	52°08.892	12°46.274	705	35.46	0.45
M61/3	589	52°08.892	12°46.274	598	35.41	0.42
M61/3	589	52°08.892	12°46.274	432	35.48	0.52
M61/3	589	52°08.892	12°46.274	337	35.55	0.56
M61/3	589	52°08.892	12°46.274	256	35.55	0.64
M61/3	589	52°08.892	12°46.274	189	35.57	0.58
M61/3	589	52°08.892	12°46.274	92	35.59	0.63
M61/3	589	52°08.892	12°46.274	38	35.60	0.67
M61/3	590	52°08.244	12°46.414	708	35.49	0.53
M61/1	205	51°27.85	11°45.07	914	35.50	0.43
M61/1	206	51°27.64	11°45.25	910	35.32	0.31
M61/1	207	51°27.44	11°45.30	868	35.50	0.40
M61/1	208	51°27.26	11°45.19	806	35.49	0.46
M61/1	209	51°27.09	11°45.12	786	35.47	0.51
M61/1	211	51°26.80	11°45.19	865	35.52	0.43
M61/1	212	51°26.69	11°45.18	893	35.52	0.43
M61/1	214	51°26.53	11°45.42	880	35.52	0.43
M61/1	213	51°26.38	11°45.48	880	35.53	0.41
M61/1	227	51°27.17	11°44.43	917	35.52	0.48
M61/1	228	51°27.13	11°44.91	884	35.52	0.47
M61/1	229	51°27.08	11°45.14	809	35.49	0.49
M61/1	230	51°27.10	11°45.29	873	35.52	0.47
M61/1	231	51°27.08	11°45.63	946	35.54	0.40
M61/1	232	51°27.11	11°45.37	973	35.54	0.42
M61/1	233	51°27.02	11°48.95	1066	35.50	0.49
M61/1	233	51°27.02	11°48.95	1051	35.48	0.46
M61/1	233	51°27.02	11°48.95	1027	35.50	0.41
M61/1	233	51°27.02	11°48.95	884	35.52	0.44
M61/1	233	51°27.02	11°48.95	795	35.53	0.41
M61/1	233	51°27.02	11°48.95	665	35.46	0.40
M61/1	233	51°27.02	11°48.95	559	35.44	0.50
M61/1	233	51°27.02	11°48.95	430	35.50	0.53
M61/1	233	51°27.02	11°48.95	250	35.54	0.58
M61/1	233	51°27.02	11°48.95	175	35.54	0.53
M61/1	233	51°27.02	11°48.95	120	35.55	0.51
M61/1	233	51°27.02	11°48.95	38	35.54	0.48
M61/1	233	51°27.02	11°48.95	8	35.55	0.41
M61/1	249	51°25.15	11°46.32	995	35.53	0.44
M61/1	250	51°25.37	11°46.34	960	35.54	0.42
M61/1	251	51°25.52	11°46.34	919	35.53	0.38
M61/1	252	51°25.70	11°46.29	850	35.54	0.41
M61/1	253	51°25.82	11°46.31	910	35.54	0.40
M61/1	254	51°25.94	11°46.23	907	35.54	0.37
M61/1	255	51°26.15	11°46.27	989	35.54	0.38
M61/1	278	51°26.47	11°47.24	1058	35.54	0.42
M61/1	279	51°24.97	11°45.97	905	35.53	0.43
M61/1	280-2	51°24.36	11°41.36	680	35.47	0.44
M61/1	283-2	51°23.86	11°48.58	1155	35.50	0.44
M61/1	283-2	51°23.86	11°48.58	1131	35.49	0.43
M61/1	283-2	51°23.86	11°48.58	1002	35.54	0.38
M61/1	283-2	51°23.86	11°48.58	750	35.46	0.45

M61/1	283-2	51°23.86	11°48.58	500	35.49	0.47
M61/1	283-2	51°23.86	11°48.58	250	35.53	0.50
M61/1	283-2	51°23.86	11°48.58	30	35.54	0.53
M61/3	547	51°26.75	11°45.11	880	35.51	0.47
M61/3	548	51°27.10	11°45.06	830	35.53	0.59
M61/3	554	51°27.60	11°45.312	908	35.55	0.54
M61/3	555	51°27.13	11°45.44	920	35.56	0.53
M61/3	562	51°27.179	11°44.333	917	35.55	0.52
M61/3	578	51°27.025	11°45.824	962	35.57	0.44
M61/3	579	51°26.98	11°45.096	822	35.57	0.46
M61/3	580	51°27.128	11°44.567	917	35.57	0.46
M61/3	581	51°26.983	11°45.926	974	35.57	0.49
M61/3	582	51°27.102	11°45.217	808	35.56	0.48
M61/3	583	51°27.222	11°44.392	919	35.58	0.35
M61/3	584	51°27.078	11°45.782	964	35.58	0.52
M61/3	585	51°27.08	11°45.155	786	35.55	0.39
P316	512	51°27.60	11°45.34	922	35.52	0.39
P316	513	51°27.46	11°45.31	908	35.51	0.43
P316	514	51°27.28	11°45.19	842	35.50	0.35
P316	515	51°27.11	11°45.17	818	35.51	0.40
P316	515	51°27.11	11°45.17	731	35.48	0.43
P316	515	51°27.11	11°45.17	594	35.46	0.46
P316	515	51°27.11	11°45.17	530	35.49	0.44
P316	515	51°27.11	11°45.17	466	35.52	0.54
P316	515	51°27.11	11°45.17	345	35.55	0.47
P316	515	51°27.11	11°45.17	119	35.58	0.54
P316	515	51°27.11	11°45.17	28	35.59	0.54
P316	516	51°27.11	11°44.87	899	35.53	0.44
P316	517	51°26.9	11°45.12	812	35.53	0.38
P316	518	51°26.65	11°45.16	896	35.50	0.46
P316	519	51°26.91	11°46.15	986	35.51	0.44
P316	520	51°26.88	11°45.80	972	35.51	0.44
P316	521	51°26.97	11°44.46	920	35.51	0.38
P316	530	51°25.99	11°48.74	1088	35.49	0.43
P316	531	51°26.44	11°47.52	1050	35.52	0.50
P316	532	51°27.18	11°44.03	898	35.53	0.39
P316	533	51°27.22	11°43.55	908	35.52	0.53
P316	534	51°27.3	11°42.63	875	35.52	0.43
P316	535	51°27.39	11°42.39	807	35.49	0.50
P316	536	51°27.44	11°42.00	691	35.51	0.56
P316	537	51°27.37	11°41.73	732	35.50	0.49
P316	538	51°27.49	11°40.66	728	35.49	0.58

*All cruises took place in 2004, M61/1 in April, M61/3 in June, P316 in August.

Table 3: $\delta^{18}O$ ratios of *Cibicidoides kullenbergi* ($\delta^{18}O_{kull}$) and *Fontbotia wuellerstorfi* ($\delta^{18}O_{wuell}$) of fraction 250 to 500 µm from gravity cores of Propeller Mound. Analytical standard deviation for $\delta^{18}O$ is ± 0.07 ‰ PDB.

Core GeoB	Depth (cm)	$\delta^{18}O_{wuell}$ (‰ PDB)	$\delta^{18}O_{kull}$ (‰ PDB)
6729-1	8	3.37	2.71
6729-1	38	2.74	2.84
6729-1	73	2.66	3.06
6729-1	108	2.35	2.34
6729-1	143	2.22	2.77
6729-1	153	2.80	2.89
6729-1	218	2.32	2.55
6729-1	268	2.56	2.54
6729-1	278	2.62	2.56
6729-1	333	2.14	2.26
6729-1	358	2.52	2.31
6729-1	418	3.32	3.05
6728-1	18	3.16	3.23
6728-1	103	2.35	2.93
6728-1	208	2.67	2.70
6728-1	318	2.41	2.91
6728-1	323	2.40	2.29
6728-1	423	2.84	2.85
6728-1	523	2.55	2.75
6727-1	18	3.46	3.78
6727-1	53	3.70	3.66
6727-1	118	3.65	3.68
6727-1	123	3.69	3.64
6727-1	143	3.39	3.60
6727-1	168	3.44	3.66
6727-1	208	3.53	3.61
6727-1	228	3.30	3.33
6727-1	253	2.67	2.82
6725-1	43	3.68	3.71
6725-1	88	3.62	3.72
6725-1	243	3.68	3.45
6725-1	348	3.40	3.39
6725-1	408	2.79	3.10
6725-1	448	2.37	2.77
6718-2	103	3.38	3.50
6718-2	218	3.83	3.84
6718-2	223	3.67	3.89
6718-2	228	3.68	3.73
6718-2	313	3.68	3.64
6718-2	423	3.59	3.73
6718-2	428	3.64	3.68

Table 4: $\delta^{18}O$ and paleo-density data of core GeoB 6730-1. Equation numbers 1, 6 and 7 correspond to main text. MIS = Marine Isotope Stages. Analytical standard deviation for $\delta^{18}O$ is ± 0.07 ‰ PDB, for paleo-density reconstruction ± 0.05 kg m^{-3}.

Depth (cm)	$\delta^{18}O$ (‰)	Paleo-density (kg m^{-3})	Equation No.	MIS
3	1.49	27.29	1	1
8	1.42	27.24	1	1
13	1.44	27.25	1	1
18	1.45	27.26	1	1
23	1.50	27.29	1	1
28	1.55	27.32	1	1
33	1.51	27.29	1	1
38	1.48	27.28	1	1
43	1.48	27.28	1	1
48	1.57	27.33	1	1
53	1.53	27.31	1	1
58	1.84	27.48	HIATUS	HIATUS
63	2.12	27.28	6	5
68	2.21	27.32	6	5
73	2.34	27.38	6	5
78	2.35	27.39	6	5
83	2.32	27.37	6	5
88	2.27	27.35	6	5
93	2.28	27.35	6	5
98	2.40	27.41	6	5
103	2.22	27.33	6	5
108	2.27	27.35	6	5
113	2.33	27.38	6	5
118	1.95	27.19	HIATUS	HIATUS
123	3.04	27.55	7	6.5
128	2.77	27.52	7	6.5
133	3.22	27.56	7	6.5
138	3.32	27.57	7	6.5
143	3.28	27.57	7	6.5
148	3.19	27.56	7	6.5
153	3.36	27.57	7	6.5
158	3.28	27.57	7	6.5
163	3.05	27.55	7	6.5
168	2.85	27.53	7	6.5
173	2.58	27.48	7	6.5
178	2.43	27.45	7	6.5
183	2.36	27.39	6	HIATUS
188	2.51	27.45	6	7
193	2.49	27.44	6	7
198	2.37	27.40	6	7
203	2.27	27.35	6	7
208	2.34	27.39	6	7
213	2.33	27.38	6	7
218	2.35	27.39	6	7
223	2.42	27.42	6	7
233	2.35	27.39	6	7
238	2.25	27.34	6	7
243	2.28	27.36	6	7
248	2.25	27.34	6	7
258	2.02	27.23	6	7
263	1.92	27.18	HIATUS	HIATUS
268	1.78	27.10	HIATUS	HIATUS
278	2.32	27.38	6	9
283	2.08	27.26	6	9

288	2.25	27.34	6	9
293	2.60	27.49	6	9
298	2.45	27.43	6	9
303	2.59	27.48	HIATUS	HIATUS
308	2.53	27.46	6	9
313	2.59	27.49	6	9
318	2.89	27.59	6	9
323	2.98	27.62	6	9
328	2.89	27.59	6	9
333	2.96	27.61	6	9
338	2.74	27.54	6	9
343	2.66	27.51	6	9
353	3.08	27.64	6	9
358	2.65	27.51	6	9

Table 5: $\delta^{18}O$ and paleo-density data of IODP core U1317C. Equation 6 is used for paleo-density reconstruction (see manuscript). Analytical standard deviation for $\delta^{18}O$ is ±0.045 ‰ PDB, for paleo-density reconstruction ±0.05 kg m^{-3}. Mbsf = meters below seafloor.

U1317C-	Depth (mbsf)	$\delta^{18}O$ (‰ PDB)[15]	Paleo-density (kg m^{-3})
16-7/4.5	141.19	1.88	27.35
16-7/14.5	141.29	1.79	27.29
16-7/24.5	141.39	1.80	27.29
16-7/34.5	141.49	1.83	27.31
16-7/44.5	141.59	1.85	27.32
16-7/54.5	141.69	1.69	27.21
16-7/64.5	141.79	1.86	27.33
16-7/74.5	141.89	1.80	27.29
16-7/84.5	141.99	1.74	27.25
16-7/94.5	142.09	1.81	27.30
16-7/104.5	142.19	2.00	27.42
16-7/114.5	142.29	1.81	27.30
16-8/4.5	142.43	1.89	27.35
16-8/14.5	142.53	1.95	27.39
16-8/24.5	142.63	2.02	27.43
16-8/34.5	142.73	2.17	27.52
16-8/44.5	142.83	2.11	27.49
16-8/54.5	142.93	2.22	27.55
16-8/64.5	143.03	2.14	27.51
16-ccw/4.5	143.16	2.52	27.71
16-ccw/14.5	143.26	2.48	27.69
17-1/4.5	143.35	2.23	27.56
17-1/14.5	143.45	2.01	27.43
17-1/24.5	143.55	1.88	27.34
17-1/34.5	143.65	2.10	27.48
17-1/44.5	143.75	1.92	27.37
17-1/54.5	143.85	2.00	27.42
17-1/64.5	143.95	2.03	27.44
17-1/74.5	144.05	1.45	27.05
17-1/84.5	144.15	2.06	27.46
17-1/94.5	144.25	2.04	27.44
17-1/104.5	144.35	1.89	27.35
17-1/114.5	144.45	1.77	27.27
17-2/4.5	144.56	1.94	27.39
17-2/14.5	144.66	1.86	27.33
17-2/24.5	144.76	1.81	27.30
17-2/44.5	144.96	2.23	27.56
17-2/54.5	145.06	2.28	27.58
17-2/64.5	145.16	1.87	27.34
17-2/74.5	145.26	1.89	27.35
17-2/84.5	145.36	1.84	27.32
17-2/104.5	145.56	1.77	27.27
17-2/114.5	145.66	1.95	27.39
17-3/6.5	145.79	2.14	27.50
17-3/13.5	145.86	1.85	27.32
17-3/20.5	145.93	1.90	27.36
17-3/27.5	146.00	2.05	27.45
17-3/34.5	146.07	1.92	27.37

17-3/48.5	146.21	2.29	27.59
17-3/55.5	146.28	2.16	27.52
17-3/61.5	146.34	2.30	27.60
17-3/97.5	146.70	2.00	27.42
17-3/104.5	146.77	1.96	27.40
17-3/111.5	146.84	2.10	27.48
17-3/118.5	146.91	1.97	27.40
17-4/6.5	147.02	1.94	27.38
17-4/13.5	147.09	1.98	27.41
17-4/20.5	147.16	1.93	27.37
17-4/26.5	147.22	2.06	27.46
17-4/32.5	147.28	2.23	27.56
17-4/41.5	147.37	2.17	27.52
17-4/48.5	147.44	2.15	27.51
17-4/55.5	147.51	1.93	27.38
17-4/62.5	147.58	2.08	27.47
17-4/69.5	147.65	2.14	27.50
17-4/76.5	147.72	1.91	27.36
17-4/85.5	147.81	2.14	27.51
17-4/90.5	147.86	2.11	27.48
17-4/96.5	147.92	2.11	27.49
17-4/111.5	148.07	0.13	25.84
17-4/118.5	148.14	0.08	25.78
17-5/4.5	148.20	0.23	25.95
17-5/14.5	148.30	0.13	25.84
17-5/34.5	148.50	0.18	25.89
17-5/44.5	148.60	0.10	25.81
17-5/54.5	148.70	0.16	25.88
17-5/64.5	148.80	0.43	26.15
17-5/74.5	148.90	-0.17	25.51
17-5/84.5	149.00	0.03	25.74
17-5/94.5	149.10	0.22	25.94
17-5/104.5	149.20	0.13	25.84
17-5/114.5	149.30	0.03	25.73
17-6/7.5	149.46	0.01	25.71
17-6/17.5	149.56	0.19	25.90
17-6/27.5	149.66	-0.02	25.68
17-6/38.5	149.77	0.11	25.82
17-6/47.5	149.86	0.15	25.86
17-6/57.5	149.96	0.08	25.78
17-6/67.5	150.06	0.11	25.82
17-6/77.5	150.16	0.26	25.98
17-6/97.5	150.36	0.08	25.79
17-6/107.5	150.46	0.20	25.91
17-6/117.5	150.56	-0.15	25.54
17-ccw/3.5	150.63	0.19	25.90
17-ccw/13.5	150.73	0.20	25.92

Chapter IV

Table 1: Meta data, environmental data, stable strontium isotopes and element ratios of *Lophelia pertusa* coral samples.

Cruise	S	Location	Province	Latitude	Longitude	T [°C]	Salinity	Depth [m]	$\delta^{88/86}$Sr [‰]	2 SEM [‰]	Sr/Ca [mmol/mol]	Mg/Ca [mmol/mol]	Li/Ca [µmol/mol]	Mg/Li [mol/mmol]	U/Ca [µmol/mol]
POS325-433	1	Stjernsund	NNR	70°16.04'N	22°27.37'E	5.9	34.97	295	0.226	0.006	9.732	4.312	15.664	0.275	1.133
POS325-433	1	Stjernsund	NNR	70°16.04'N	22°27.37'E	5.9	34.97	295	0.191	0.002					
PS70/40-4	2	Sotbakken	NNR	70°45.35'N	18°40.04'E	6.6	35.2	265	0.195	0.006	9.792	4.720	16.296	0.29	1.228
PS70/40-4	2	Sotbakken	NNR	70°45.35'N	18°40.04'E	6.6	35.2	265	0.210	0.014					
POS391-552-1	2	Lopphavet	NNR	70°26.80'N	21°10.38'E	6.5	35	230	0.194	0.014	10.051	3.809	14.276	0.267	1.309
POS391-552-1	2	Lopphavet	NNR	70°26.80'N	21°10.38'E	6.5	35	230	0.209	0.001	9.967	4.445	16.316	0.272	1.163
POS391-552-1	2	Lopphavet	NNR	70°26.80'N	21°10.38'E	6.5	35	230	0.189	0.009					
POS391-552-1	2	Lopphavet	NNR	70°26.80'N	21°10.38'E	6.5	35	230	0.179	0.011					
POS325-356/1	1	Trænadjupet	TD	66°58.40'N	11°06.53'E	7.2	35.2	300	0.210	0.005					
POS325-356/1	1	Trænadjupet	TD	66°58.40'N	11°06.53'E	7.2	35.2	300	0.224	0.027					
POS391-561-1	2	Sula-Reef	SR	64°05.98'N	08°05.86'E	7.6	35.3	290	0.191	0.005	9.968	3.850	13.771	0.28	1.379
POS391-561-1	2	Sula-Reef	SR	64°05.98'N	08°05.86'E	7.6	35.3	290	0.195	0.009					
Røberg #3	1	Trondheimsfjord	TF	63°28.61'N	09°59.72'E	8.1	31.2	240	0.172	0.020	9.533	4.357	14.365	0.303	1.062
POS391-574-1	2	Oslo Fjord	OF	59°04.01'N	10°44.31'E	8.2	35.2	115	0.179	0.002	9.966	3.870	13.743	0.282	1.081
POS391-574-1	2	Oslo Fjord	OF	59°04.01'N	10°44.31'E	8.2	35.2	115	0.191	0.001					
M61/1-218	1	Little Galway Mound	PSB	51°26.51'N	11°45.43'W	8.96	35.53	881	0.189	0.014	9.785	3.941	11.489	0.343	1.250
M61/3-551	1	Galway Mound	PSB	51°26.94'N	11°45.16'W	9.54	35.53	837	0.166	0.004					
M61/3-551	1	Galway Mound	PSB	51°26.94'N	11°45.16'W	9.54	35.53	837	0.174	0.010	9.603	3.242	11.143	0.291	1.634
POS265-499 (CoC)	2	Propeller Mound	PSB	52°08.89'N	12°46.31'W	9.6	35.5	729	0.166	0.014	9.375	5.706	17.388	0.328	1.900
POS265-499	2	Propeller Mound	PSB	52°08.89'N	12°46.31'W	9.6	35.5	729	0.190	0.002	9.471	3.250	10.333	0.315	1.531
POS265-499	2	Propeller Mound	PSB	52°08.89'N	12°46.31'W	9.6	35.5	729	0.203	0.016	9.49	3.773	11.343	0.333	1.396
POS265-499	2	Propeller Mound	PSB	52°08.89'N	12°46.31'W	9.6	35.5	729	0.194	0.012					
B10-17b Dive 4	2	Whittard Canyon	WC	48°46.79'N	10°34.20'W	9.79	35.5	835	0.143	0.001					
B10-17a Dive 1	2	Guilvinec Canyon	GC	46°56.20'N	05°21.60'W	10.2	35.6	800	0.198	0.010					
GeoB12738-1	2	Gulf of Cadiz	GoC	34.59.98'N	07°04.51'W	10.2	---	738	0.179	0.007	9.732	2.986	8.857	0.337	1.923
M70/1-677	2	Urania Bank	UB	36°50.34'N	13°09.31'E	13.5	38.8	651	0.171	0.014	9.393	3.618	9.343	0.387	1.754
M70/1-677	2	Urania Bank	UB	36°50.34'N	13°09.31'E	13.5	38.8	651	0.196	0.001					
M70/1-677	2	Urania Bank	UB	36°50.34'N	13°09.31'E	13.5	38.8	651	0.197	0.007					
M70/1-677	2	Urania Bank	UB	36°50.34'N	13°09.31'E	13.5	38.8	651	0.200	0.007					
M70/1-677	2	Urania Bank	UB	36°50.34'N	13°09.31'E	13.5	38.8	651	0.183	0.011					
M70/1-677 (CoC)	2	Urania Bank	UB	36°50.34'N	13°09.31'E	13.5	38.8	651	0.193	0.005					
COR2-111	2	Santa Maria de Leuca	SML	39°34.89'N	18°23.00'E	13.6	38.69	496	0.203	0.015	9.267	4.263	11.262	0.378	1.222

Note* S = Source; 1 = Rüggeberg et al. (2008), Source 2 = this study, NNR = Northern Norwegian Reefs, PSB = Porcupine Seabight. CoC = Centers of calcification

Chapter V

Table 1: Elemental ratios of *Lophelia pertusa* samples from IODP Site 1317

LabNr	Depth E (mbsf)	Li/Ca [μmol/mol]	Mg/Ca [mmol/mol]	Ba/Ca [μmol|mol]	Mg/Li [mol|mmol]
900-10	0,08	10,62	3,23	9,78	0,30
901-10	4,01	10,77	3,09	7,85	0,29
908-10	3,94	9,43	2,91	8,12	0,31
909-10	7,87	10,02	2,85	8,91	0,28
907-10	12,51	11,70	2,84	9,53	0,24
903-10	19,01	16,05	4,84	16,44	0,30
899-10	20,75	13,24	3,64	11,71	0,28
897-10	21,09	11,66	3,23	11,21	0,28
896-10	25,95	12,66	3,21	12,77	0,25
346-09	110,13	13,90	3,75	15,57	0,27
350-09	125,51	15,11	3,45	22,78	0,23
353-09	151,25	15,75	3,89	41,79	0,25

Table 2: Stable carbon isotopes and Mg/Ca ratios of benthic and planktonic foraminifera from IODP Site 1317

Depth E (mbsf)	*P.ariminensis* Mg/Ca [mmol/mol]	*G.bulloides* $\delta^{13}C$ (‰)
0,08	2,69	
2,45		-0,32
3,63	2,60	0,04
3,70	3,43	-1,16
3,71	2,99	0,14
3,76		0,09
3,83	3,06	0,15
4,01	3,07	
4,09	2,98	0,31
4,17	2,83	0,03
4,24	2,58	0,14
4,43	2,61	0,21
4,53		0,29
4,68	3,10	-0,05
4,97	2,48	
5,25		-0,19
5,41	2,64	
5,72		
5,88	3,03	-0,27
7,08		
7,39		
7,71		
7,87		-0,13
8,02		
8,18		
8,34	2,92	0,40
8,42	2,54	0,19
8,56		
8,72	2,88	0,10
8,88	2,93	-0,02
9,66	3,34	
10,29	2,88	
10,36		
10,40	2,99	-0,31
10,40	2,99	
10,66		
10,97	2,79	
11,27		
11,41		-0,23
11,90	2,90	-0,53
12,04	2,62	-0,42
12,51	3,15	
13,78		-0,62
14,59		-0,39
16,20		-0,36
16,99		-0,61
17,25	2,92	-0,66
17,81	3,30	-0,89
17,87	2,65	-0,57

17,90		-0,90
17,90	3,02	-0,67
17,96		-0,71
18,00	3,10	-1,14
18,03		-0,98
18,06		-0,89
18,10		-0,43
18,13		-0,87
18,20		-1,07
18,92		-1,00
19,01		-0,82
20,38	2,78	-1,41
20,68		
20,75		-1,10
21,09		-1,10
21,25		
21,31		-1,38
22,69		-1,29
23,04		-1,15
23,88		-0,76
24,00		-1,18
24,40		-3,26
25,44		-2,28
25,62		-1,25
25,95		-1,66
35,95	2,85	-1,44
41,90	3,68	
41,90	3,68	-3,12
52,90	2,91	
52,90	2,91	-1,80
61,85	1,87	-0,97
68,98	2,17	-1,14
78,48	2,89	-1,79
87,98	3,01	-1,75
97,51	2,56	
97,51	2,56	-1,18
106,97		-0,91
115,04		-1,53
123,02		-1,91
130,96		-1,80
137,58		-0,67
141,97	2,11	-1,01
146,45	2,40	-0,44
146,45	2,40	
151,40		-1,16